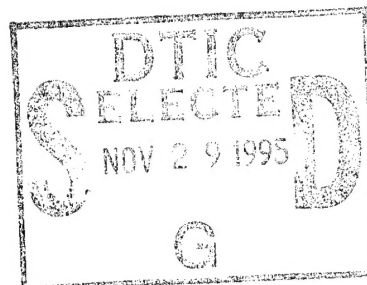NASA Contractor Report 3976
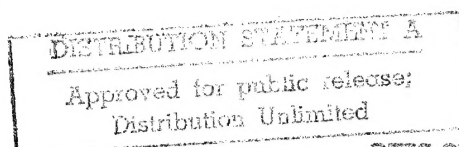
Ultrasonic Stress Wave Characterization of Composite Materials

John C. Duke, Jr., Edmund G. Henneke II, and Wayne W. Stinchcomb

DTIC
SELECTED
NOV 2 9 1995
G

19951121 088

NASA

```
--     1   OF      2
--                        ***DTIC DOES NOT HAVE THIS ITEM***
-- 1 -  AD NUMBER: D440028
-- 5 -  CORPORATE AUTHOR: VIRGINIA POLYTECHNIC INST AND STATE UNIV
--         BLACKSBURG  DEPT OF ENGINEERING SCIENCE AND MECHANICS
-- 6 -  UNCLASSIFIED TITLE:    ULTRASONIC STRESS WAVE CHARACTERIZATION OF
--         COMPOSITE MATERIALS,
--10 -  PERSONAL AUTHORS: DUKE,J. C. , JR.;HENNEKE,E. G. ;STINCHCOMB,W. W. ;
--11 -  REPORT DATE:        MAY   , 1986
--12 -  PAGINATION:     158P
--15 -  CONTRACT NUMBER:  NAG3-323
--18 -  MONITOR ACRONYM:  NASA
--19 -  MONITOR SERIES:   CR-3976
--20 -  REPORT CLASSIFICATION:  UNCLASSIFIED
--22 -  LIMITATIONS (ALPHA):    APPROVED FOR PUBLIC RELEASE; DISTRIBUTION
--         UNLIMITED. AVAILABILITY: NATIONAL AERONAUTICS AND SPACE
--         ADMINISTRATION, WASHINGTON, D.C. 20546. NASA-CR-3976.
--33 -  LIMITATION CODES:  1  24
--******
--     2   OF      2
--                        ***DTIC DOES NOT HAVE THIS ITEM***
-- 1 -  AD NUMBER: D323057
-- 5 -  CORPORATE AUTHOR: VIRGINIA POLYTECHNIC INST AND STATE UNIV


--         BLACKSBURG  DEPT OF ENGINEERING SCIENCE AND MECHANICS
-- 6 -  UNCLASSIFIED TITLE:    ULTRASONIC STRESS WAVE CHARACTERIZATION OF
--         COMPOSITE MATERIALS
--11 -  REPORT DATE:        MAY   , 1986
--12 -  PAGINATION:     158P
--15 -  CONTRACT NUMBER:  NAG3-323
--18 -  MONITOR ACRONYM:  NASA
--19 -  MONITOR SERIES:   CR-3976
--20 -  REPORT CLASSIFICATION:  UNCLASSIFIED
--22 -  LIMITATIONS (ALPHA):    AVAILABILITY: FOR SALE BY NTIS, SPRINGFIELD,
--         VA 22161 (N86-27556)
--33 -  LIMITATION CODES:  1  24
--******
--                     END OF DISPLAY LIST

--                     <<ENTER NEXT COMMAND>>
```

NASA Contractor Report 3976

Ultrasonic Stress Wave Characterization of Composite Materials

John C. Duke, Jr., Edmund G. Henneke II,
and Wayne W. Stinchcomb

Virginia Polytechnic Institute and State University
Blacksburg, Virginia

Accesion For		
NTIS CRA&I		☒
DTIC TAB		☐
Unannounced		☐
Justification		
By		
Distribution /		
Availability Codes		
Dist	Avail and / or Special	
A-1		

NASA
National Aeronautics
and Space Administration

Scientific and Technical
Information Branch

1986

Table of Contents

Preface

The final report of work performed with support from NASA Grant NAG 3-323 is presented in three parts. The first consists of three senior projects which examine:

1) the sensitivity of the acousto-ultrasonic evaluation method to subtle forms of damage development in cyclically loaded composite material,

2) the ability of the acousto-ultrasonic evaluation method for detecting initially existing imperfect material condition that promotes damage localization and final specimen failure, and

3) the use of a well-characterized receiving sensor (an NBS/Proctor transducer) in performing acousto-ultrasonic evaluation of laminate composite materials.

The second examines the nature of the wave propagation that occurs during acousto-ultrasonic evaluation of composite plates. It clearly demonstrates the part played by Lamb or plate wave modes and discusses how this may be utilized for characterizing such materials.

Part III describes work done to replace the receiving transducer in the acousto-ultrasonic measurement procedure with calibrated noncontact "practical" optical detection system.

A closure section presents a consolidated list of the conclusions of all these efforts.

Part I

THREE SENIOR STUDENT RESEARCH PROJECTS INVOLVING THE CHARACTERIZATION OF COMPOSITE MATERIALS USING ACOUSTO-ULTRASONIC METHODS

Seniors: Jonathan Buttram
          Paul Douglas
Advisor: J.C. Duke, Jr.

Senior: Thomas Lubnow
Advisor: E.G. Henneke, II

Materials Response Group
Engineering Science and Mechanics
Virginia Polytechnic Institute and State University
Blacksburg, Virginia 24061-4899

Preface

The work herein is a result of work performed by three senior students in the Engineering Science and Mechanics Department in fulfillment of the requirement of the Senior Project and Report. The work is part of an ongoing overall effort to extend the understanding and increase the areas of application of Nondestructive Evaluation of Advanced Composite Materials by Means of Acousto-Ultrasonic Methods. Support in part for this work through the NASA/LeRC Grant NAG 3-323 (technical monitor: Alex Vary) is gratefully acknowledged. The project advisors, J.C. Duke Jr. and E.G. Henneke, II, principal investigators of this grant, and Michael Kiernan, a graduate research assistant supported by this grant, have provided technical assistance. The financial support of the Engineering Science and Mechanics Department is gratefully acknowledged as well.

Assessment of Damage Development

During Stiffness Degradation Plateaus

in Cyclically Loaded Graphite Epoxy Laminates

Paul B. Douglas

Abstract

The damage mechanisms that occur in cyclically loaded composite materials that experience a stiffness plateau are not known. This paper examines several nondestructive techniques which can be utilized to provide information on local and global material condition. It is found that the damage mechanisms affect sound attenuation in composite materials as shown by Stress Wave Analysis.

I. Introduction

The increasing use of composite materials in critical structural components requires the designer to know specifics about their characteristics and behavior. Like composite materials' conventional counterparts, the "engineering metals", knowledge of the nature of the stress, strength/life, stiffness, and overall material condition is required to complete the design process and predict behavior. Unlike engineering metals, however, difficulties arise when defining composite characteristics and predicting behavior. First, composite properties are very direction-dependent; namely, individual lamina and laminates are anisotropic. Second, composites are the combination of two or more materials. As a result, lamina properties are a function of both the matrix and fiber properties. Lastly, as a consequence of both of the above, any behavior prediction process must consider the discontinuities and large gradients that arise at matrix-fiber interfaces and must include the favored failure modes and orientations.

To complete composite material characterization, the previously mentioned inhomogeneities must be coupled with the element of time. In general, applied loads (stresses), ultimate strength or life, stiffness, and overall material condition are a function of both location in the material and time. Behavior prediction for composites, then, is very complicated and is a function of position and time.

The goal of the design process and behavior prediction is to maximize component life and minimize cost and/or weight. Its ultimate goal is to accomplish this task and determine, or be able to determine through nondestructive methods, both the location and time component

performance will fall below design specifications -- when, where, and how failure will occur.

Several schemes are available to predict failure in composite materials. The Tsai-Wu and Tsai-Hill equations are popular examples which rely on the introduction of ply stresses which are estimated by laminate analysis for a given load. In conjunction with laminate analysis, discount schemes are used to reduce stiffness in failed plies and permit calculation of new ply stresses as damage develops. This process of damage development and stiffness reduction is repeated until the failure criterion (equation) yields a load that falls below the design specification.

Damage development in composite laminates subjected to cyclic loading is continuous. The degradation of stiffness, however, is not continuous and exhibits plateaus at various points. The damage mechanism(s) active during these plateau regions which leads to additional sitffness degradation are unknown. This makes it difficult to determine the condition of the material along the stiffness plateau. How close is the composite stiffness from falling off the plateau and subsequently failing?

The objective of this project is to utilize laminates which exhibit long plateaus and apply nondestructive means of evaluation to identify the degradation mechanism(s).

II. Specimen Preparation

This study was performed on T300/5208 graphite epoxy as supplied by NARMCO Materials, Inc. Specimens were fabricated locally with a flat face press using the cure time/temperature information found in Table 1 [1]. The fiber orientation configuration was $[0,\pm45]_s$. Specimens were cut using a circular saw with a diamond wheel blade. They measured 1.021 by 10.0 inches and had a cured thickness of 0.032 inches. Specimen geometry is shown in Fig. 1.

To improve gripping in the loading machine, the specimens were reinforced with Miller-Stephenson Epoxy 907 on all surfaces for a length of 2.0 inches on each end. The edges were also reinforced with the epoxy except for the 1.0 inch gage section in the middle of the section. This was done in an attempt to concentrate damage development and enhance damage detection in the 1.0 inch gage length monitored by the extensometer. To accommodate the extensometer, aluminum tabs with V-shaped grooves were bonded to the specimen gage area with 3M Adhesive/Sealant Silicone (No. 03608). The reinforced specimen with attached extensometer tabs is shown in Fig. 2.

Table I. Cure Data[1] for T300/5208 Graphite Epoxy Material

Cure Temperature (°F) (°C)   275 (135)

Cure Pressure (psi) (MPa)   70 (0.5)

Cure Time (min.)   105

Post-cure Temperature (°F) (°C)   325 (163)

Post-cure Pressure (psi) (MPa)   70 (0.5)

Post-cure Time (min.)   120
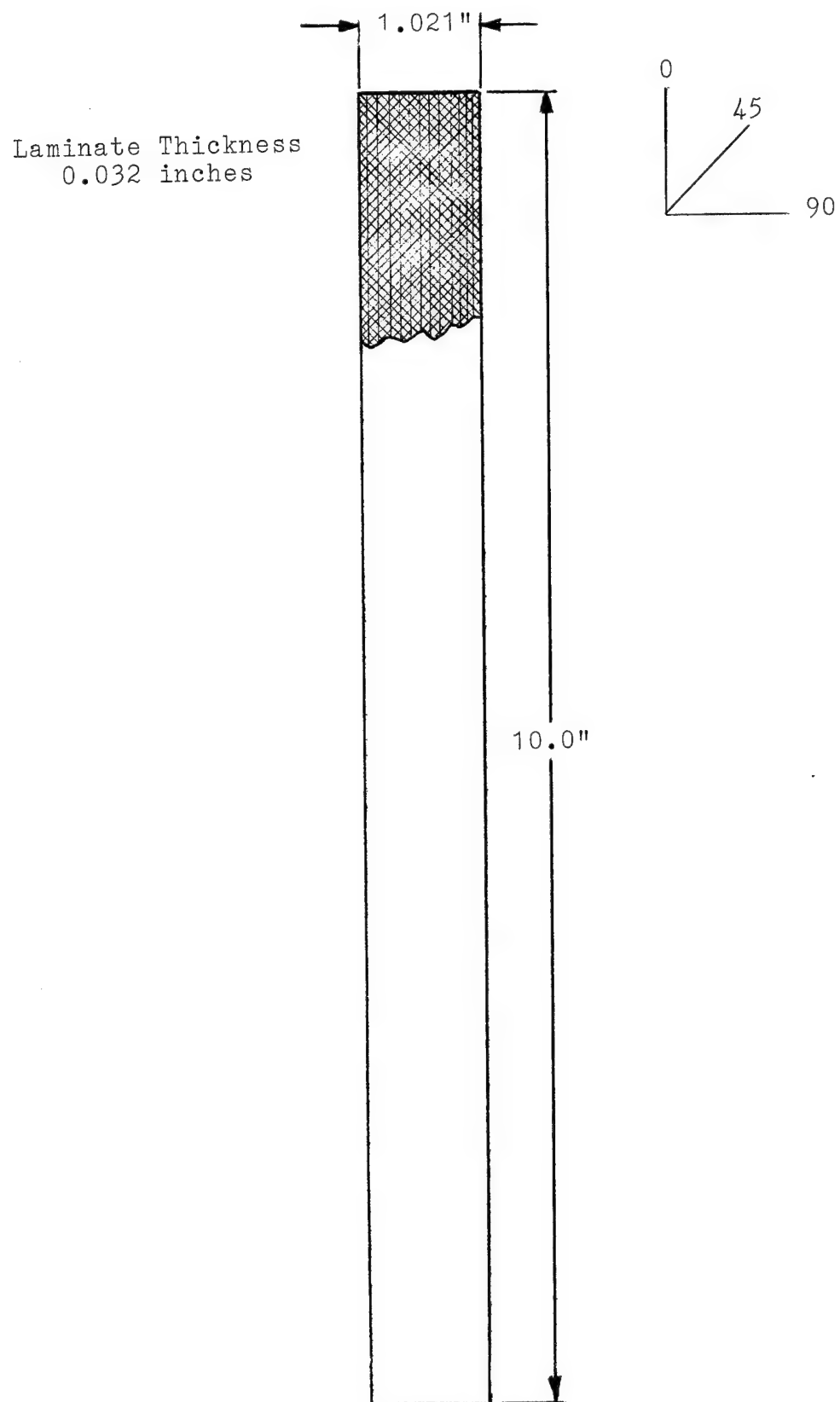

[1] Supplied by manufacturer
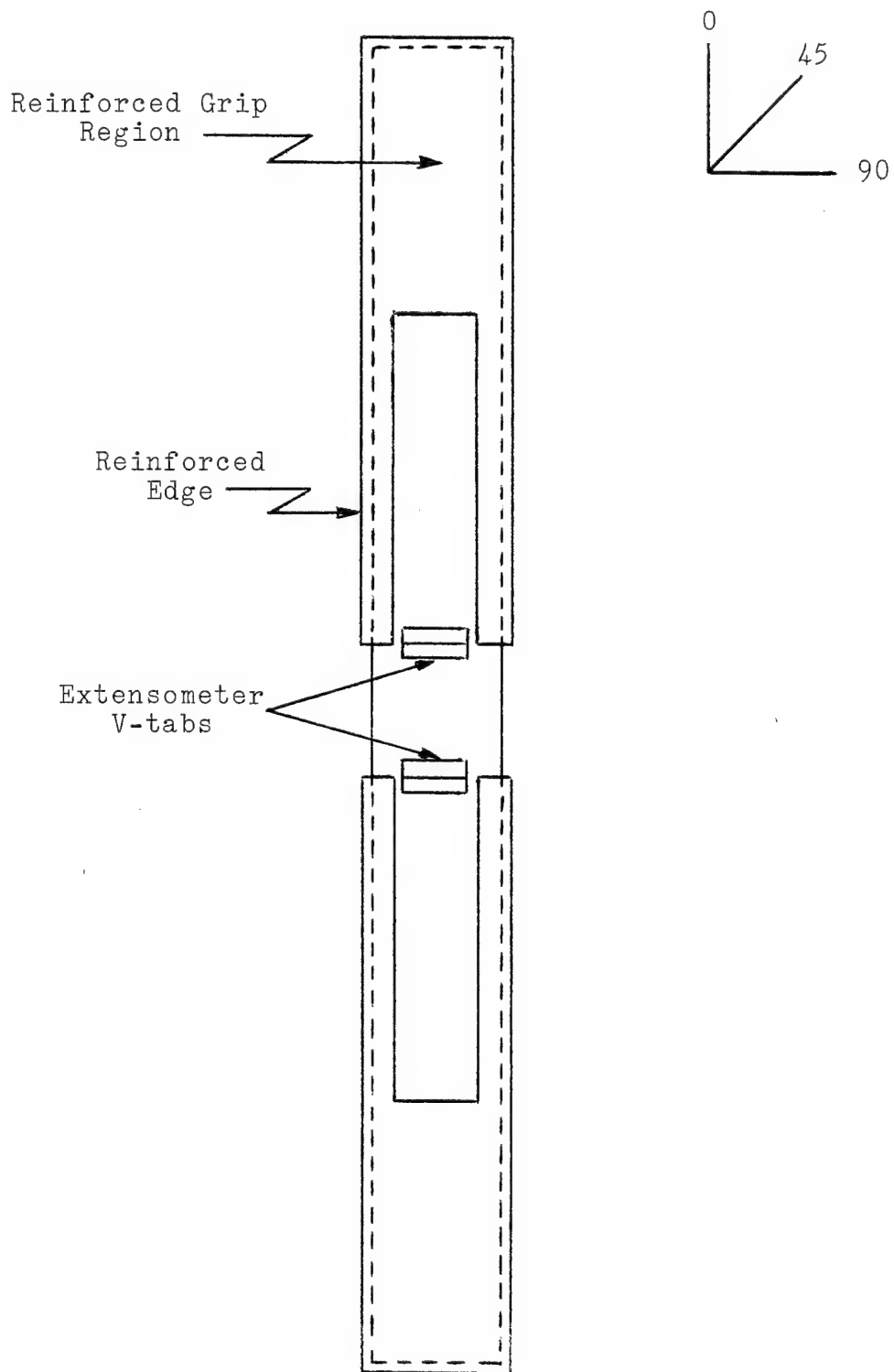
Fig. 1. Specimen configuration.

Fig. 2. Specimen grip area and edge reinforcement, and extensometer V-tab location diagram.

III. Mechanical Testing

Specimens were tested in tension-tension fatigue with $\sigma_{min}/\sigma_{max}$ = 0.1 and σ_{max} = 67.1 ksi [2]. This loading produces rapid initial degradation to the desired stiffness plateau. Fatigue tests were conducted using a MTS hyudraulic testing machine in the load control mode. Figure 3.0 is a block diagram of the testing machine and its monitoring equipment. Tests were run at 10 cycles/sec. Stiffness degradation was monitored by measuring the decrease in the secant modulus versus cycles. Strain measurements were made using an 1.000 inch extensometer and were read directly from the MTS Digital Indicator in percent strain.

IV. Nondestructive Testing

The Stress Wave Factor (SWF) has been shown to be useful to detect the relative condition of a composite material. In tensile tests performed on composites, correlation between the point at which the specimen fails and the region having the lowest SWF value have been found [3]. Using this result, one can say that if failure occurs or is initiated at a point where maximum material degradation has taken place, then the SWF should be a means of monitoring relative material condition over time. The Stress Wave Factor is utilized to try to detect a change in the fatigue specimen condition which either shows the degradation
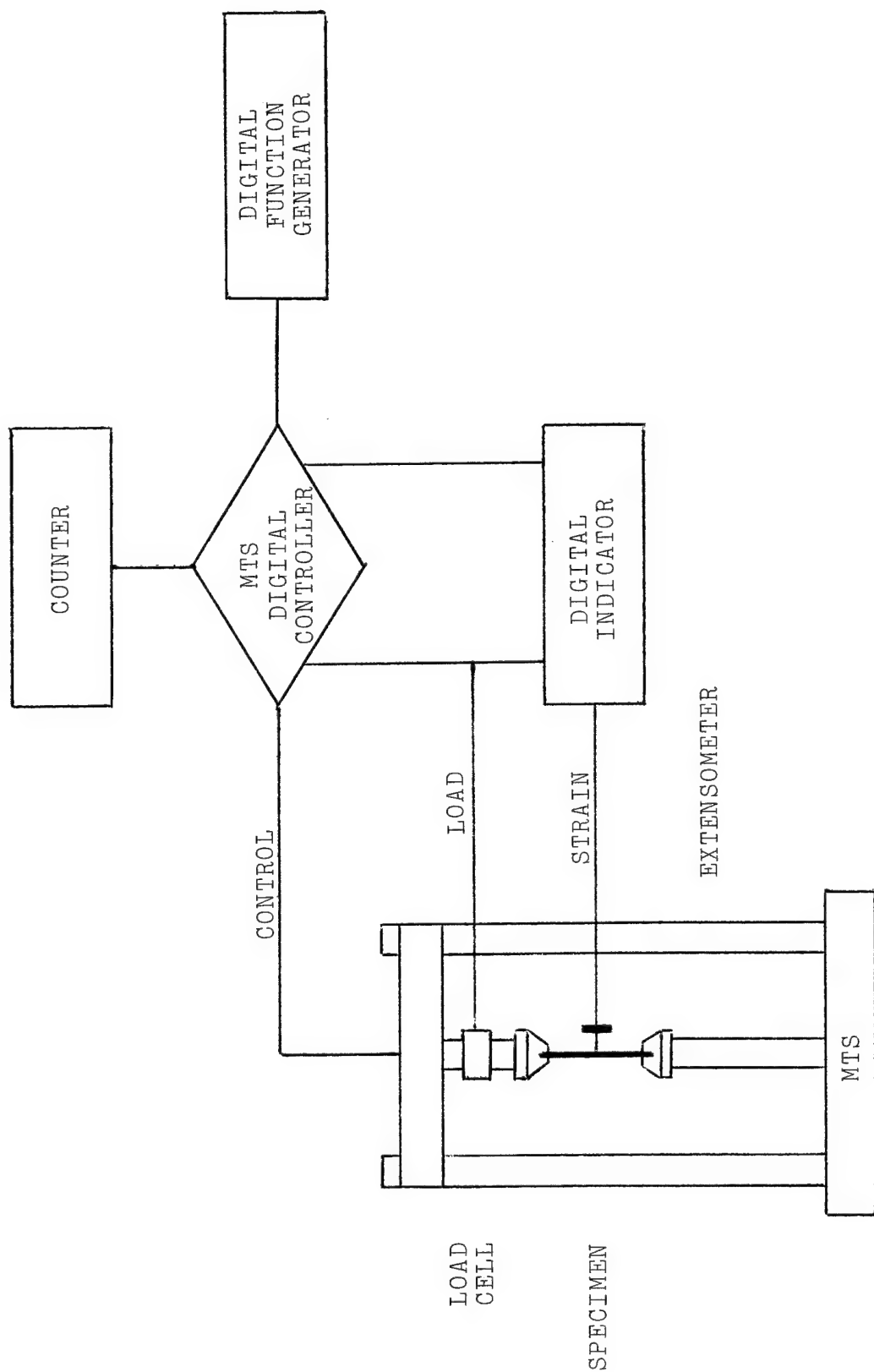
Fig. 3. Schematic of the mechanical testing and monitoring equipment.

occurring during the stiffness plateau or marks the end of the plateau or both.

During the cyclic tests, Stress Wave Factor values were recorded at points during the cyclic loading. Values were obtained at three (3) load levels -- minimum, mean, and maximum. The extensometer was removed from the specimen while these values were obtained. Two (2) one-half inch Panametric Transducers were secured to the specimen via a mounting block as shown in Fig. 4.0. Echo Laboratories' Ultragel II was the couplant used in the SWF tests. Equipment associated with the SWF is illustrated in Fig. 5.0.

X-ray radiography is a method well suited for internal flaw detection in composite materials. Radiographic techniques can readily detect macroscopic matrix cracks and delamination in composite laminates. Specimens were prepared for each radiograph while still in the MTS loading machine. To enhance detection of flaws, a solution of 60g zinc iodide, 10 ml water, 10ml isopropyl alcohol, and 10ml Kodak "Photo-Flo 600" was applied to the specimen before each radiograph. The solution was painted on the exposed edges of the laminate in the gage length while at mean load. After application, the specimen was cycled once manually using the set point load control, the zinc iodide solution was reapplied, and the cycle was repeated. The specimen was then unloaded and removed from the test machine. At this point, each specimen was washed with acetone and dried to ensure that none of the X-ray opaque zinc iodide solution remained on the surface.

A Cabinet X-ray was used to make radiographs of the specimens. All radiographs wre made with an exposure of 25kV for three-tenths of one minute. Negatives were processed using a four-step developing
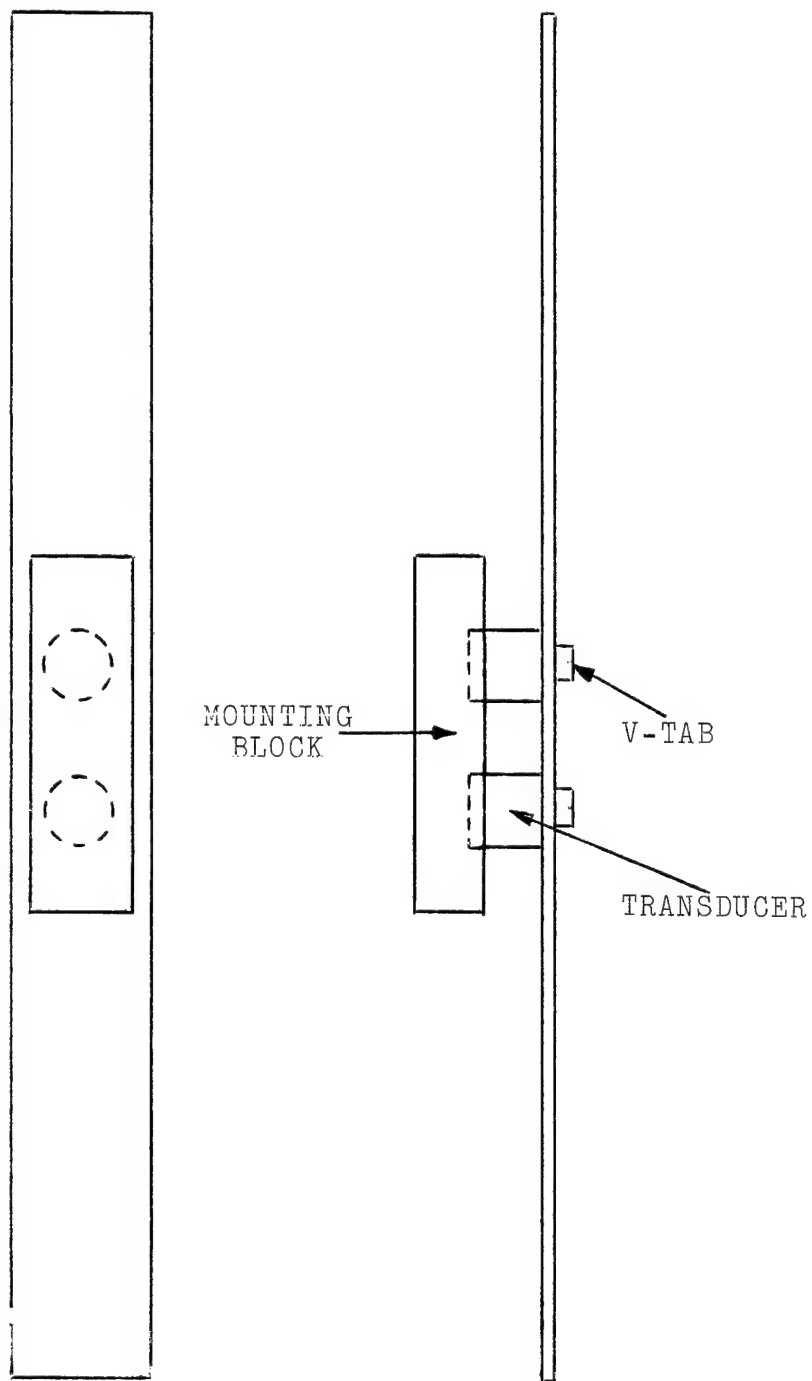
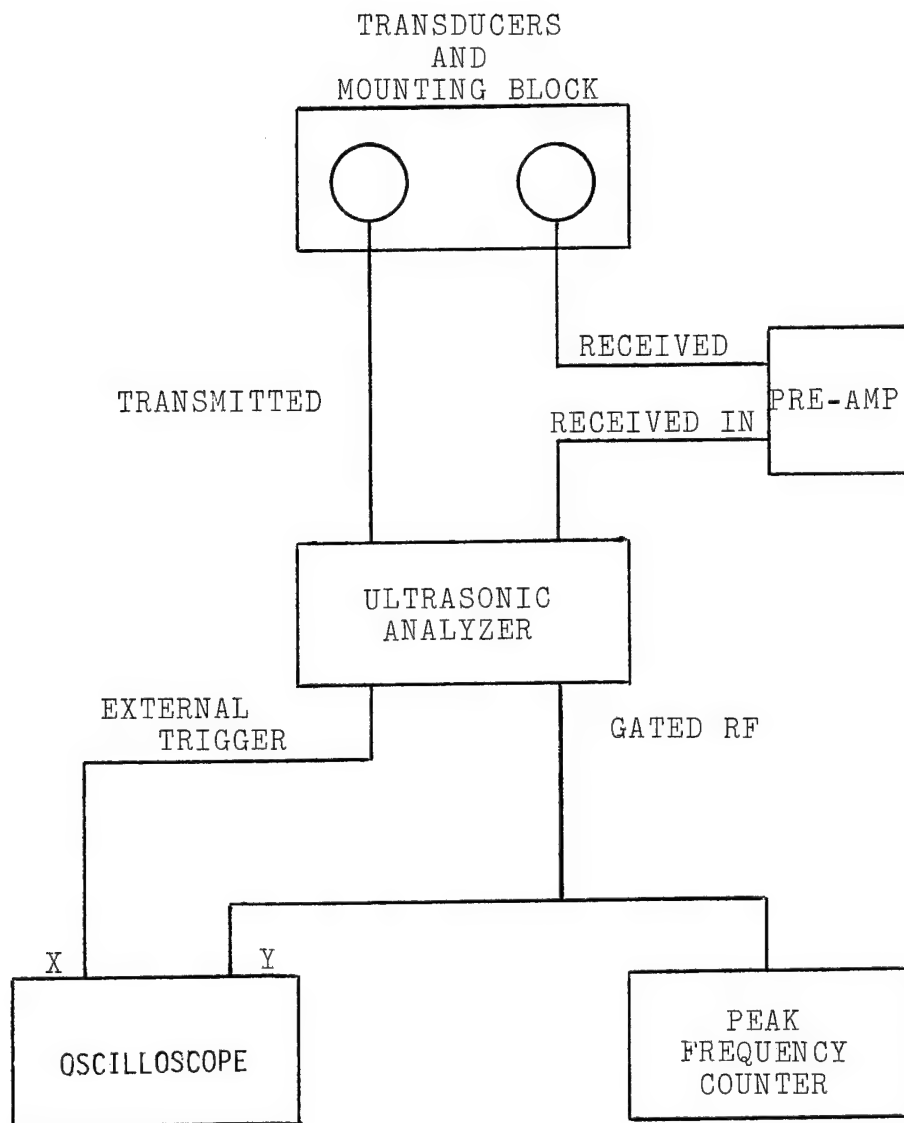Fig. 4. Transducer placement and spacing arrangement.

I-13

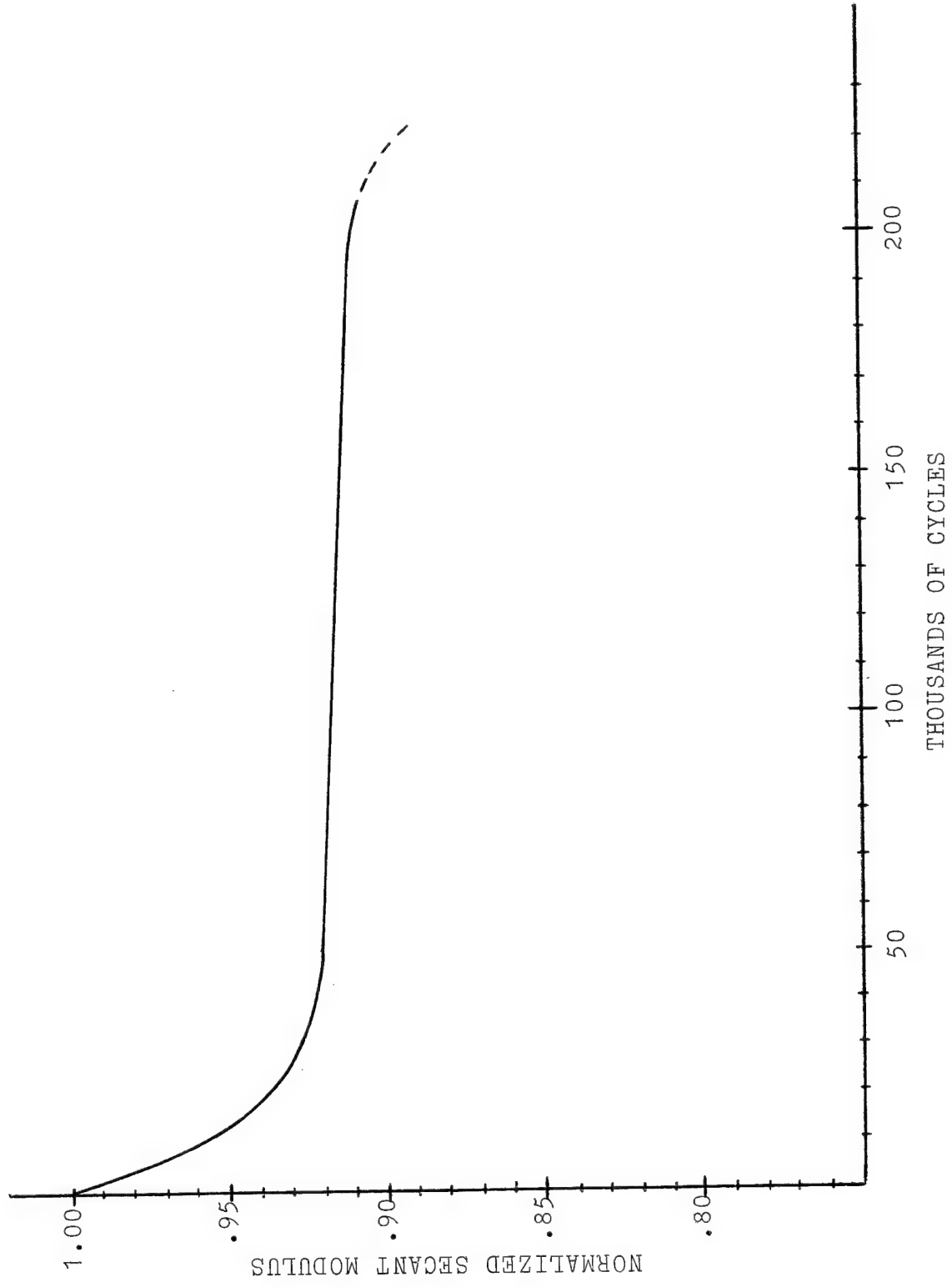Fig. 5. Schematic of the Stress Wave Factor testing system.

Fig. 6. Normalized secant modulus versus loading cycles. (R=0.1).

process: 1) 5 minutes in developer,   2) 30 second stop bath,   3) 3 minutes in fixer, and   4) 10 minute water bath.   All prints wre made on high contrast grade 5 Ilford black and white print paper.

V.   Results and Discussion

The specified fatigue loading produced a rapid initial decrease in stiffness to the anticipated stiffness plateau.   A graph of the normalized secant modulus versus cycles is plotted in Fig. 6.0.

Specimen #1 was tested to 195,000 cycles at which time a decrease in stiffness was observed.   This decrease, although seemingly small, occurred in a span of 10,000 cycles and was accelerating.   The test was stopped and a visible edge delamination was found.   It is believed that delamination was responsible for the drop off in stiffness.

Stress Wave Factor values obtained using the procedure outlined in Section IV produced no correlation between the number of cycles and the degree of degradation of the specimen.   Figure 7.0 shows this lack of correlation between stiffness and the SWF values.   SWF values were taken at five (5) points during the 195,000 cycle test period of specimen #1.   Obtaining values for these five (5) points involved stopping the loading machine after the required number of cycles.   The transducers were attached as shown in Fig. 4.0 and the couplant was introduced to the transducer/specimen interface.   The load was cycled several times to each test load using the set point, and SWF values were recorded.   No general trend towards lower SWF values with respect to time at any of the test loads (min., mean, max.) could be found.   In fact,
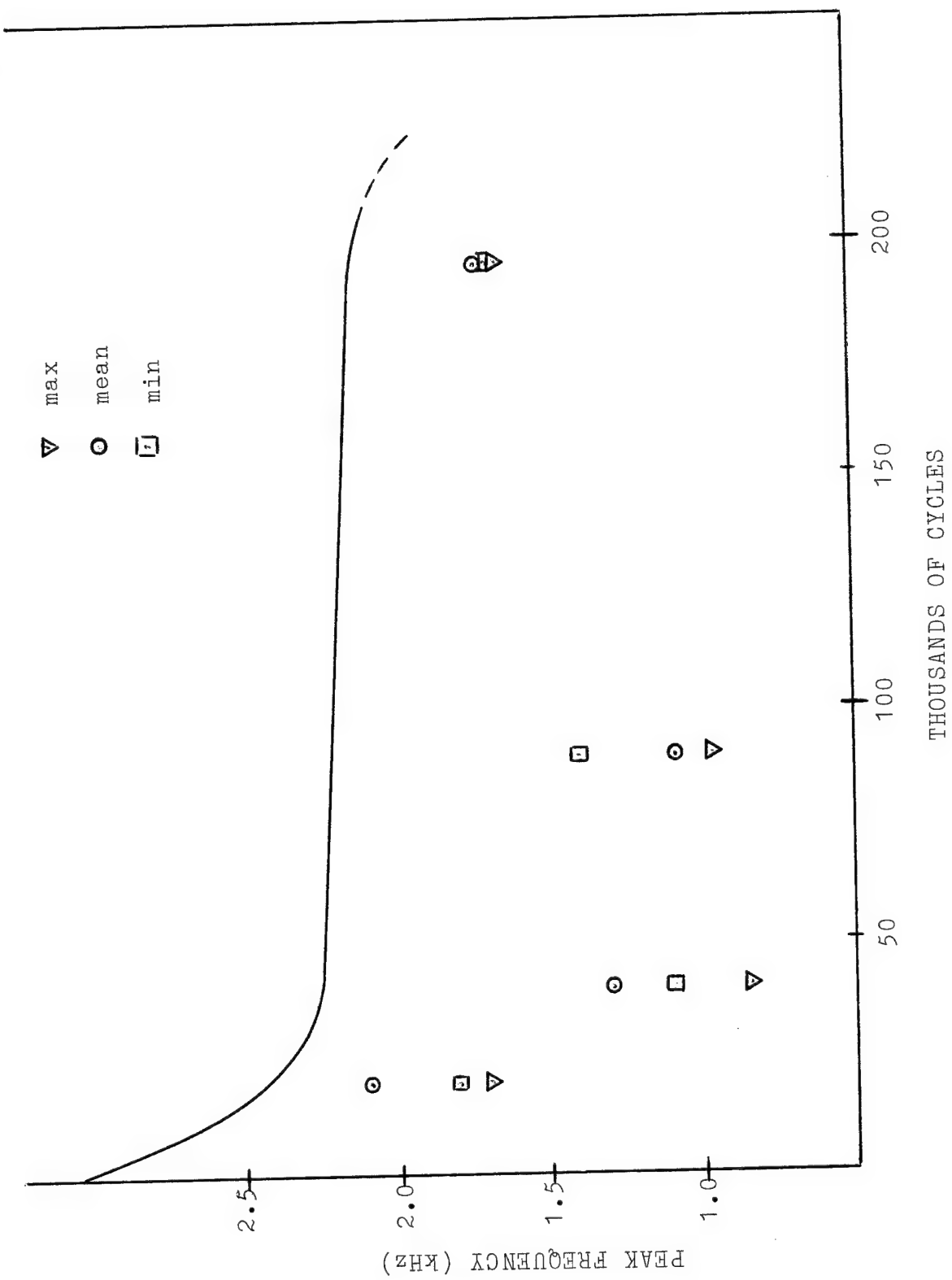
Fig. 7. Peak Frequency Count (sWF) versus loading cycles.

reproducibility of a SWF value at a given load for a given number of cycles was difficult. This difficulty in reproducing values is inherent in any type test involving the SWF. However, previous work has shown that by carefully controlling test variables, reproducibility of 10% is obtainable [3].

The test configuration described in Section IV did not permit good control of the test variables. Specific deficiencies were as follows:

1. <u>Vertical Test Position</u> -- allowed ultrasonic couplant to flow from between the transducers and test specimen under the force of gravity. The SWF value decreased with the length of time the transducers were left on the specimen.

2. <u>Transducer Placement/Orientation</u> -- complicated the ability to "look" at the same location in the same way from point to point on the stiffness plateau. Either translation of the mounting block along the specimen or rotation of a transducer in the mounting block varied the SWF value.

3. <u>Elastic Connecting Bands</u> -- complicated the ability to reproduce transducer/specimen contact pressure. The SWF value decreased with increasing contact pressure.

It was initially thought that obtaining SWF values at "load" would increase the detectability of material flaws. For instance, if flaws are some type of micro- or macroscopic crack, an applied load would tend to open the crack and increase sound impedance. This increase in detectability, however, did not account for, nor did it override, the loss of reproducibility imposed by the geometric constraints of the loading machine.

Four (4) radiographs were made of specimen #1 during the 195,000 cycle test. These are shown in Fig. 8.0. All except the last radiograph were taken when the material was still on the stiffness plateau. Figure 8.0d was taken after the decrease in the secant modulus
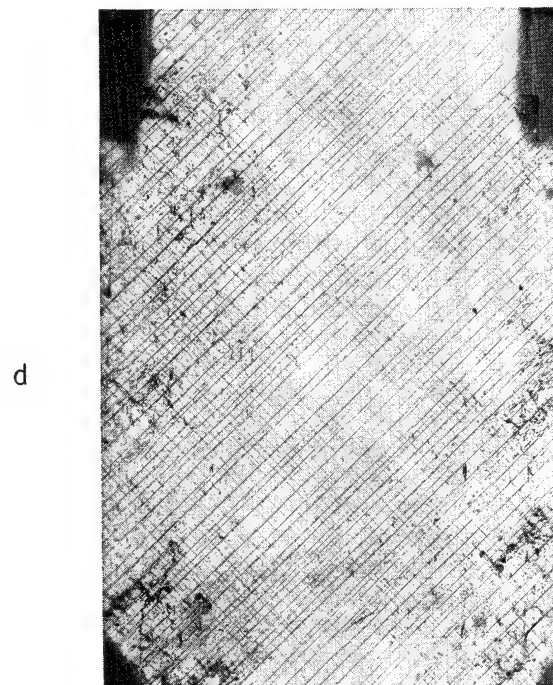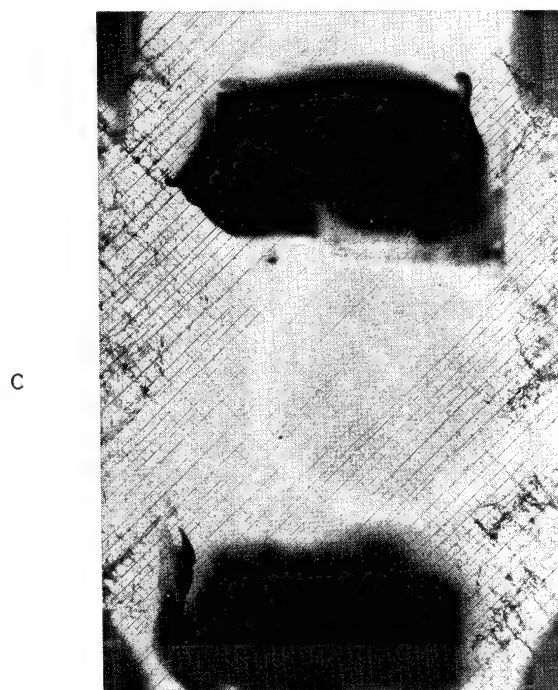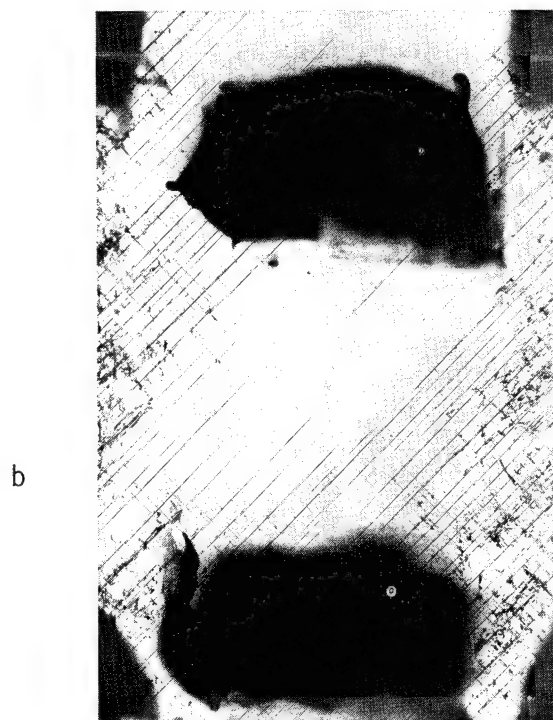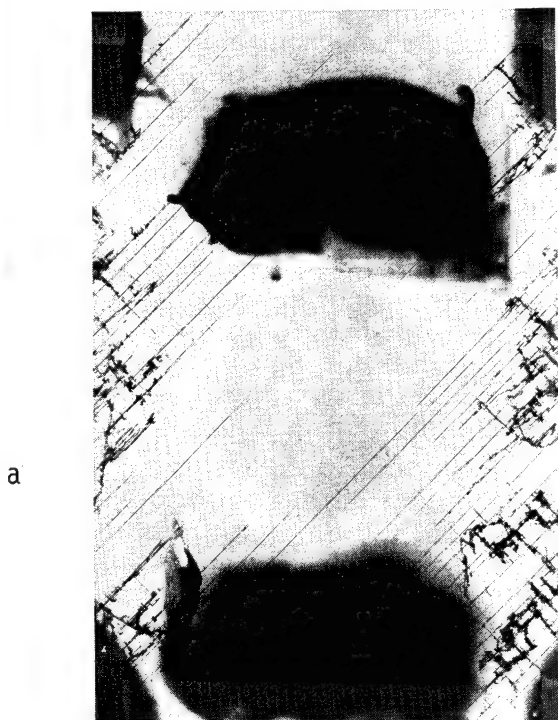
Fig. 8. Penetrant enhanced X-ray radiographs of specimen #1 after
a) 40,000, b) 90,000, c) 115,000, and d) 195,000 loading
cycles.

was observed. Also note that the V-tabs were removed from this specimen before the radiograph was made.

First analysis of these photographs indicates that macroscopic damage is occurring while cycling along the stiffness plateau. It must be carefully noted, however, that damage (matrix cracks) is only visible because the zinc iodide solution has managed to work its way onto the cracks. Further, if the density of the photographed crack damage is related to the distance from the laminate edge (point of entry for the zinc iodide), a relation is seen. The material furthest from the source of the zinc iodide shows the lowest crack density. It should also be noted that the sequence of damage development shown in Fig. 8.0a-d would have most certainly produced a reduction in stiffness. With the above remarks noted, the following must be considered when analyzing zinc iodide enhanced X-ray radiographs of cyclically loaded composite materials:

1. A radiograph does <u>not</u> show damage; it indicates where the enhancing dye is present.

2. A sequence of radiographs does <u>not</u> show crack development but rather the extent of dye penetration.

3. As a result of 1. and 2., and by observing the sequence of photrographs in Fig. 8.0, it can be proposed that the degree of macroscopic cracking between two (2) points on the stiffness plateau is very nearly the same, but might appear quite different with comparison of radiographs taken at each point.

4. The cyclic nature of the load may act as a pumping mechanism to get the dye (zinc iodide) into the developed cracks.

A somewhat different approach was used for the analysis of specimen #2. Seeing that the Stress Wave Factor (SWF) data for specimen #1 yielded no correlation between damage development and position along the

stiffness plateau (cycles), it was decided to modify the signal interpretation. Increased sensitivity and reproducibility were accomplished by removing the testing deficiencies imposed by the loading machine. Namely, SWF data was obtained with the specimen removed from loading machine grips and positioned on a horizontal surface. The transducers were mounted as shown in Fig. 9.0 and their initial position was marked on the specimen with a white marker. Signal interpretation was changed from recording the peak frequency count to performing a Fast Fourier Transform of the Stress Wave Signal and looking at the "zeroth moment" of this transform [5]. The zeroth moment is the square root of the area under the frequency versus amplitude curve and gives a measure of the energy reaching the receiving transducer. Plots of the peak frequency count (amplitude versus time) and the transformed Stress Wave Signal (frequency versus amplitude) are shown in Fig. 10.0 and Fig. 11.0 respectively.

The zeroth moment calculation was performed at three (3) points along the stiffness plateau curve of specimen #2 plotted in Fig. 12.0. Preliminary results shown in Fig. 12.0 correlate a decrease in the moment calculation with increasing cycles. This is a very significant result because it indicates a continuous degradation of material condition not associated with a change in stiffness. As the composite was cycled and damage progressed, there was an increase in signal attenuation.

Two (2) radiographs of specimen #2 were made. They are shown in Fig. 13.0. The comments made concerning radiographic evaluation of fatigued composites from the discussion of specimen #1 apply.

Fig. 9. Testing configuration for stress wave analysis with the specimen removed from the testing machine.

MOUNTING BLOCK

TRANSDUCER

PLOT OF TIME VERSES VOLTAGE

Fig. 10. Time domain received signal as gated for analysis.

PLOT OF FREQ VERSES AMPL

Fig. 11. Fast Fourier Transform (FFT) analysis of the time domain
signal of Fig. 10.

I-24

Fig. 12.   Zeroth Moment of the frequency spectra of stress wave signals at various points during the cyclic loading.

Fig. 13. Penetrant enhanced X-ray radiographs of specimen #2 after a) 70,000, b) 170,000 loading cycles.

VI. Conclusions

The following conclusions are made:

1. Zeroth moment calculations indicate an increase in sound attenuation with increasing cycles in a $[0,\pm45]_s$ composite laminate, with no corresponding increase in observable damage.

2. Stress Wave Frequency Counts do not correlate with the continuous degradation occurring in a $[0,\pm45]_s$ composite laminate.

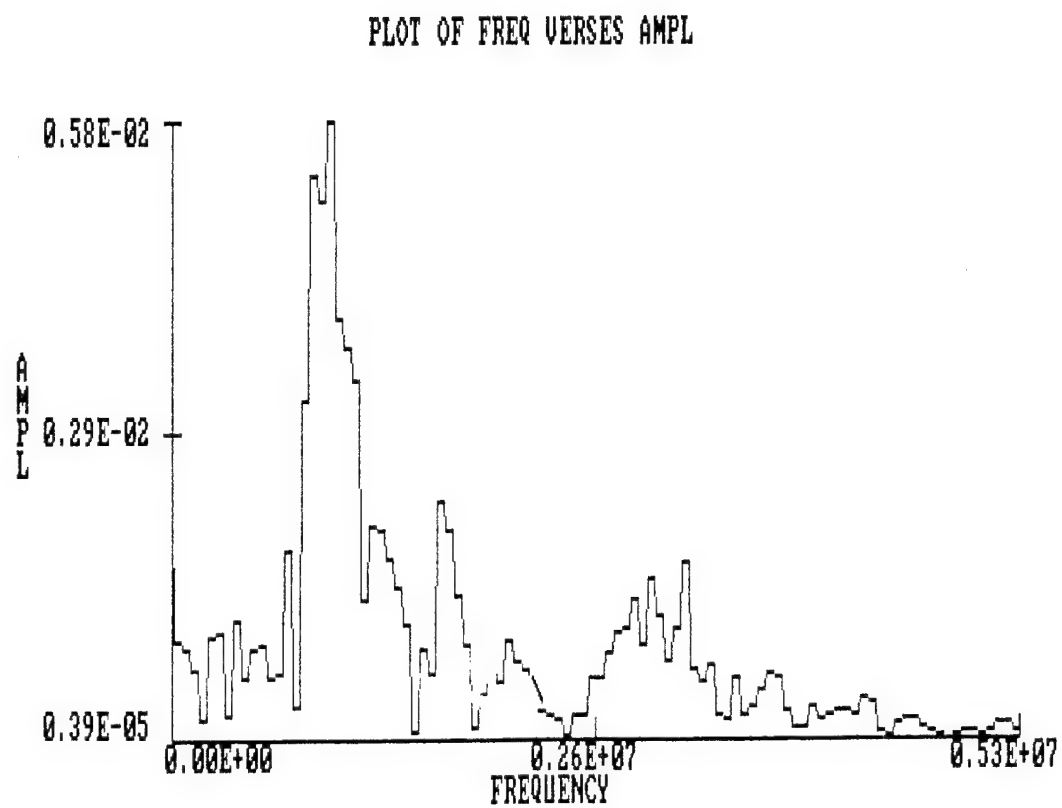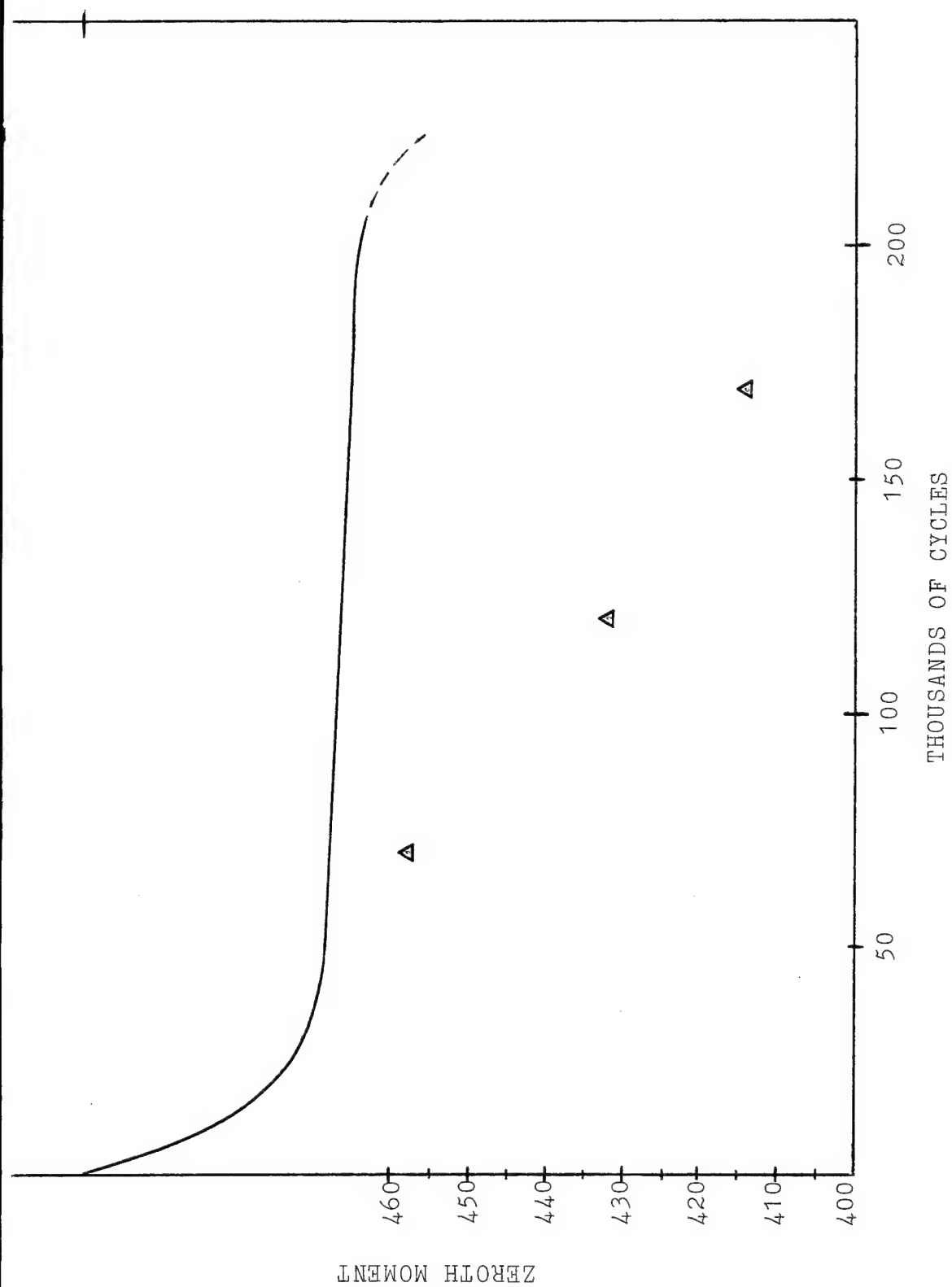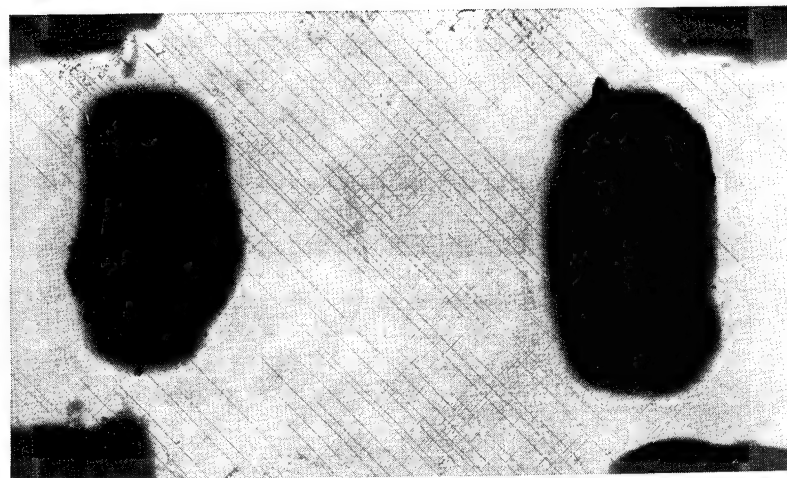3. X-ray radiography yields misleading visual information about the degree of material degradation occurring in a $[0,\pm45]_s$ composite laminate under cyclic loading.

References

1. Jamison, R. D., "Advanced Fatigue Development in Graphite Epoxy Laminates," Ph. D. Dissertation, VPI & SU, August 1982, p. 27.

2. Reifsnider, K. L. and Jamison, R., "Fracture of FAtigue Loaded Composite Laminates," Int'l. J. of Fatigue 4 no. 4 (1982) pp. 187-198.

3. Henneke, E. G., Duke, J. C., Stinchcomb, W. W., Govada, A. and Lemascon, A., "A Study of the Stress Wave Factor Technique for the Characterization of Composite Materials," NASA Contractor Report 3670, Feb. 1983, p. 2.

4. Govada, Anil K., "Nondestructive Assessment of Composite Material Condition by Means of Acousto-Ultrasonics," Thesis for the Master of Science, Engineering Mechanics, Virginia Polytechnic Institute and State University, June 1984.

A Study of the Final Failure Event

for Uniaxial Tensile Loading

of Graphite Epoxy Laminates

Jonathan D. Buttram

Abstract

Identifying areas of low strength in a composite material is a problem of which little is known. This experiment approaches this problem by identifying damage characteristics that are related to areas of low strength through the use of stress wave factor analysis, edge replication, and X-ray radiography.

The data obtained indicated a relationship between areas of low structural strength and those which produced low stress wave factor (SWF) values. Using this relationship, which provided the means to predict failure areas, and the ability to visually monitor these areas through the use of replicas and radiographs during increasing load increments, data was obtained which suggests that damage is a local phenomena that eventually governs failure. Visual damage characteristics found in the edge replicas and radiographs were found not to be as significant as stress wave factor data, which, if used properly, can be a characteristic of otherwise undetected damage.

I. Introduction

The identification of potentially weak areas in a composite material has become a major problem in the forecasting of durability. Although there are many nondestructive testing techniques that can be used on composites, the interpretation of the results from these tests can be difficult and unsure. If certain distinguishing damage characteristics were to be found which correlated directly to areas of structural failure, then these could be used to assist in the nondestructive evaluation process. This project addresses this problem by initiating damage in a quasi-isotropic material by applying uniaxial tension to sample specimens. Using nondestructive testing techniques such as X-ray radiography, acoustic emission monitoring, stress wave factor analysis, and edge replication, a direct relationship between some distinct damage feature and the probable failure area is sought. To understand this more clearly, certain assumptions must be discussed and related to the procedures and final outcome.

First one must ask the question,"Why does a failure occur at a particular location?" Theoretically if a material were perfect with no flaws, then a uniform specimen would just disintegrate under uniaxial tension. Since every point on the specimen has the same strength properties with no defects, then failure should simultaneously occur at every point along the specimen. This of course does not happen in reality because of imperfections in the material. In this experiment the assumption is made that as the specimen becomes stressed under load, the point with the most significant damage becomes increasingly more damaged. Immediately before failure the damage here is more advanced

than at other points throughout the sample. The density of this damage is also assumed to decrease as one moves farther from the failure area. Therefore if long specimens are used and the approximate location of failure can be determined, then it is assumed that another area that is much farther away will be less damaged.

The detection of the failure area presents another problem. Because of the dynamic nature of failure under high stresses, unwanted destruction can be imposed on the material if actual rupture occurs during testing. Because of this, a stress wave factor analysis was used to predict areas of failure before failure occurred. Stress wave factor (SWF) is a relatively new nondestructive testing technique which utilizes high frequency stress waves to predict relative material strengths [2,3]. This method assumes that as a stress wave propagates through a material, imperfections such as voids, cracks, defective bonds, broken fibers, etc., will attenuate the signal. During the testing process, high frequency pulses are transmitted by one transducer and received by another that is at a fixed distance away. A scanning process is set-up so that an entire specimen can be examined, a segment at a time. Accordingly, if a segment of a material exhibits a signal of particularly low amplitude, then one can assume the presence of imperfections or areas of low strength. This method is vital in this experiment since it allows the prediction of low strength areas that can be scrutinized during the testing and analysis process.

II. Objective

The purpose of this experiment is to find distinguishing damage characteristics that are directly related to predicted areas of low

structural strength through the use of acoustic emission, stress wave factor, edge replication, and X-ray radiography.

Approach

The basic experimental approach was to use the stress wave factor technique to first predict an area of low structural strength. Then samples were loaded to various levels and radiographs plus edge replicas were used to observe internal damage. The objective was to unload the specimen immediately before failure was expected, paying particular attention to the area of low strength predicted by the SWF analysis. Acoustic emission monitoring was also used so that failure could be anticipated from emission occurring during loading.

III. Procedures

A. Sample Preparation

Six samples were cut from a $[+45,-45,90,0]_s$, a graphite epoxy laminated sheet. These samples varied from 12 to 16 inches long and were ½ inch wide. Because of their length, some of the longer samples were cut so that they would fit the testing machine. All specimens were cut using a diamond impregnated cut off wheel employing continuous coolant flow.

B. Testing Platform Preparation

To achieve consistent results from the stress wave factor analysis, a position platform was designed (Fig. 1). The platform held the sample securely and provided a means by which to position the transducers accurately in the center of the specimen. Quarter inch marks were placed on the transducer rest so that a precise location of the

NOTE: After making all adjustments, washers and
      wingnuts were used on bolts.

Spacer

Adjustable Transducer Rest
with Position Marks

a)

Transducer

Adjustable Specimen Holder

Specimen

b)

Bottom View

|←— 1 in —→|

End View

Side View

Fig. 1. a) Testing platform b) Transducer holder.

specimen could be recorded and reproduced. The transducers were maintained 1 inch apart by a simple fixture also shown in Fig. 1. The previously mentioned tools were used in the stress wave factor analysis in order to improve the accuracy of the results.
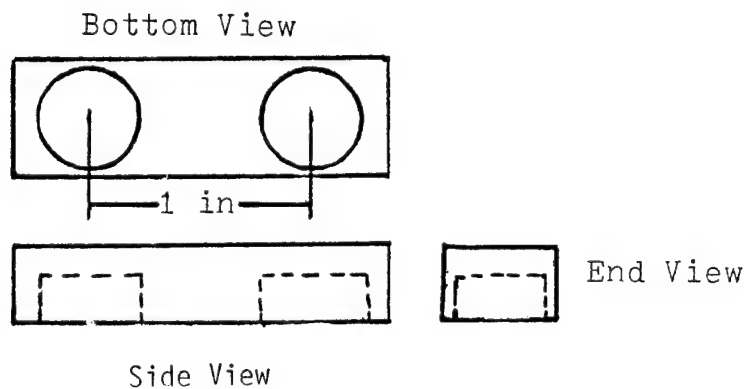
C. Stress Wave Factor

An understanding of the basic equipment set-up and its function must be obtained before the procedures for the SWF can be appreciated. The first step in the process is the production of ultrasonic pulses. These pulses are produced by an ultrasonic pulser which can be adjusted depending on the desired energy and repetition rate desired (Fig. 2). The pulse then travels to the transmitting transducer and propagates through the specimen to the receiving transducer. The signal is then amplified, filtered, and gated. This gated signal is sent to a counter which counts cycles over an adjustable threshold (voltage level) in a desired time period. The number of cycles counted was recorded according to specimen location. In order to smooth out any abrupt changes in data values, a computer program was written. This program took the data values and averaged each with its two neighbors. For example:

$$X'_3 = \frac{(X_2 + X_3 + X_4)}{3.0}$$

or

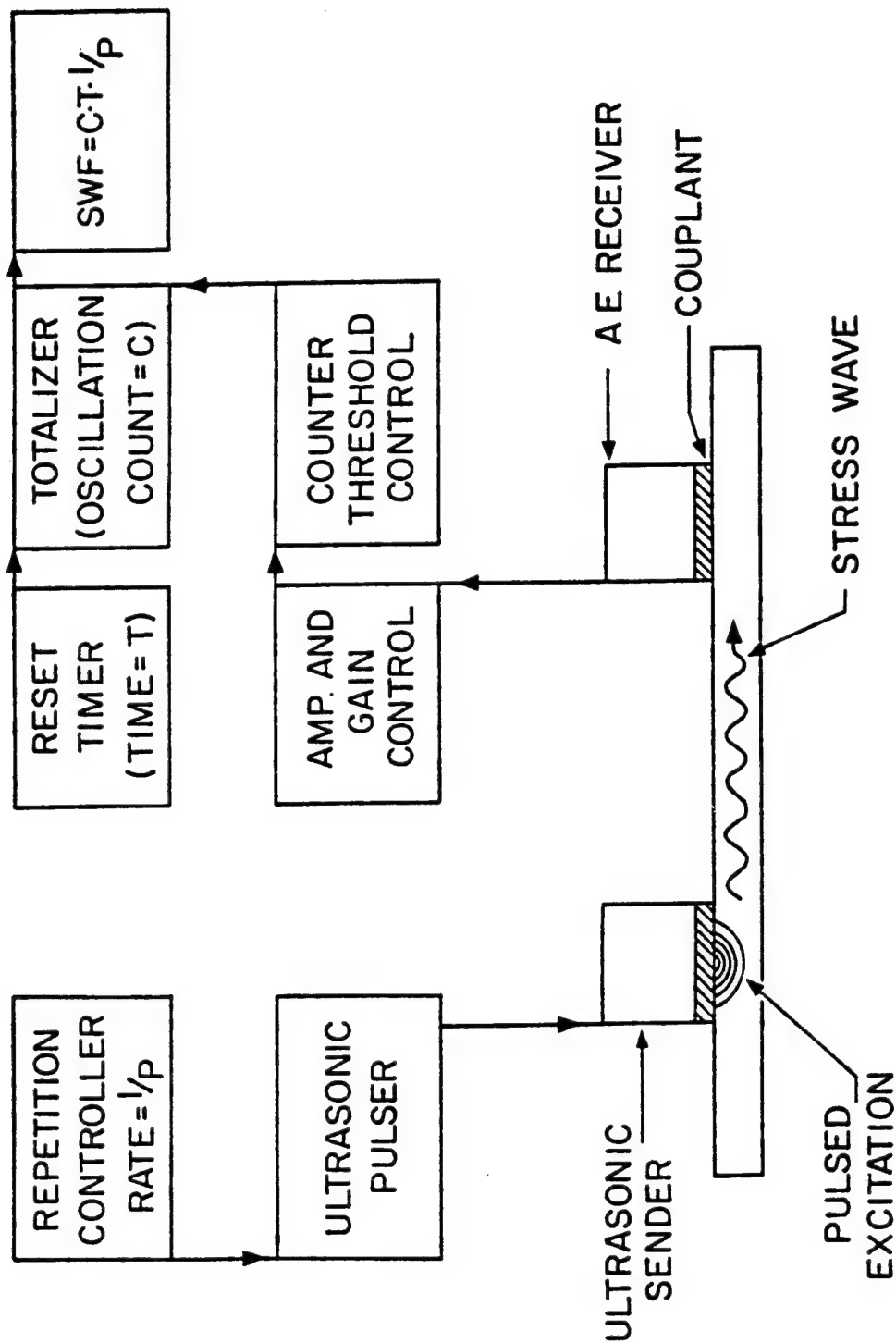$$X'_n = \frac{(X_{n-1} + X_n + X_{n+1})}{3.0}$$

I-33

Fig. 2. Schematic of the stress wave factor testing set-up.

where X_n represents the actual data and X'_n represents the new calculated data. This method only made data more plottable but did not change data trends which are essential in this experiment. For more detailed information pertaining to topics concerning SWF, refer to the appendix.

The following steps were preformed in the analysis.

Step 1: The specimen was placed in the positioning platform and adjustments performed so that the center of the transducers were positioned directly above the center (of width dimension) of the specimen. A small overhang of the transducers was experienced in this case because of the dimensions of the transducer and specimen.

Step 2: The transmitting and receiving transducers were fixed at 1 inch apart. A starting point was designated and a large drop of couplant was applied, and another, 1 inch along the sample. The couplant was then spread into a thin, even film using a razor blade.

Step 3: The transducers were set in the couplant and a 50 gram mass was placed on each transducer. The transducers were allowed to set for 25 seconds so that an even and uniform layer of couplant was achieved.

Step 4: After the 25 seconds had expired, the counter was reset and signal preamplifier turned on. Twenty more seconds were allowed to pass and a reading from the counter was then recorded.

Step 5: The transducers were removed from the specimen and all couplant cleaned from the transducer and specimen surfaces.

Step 6: The tandem transducer assembly was translated ¼ inch along the specimen to the next measurement location and steps 2-5 repeated until the entire testing area was examined. (Two inches on the

ends of each sample were not tested because they were located in the testing machines grips.)

Step 7:   The data was then entered into a computer program which calculated and plotted the results.

D.   Sample Test

A preliminary test was run on one of the samples in order to determine a representative ultimate strength.

E.   Edge Replication Technique

Edge replication is a simple and quick method to examine damage on an exterior surface.   It provides a "fingerprint" of the desired surface showing damage such as cracks, delaminations, voids, etc.   A special tape is used which softens with the application of acetone.   If pressed against a surface during this soft condition, the tape will be impressed with features from that surface.   The steps in the procedure are as follows.

Step 1:   The edges of the sample to be tested were cleaned. (These surfaces should be smooth.)

Step 2:   A thin piece of replica tape was cut from the roll and securely fastened to the edge of the specimen by taping it at the ends.

Step 3:   Acetone was then applied to the crevice between the replica tape and specimen edge by means of a syringe.

Step 4:   An object with a flat, smooth surface was rubbed over the back of the tape, pressing it against the sample surface.   Approximately 45 seconds was allowed to pass before the tape was removed.   This provided time for the acetone to dry and the tape to harden.

Step 5:   The samples were marked where replicas were taken.   The edge replicas were placed on a glass slide and viewed under magnification.

F. Second Stress Wave Factor

Another stress wave factor analysis was performed after load of the specimens. (Refer to part C for the precise procedure.) These results were later compared to the SWF results obtained prior to loading so that a more accurate prediction of the low strength area could be made. It was believed that the 1000 lb. loading might produce damage in the predicted weak spots and enhance the SWF data.

G. Tests to Failure

Step 1: Each specimen was positioned in the Instron constant crosshead rate testing machine grips so that uniaxial tension was applied with no shear forces or bending moments present. A transducer was clamped to the specimen which monitored the acoustical signal. This signal was directed into a preamplifier and then to a high pass filter. After being filtered, the signal was further amplified and sent to an oscilloscope that provided a real-time display. This set-up (as shown in Fig. 3) was used during the monitoring of the acoustic signals emitted during the damage process.

Step 2: The sample was then loaded to 1200 lbs. and zinc iodide (ZnI_2 was generously applied to the samples' edges. The ZnI_2 was allowed 3-4 minutes to penetrate all the cracks that were present. The ZnI_2, which is radiographically opaque, was applied so that any delaminations or cracks would be enhanced on the X-ray radiographs. Edge replicas were then taken and the specimen was unloaded. X-ray radiographs were made.

Step 3: The sample was reloaded to 1250 lbs again following the procedures outlined in step 2.
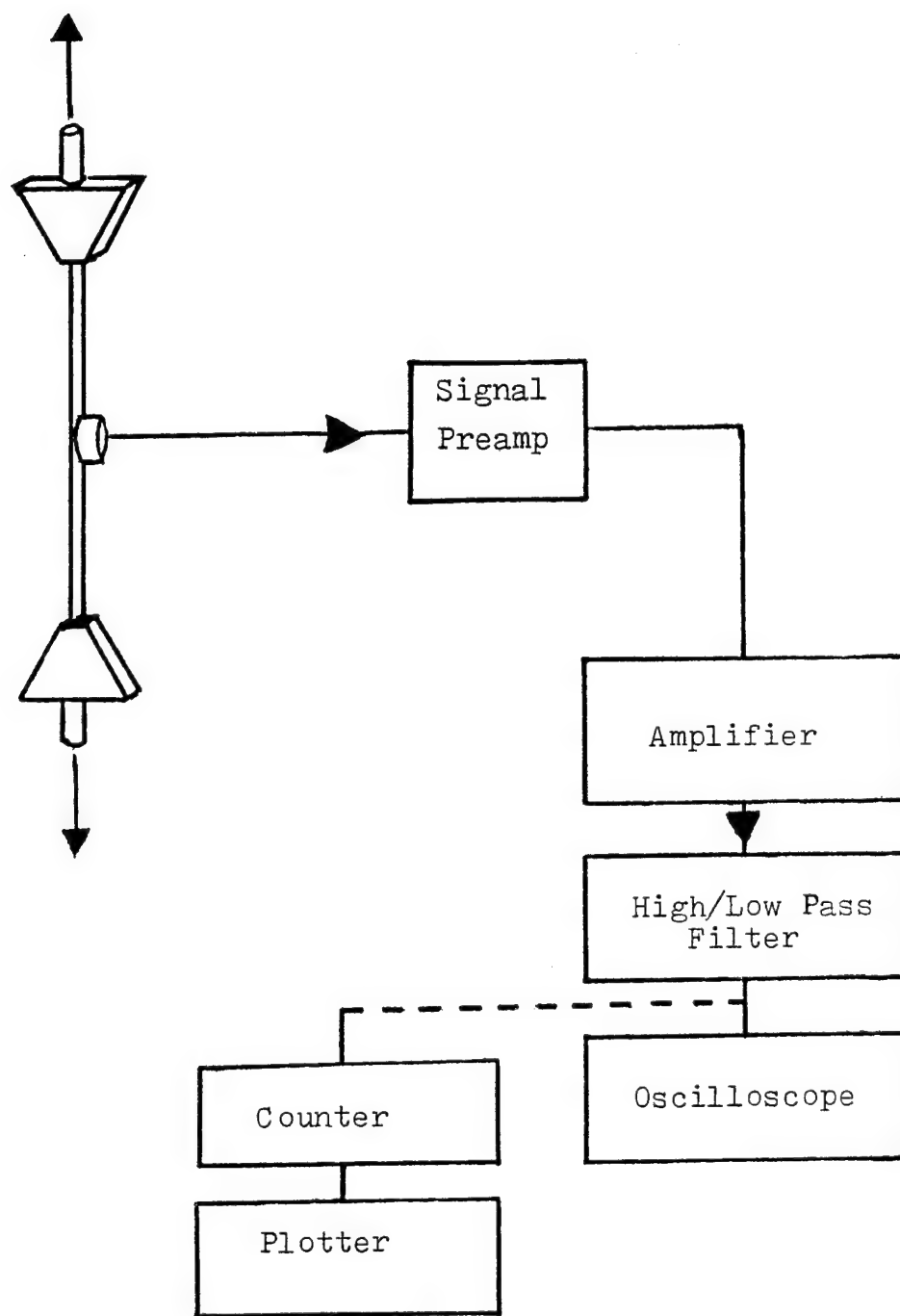
Fig. 3. Schematic of the acoustic emission monitoring set-up for tensile loading.

Step 4: The sample was loaded to 1300 lbs. The procedures explained in step 2 were repeated.

Step 5: The specimen was reloaded and the load increased again in 50 lb. increments while the procedures explained in step 2 were repeated until either the breaking of zero degree fibers was heard, the next increment was reached, or failure occurred. Because of the high stresses incurred at this stage, the specimens were unloaded to approximately 900 lbs. for the application of ZnI_2 and replication procedure. This was done so that further damge would not occur while the load was maintained.

H. X-ray Radiography Technique

X-ray radiographs were taken so that any internal flaws could be detected. A cabinet type X-ray machine was used in this experiment. A tube voltage of 25kV was used with an exposure time of .9 minutes.

IV. Results

Six samples were tested in this study. Three of the specimens broke in or near the testing machine's grips. Knowing that the grips can cause undesired stresses, initial nondestructive examination was not performed on these areas. Therefore these specimens were not given further consideration because of the lack of SWF, X-ray and replica data. The location of failure and four lowest SWF measurements are tabulated below.

Sample Number	Position of Failure (inches)	Position Predicted by SWF Before Failure (inches)				Position Predicted by SWF After Loading (inches)			
		1	2	3	4	1	2	3	4
1	GRIPS	--	--	--	--	--	--	--	--
2	11.25	12.0	12.25	12.5	11.75	8.5	6.5	8.75	12.35
3	4.0	5.75	6.0	5.5	3.0	4.25	4.5	3.75	3.0
4	6.0	0.5	0.25	6.5	6.75	7.25	7.0	.25	1.0
5	GRIPS	--	--	--	--	--	--	--	--
6	GRIPS	--	--	--	--	--	--	--	--

V. Data Analysis

Stress Wave Factor

When examining the data from the stress wave factor tests (Figs. 4,5,6), a number of observations can be made. The first of these deals with the correlation between the predicted site of failure and the actual rupture location. Remembering that the low strength area should, by assumption, correspond to the lowest valued data points, a comparison between the failure site and the obtained data can be made.

Sample 2 broke at position 45 which was located 11.25 inches from the end of the sample. As shown in Fig. 4, the SWF before the 1000 lb. loading predicted an area of low strength at 12.0 inches. If the 4 lowest points are considered, then a more accurate 11.75 inches can be obtained. The SWF fater the specimen had been subjected to the 1000 lb. loading predicted (lowest point) that failure should have occurred at 8.5 inches (Fig. 5). This location corresponds to the lowest point, with 12.25 inches being the fourth lowest and most accurate. This seems
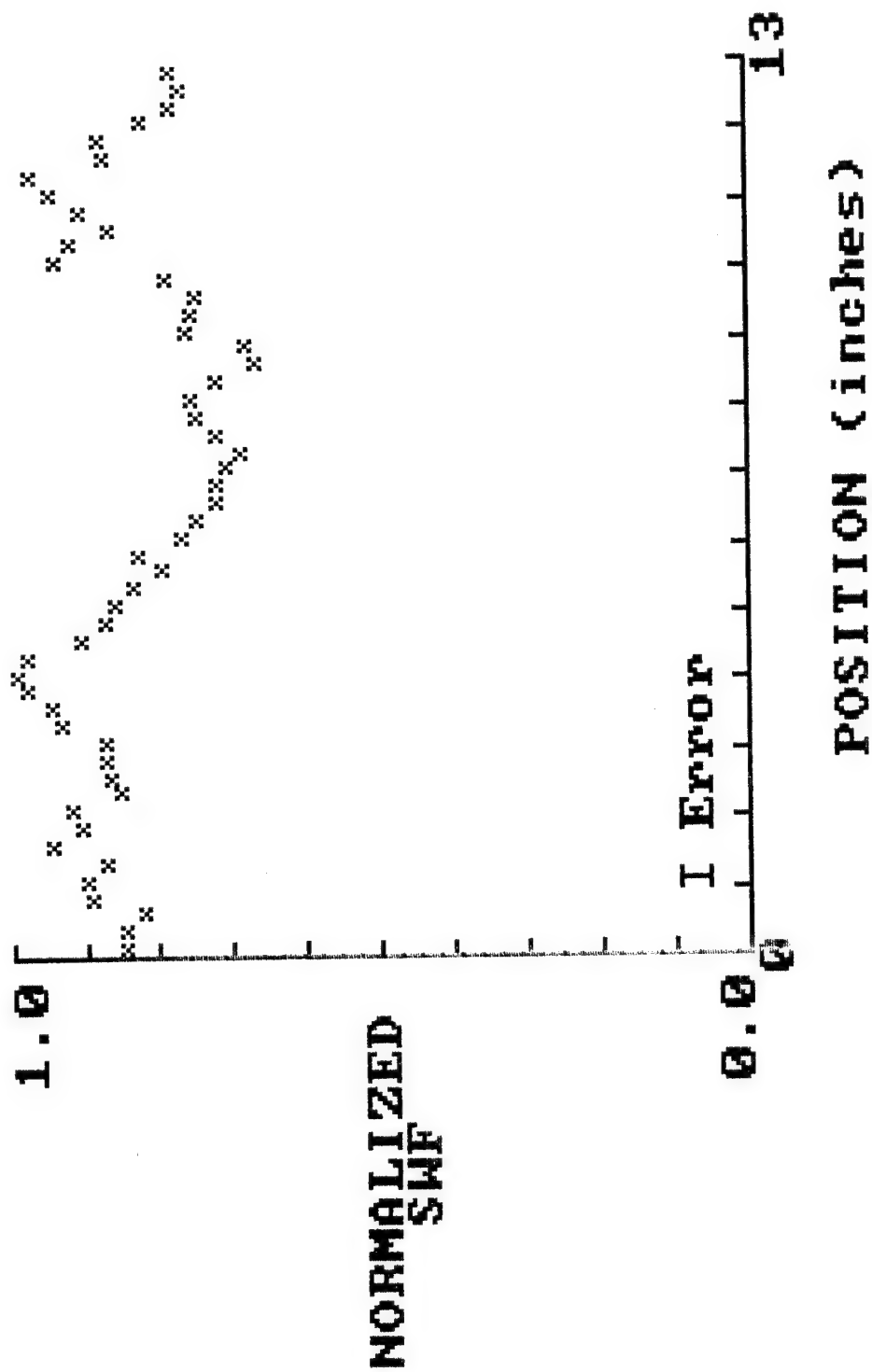
Fig. 4. Normalized SWF versus specimen position for specimen #2 before tensile loading.
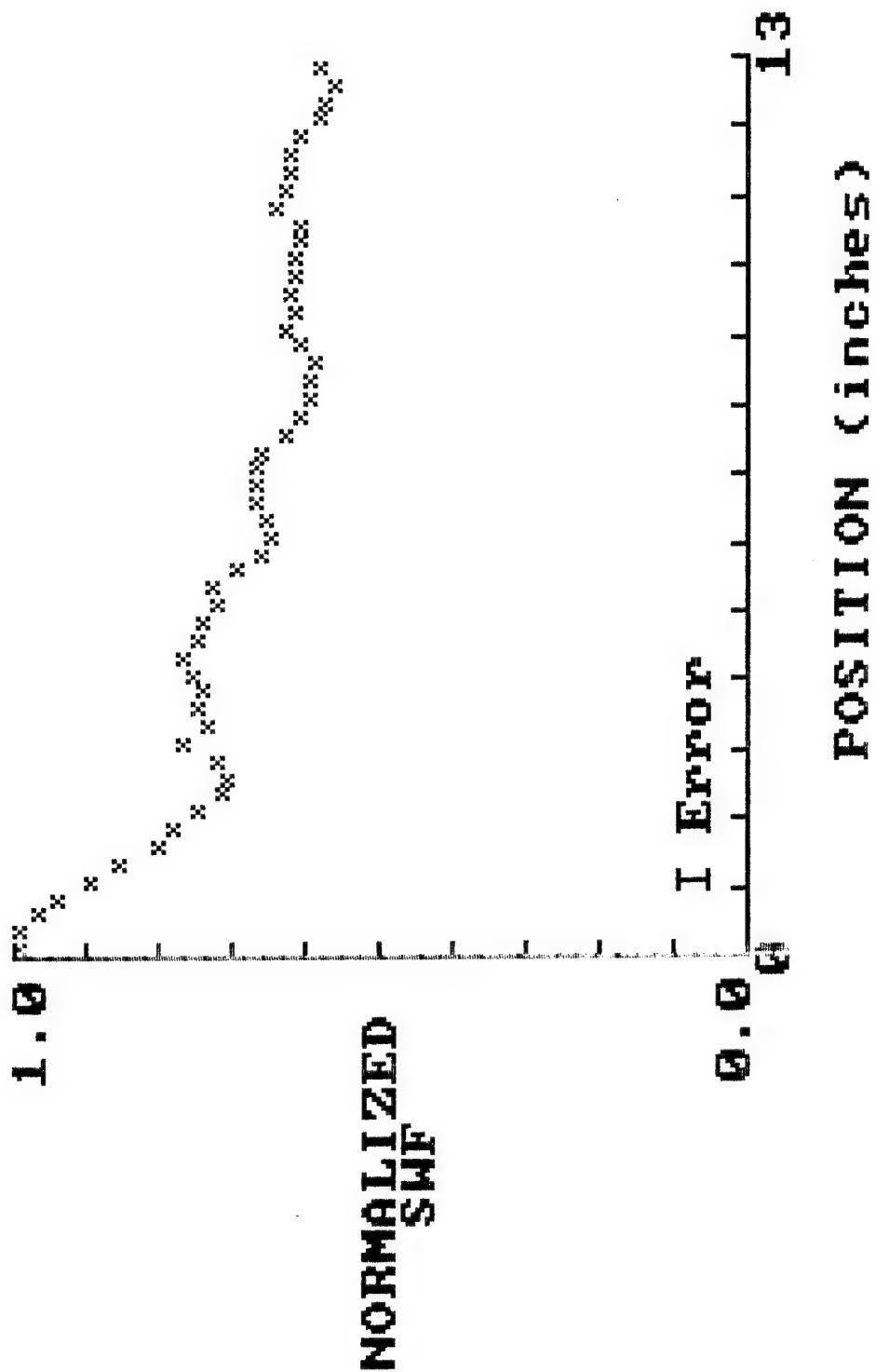
Fig. 5. Normalized SWF versus specimen position for specimen #2 after loading but before failure.

to suggest that failure can occur at low data regions that are not always the lowest in value. This topic will be discussed further, later in this paper.

Examination of sample 3 showed that failure occurred 4 inches from the end of the sample. The stress wave factor analysis before and after the 1000 lb. loading indicated areas of low structural strength at 5.75 and 4.25 inches from the end, respectfully. These again refer to the lowest values obtained from the SWF data. Table 2 illustrates that more accuracy can be obtained if more low points are considered. Plots of the SWF for sample 3 are found at Figs. 6 and 7.

The last sample, 4, failed at exactly 6 inches from the end of the sample. Figure 4 illustrates that the data obtained before the 1000 lb. loading predicted a weak area at 6.5 inches (Fig. 8). The data obtained after the 1000 lb. loading (Fig. 9) indicates a low area at 7.0 inches from the end.

The results above indicate remarkable accuracy if certain limitations are realized. Observations revealed that the procedures used entailed enough experimental error that the lowest value obtained does not necessarily correspond to the position of failure. A more accurate method for analyzing this data would be to look at the relative low spots on a normalized plot and be cautious of these areas. For clarity, consider the chart on the following page.

LOW POINTS	ERROR (inches)	
CONSIDERED	BEFORE LOADING	AFTER LOADING
1	2.67	1.5
2	2.67	1.41
3	.92	1.25
4	.67	.75

Table 2. Averaged Error Values Between Predicted and Actual Failure Positions.

Fig. 6. Normalized SWF versus specimen position for specimen #3 before loading.

Fig. 7. Normalized SWF versus specimen position for specimen #3 after loading.
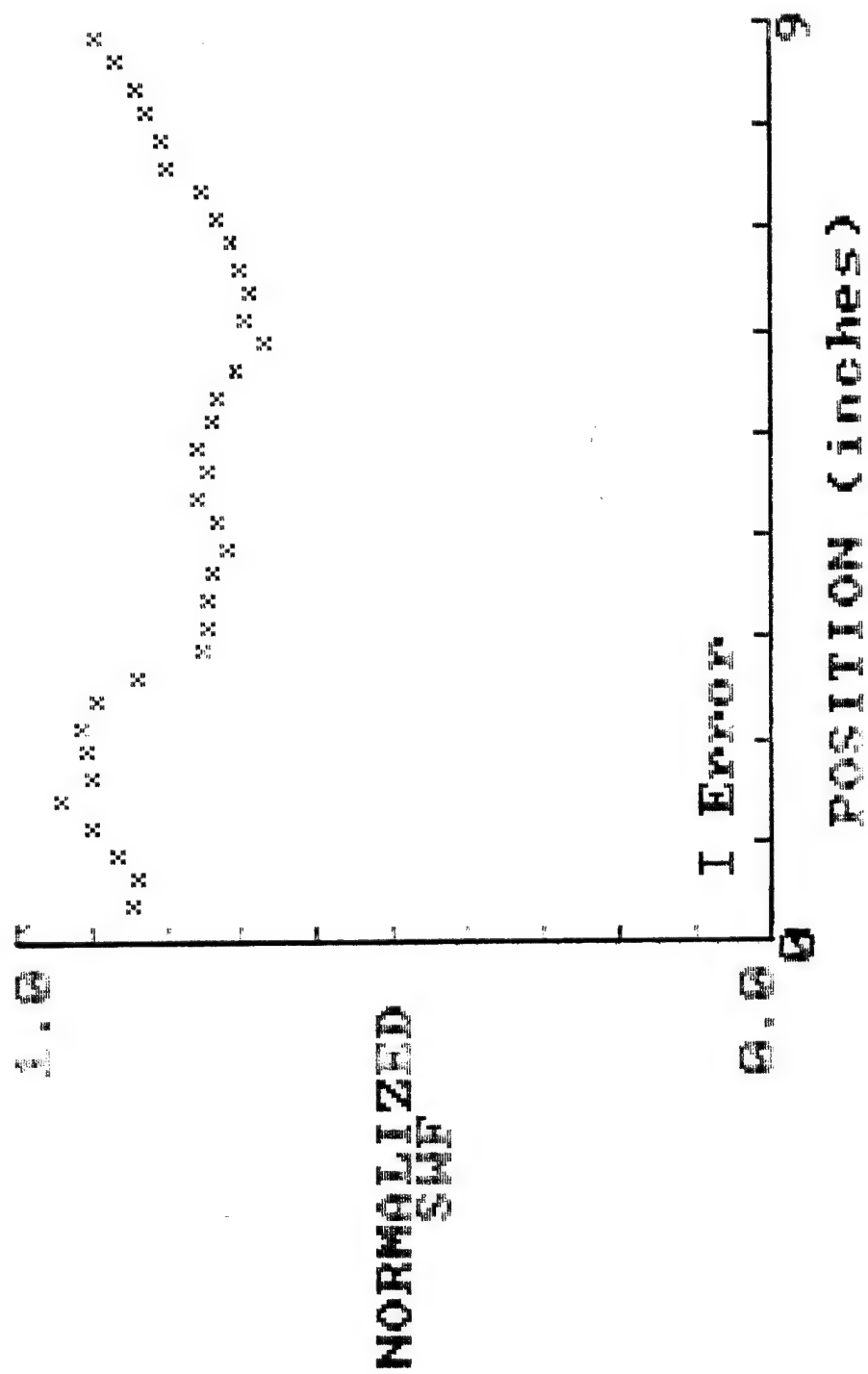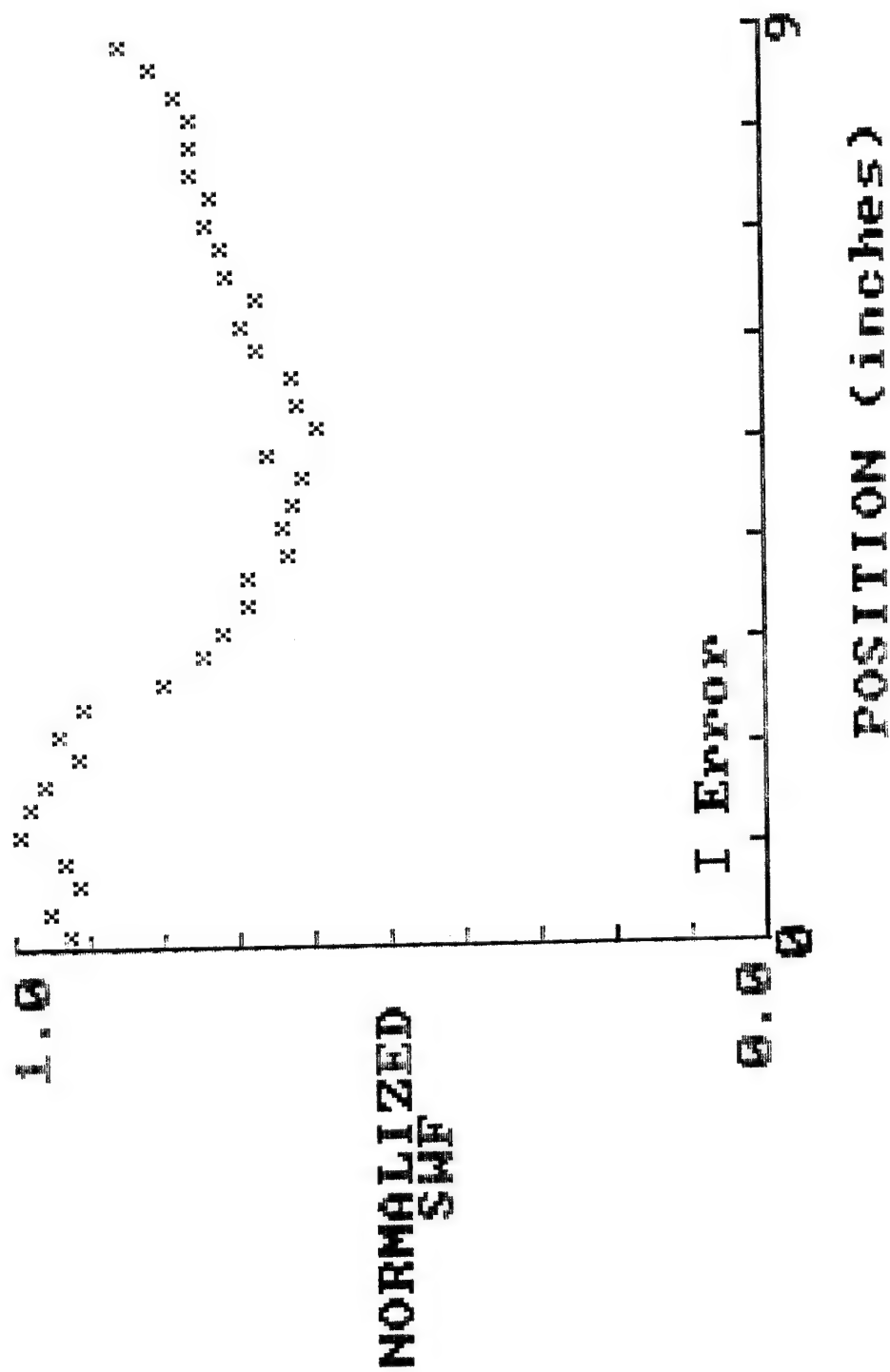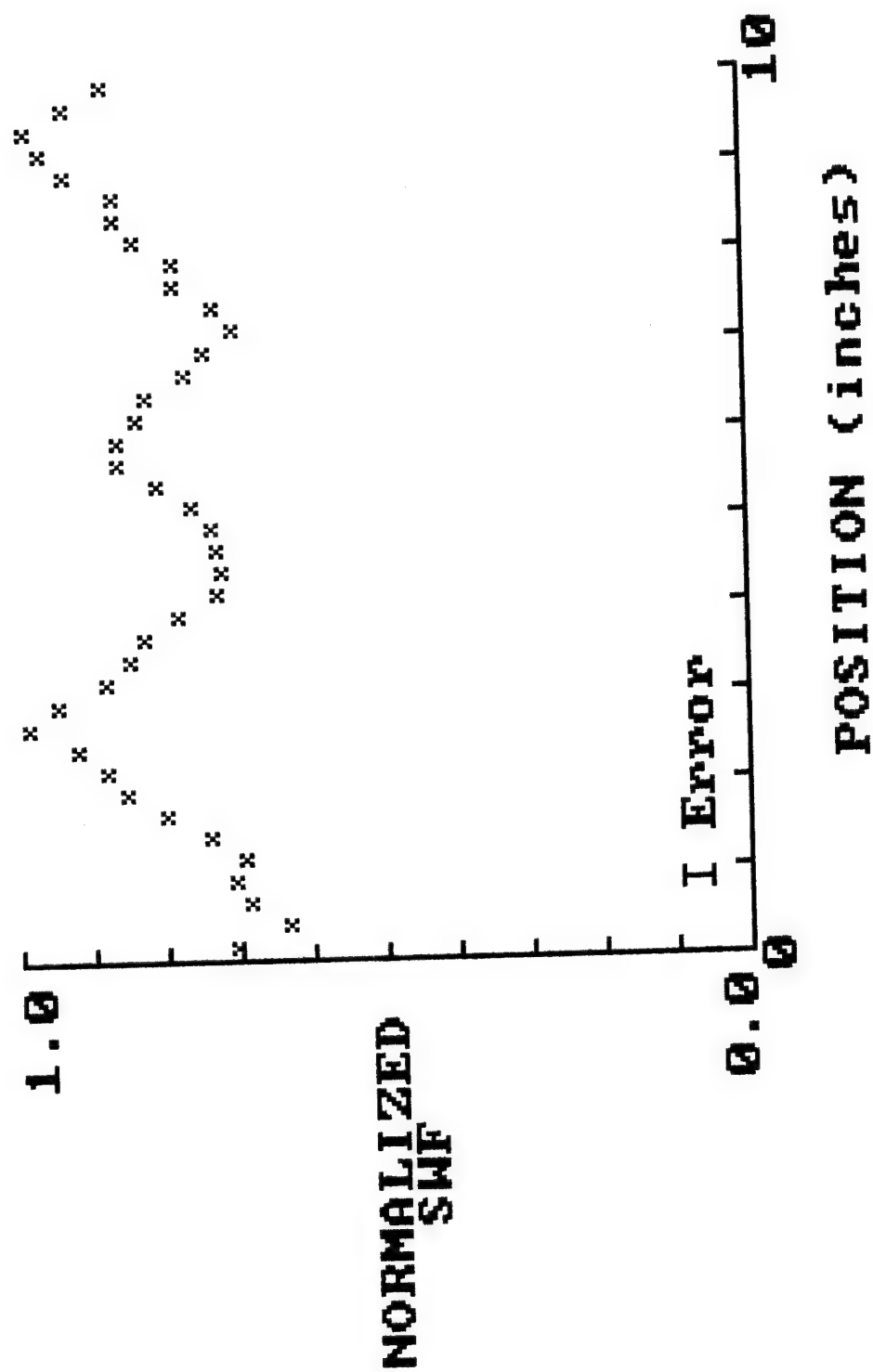
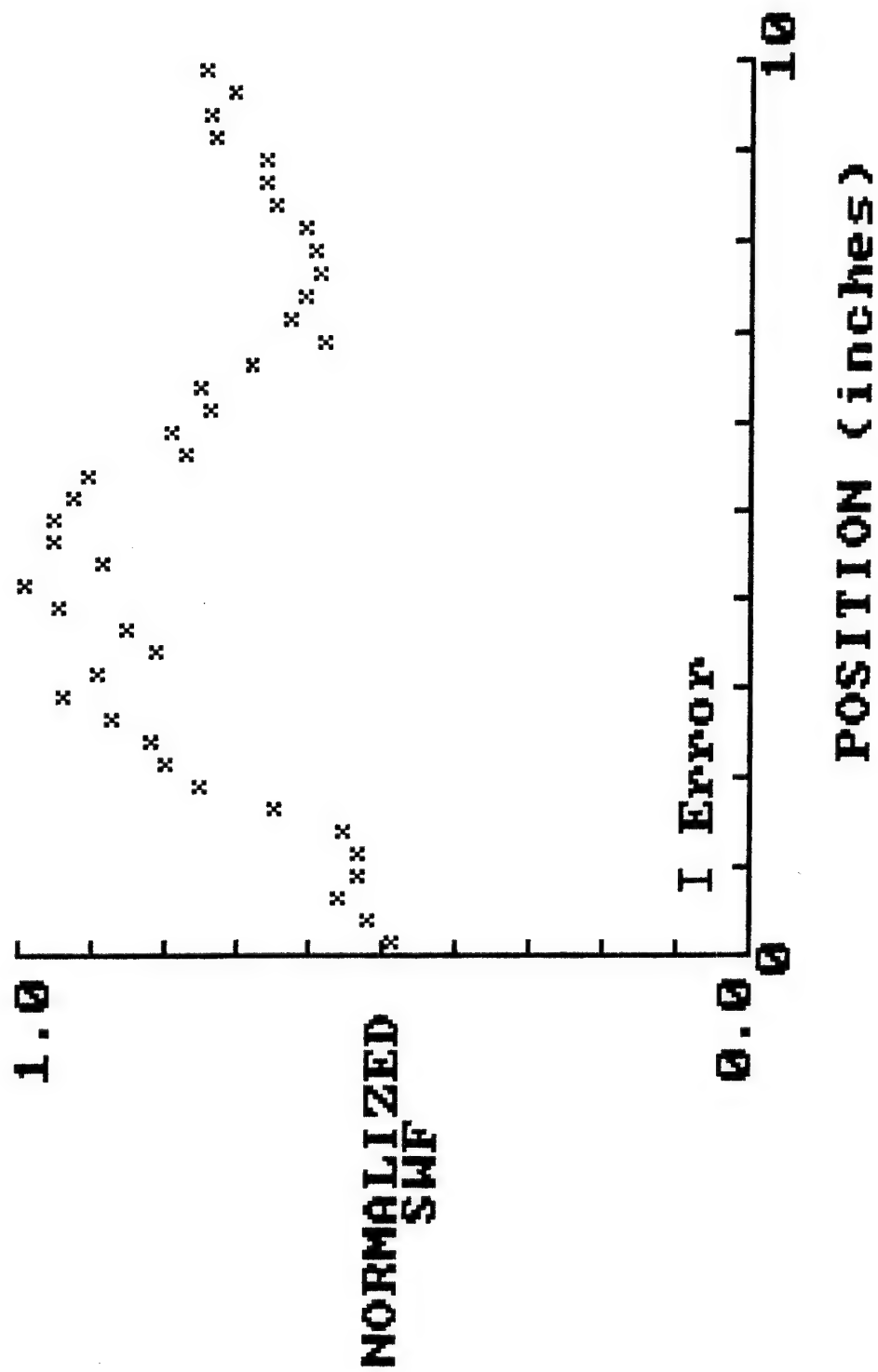Fig. 8. Normalized SWF versus specimen position for specimen #4 before loading.

Fig. 9. Normalized SWF versus specimen position for specimen #4 after loading.

This chart illustrates the averaged distance that the predicted position differed from the actual position of failure if the indicated number of low spots were considered. For instance, if the SWF data obtained after the 1000 lb. loading was used and if the positions of the four points of lowest value were considered, the failure occurred approximately .75 inches from one of these points. As the number of low points considered decreases, so does the location accuracy.

Examining the SWF vs. POSITION plots given in this section, a tendency for low valued data points to bunch up in certain areas is noticed. Therefore if 4 low points are considered, and 3 of those points are located in one general area, then only two areas would have to be concentrated on for failure. The error related to this case would then only correspond to two locations instead of four, making the overall total area of predicted failure less.

Another interesting observation that is found in the previous chart is that the predictions made after the 1000 lb. loading appear better than those taken before the loading if only the lowest two points are considered. As more low points are considered, the two accuracy values become much closer in value. This seems to illustrate that the SWF data obtained before loading had low areas that became even lower relative to their neighbors after loading. In other words, areas which were weak but not the weakest before loading were transformed into the weakest positions during the initiation of damage. Since the first SWF analysis predicted areas of low structural strength, then these areas should be the first to develop damage during the 1000 lb. loading, causing the second SWF to become more pronounced. Figures 10, 11, and 12 are superimposed graphs of the before and after loading SWF plots. These
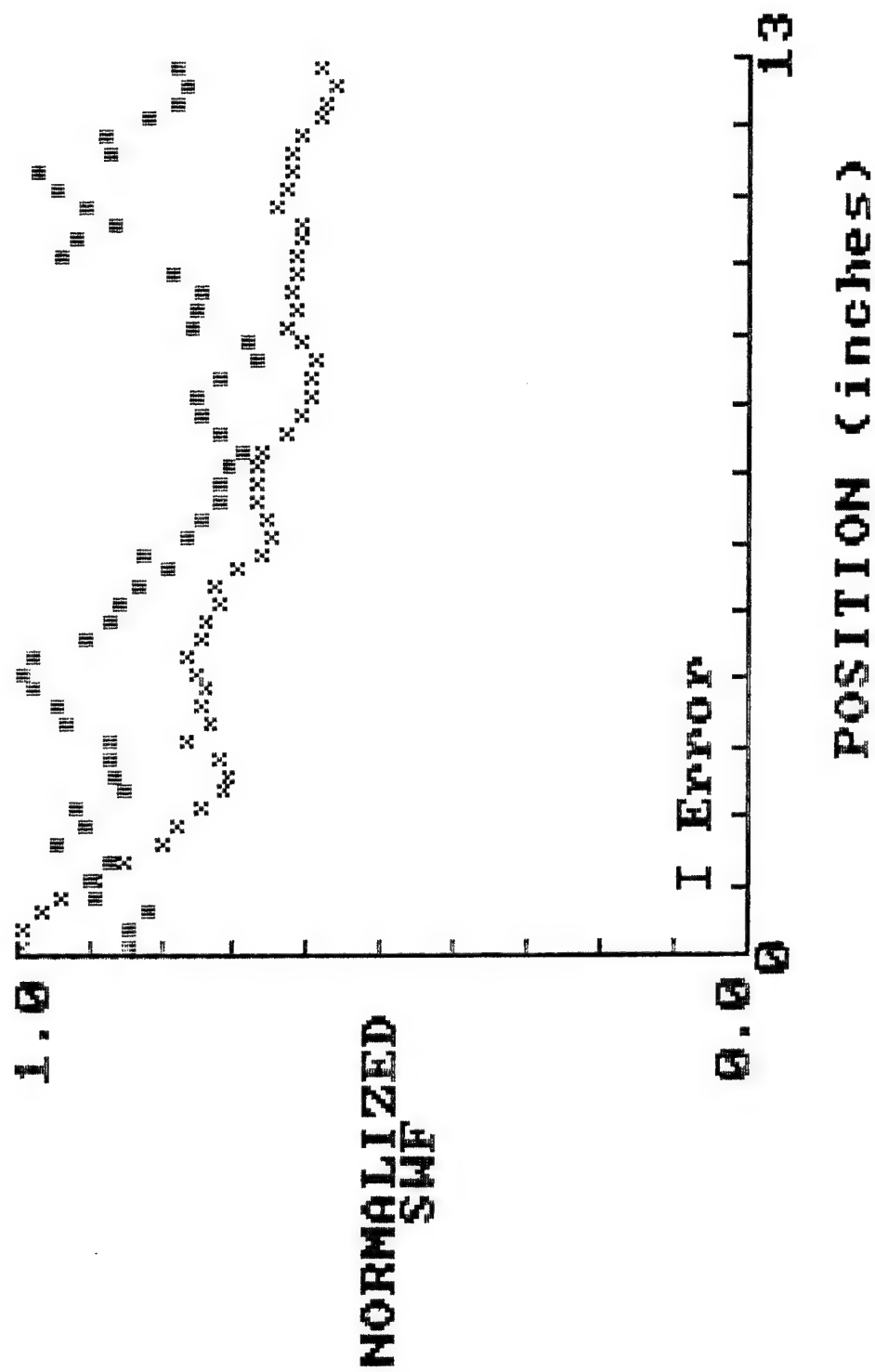
Fig. 10. Combined before and after loading normalized SWF versus specimen position for specimen #2.
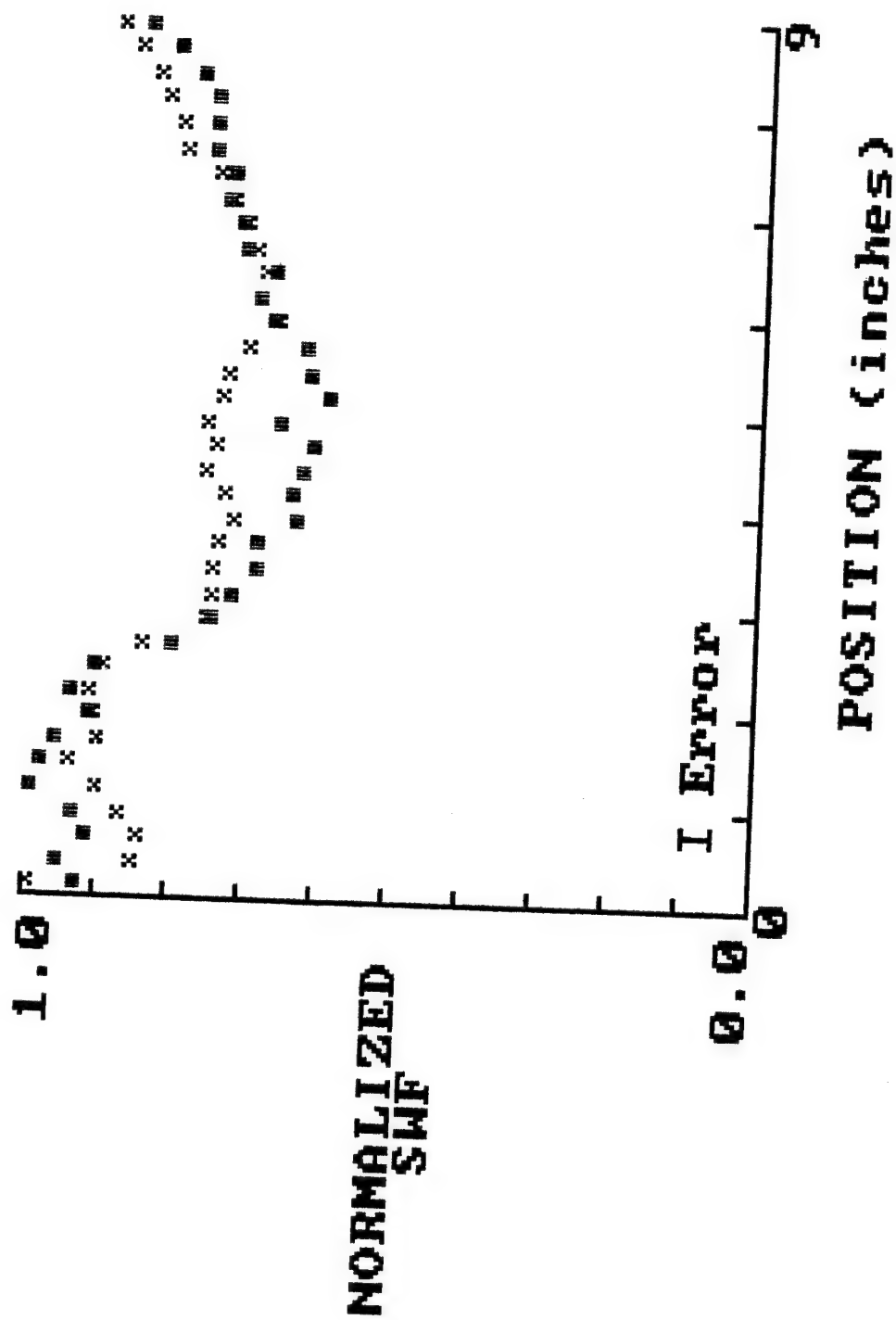
Fig. 11. Combined before and after loading normalized SWF versus specimen position for specimen #3.

Fig. 12. Combined before and after loading normalized SWF versus specimen position for specimen #4.

graphs show that in most cases the low spots remain low or become lower. There are cases where previously low spots become high, but these are not very common. Considering the numerous experimental variables that could affect the outcome (see error section), the b efore and after loading SWF plots are basically similar. The accuracy of the SWF data was estimated to be 5% based upon previous experimental tests.

Edge Replicas

Figures 13, 14, and 15 display prints of replicas taken of the failure areas prior to actual failure. They all show damage that eventually led to the failure.

Sample 2 shows a severe longitudinal crack which reaches the edge of the sample at the location of failure. The crack is believed to have started at the failure area and then propagated down through the sample. This damage appears to be a combination of transverse cracks and delaminations. The crack uses the 90 deg ply to propagate for most of its length, except near the failure area where it breaks through the +45, -45 plies.

Sample 3, Fig. 14, again shows delamination associated with its failure region. The print illustrates a crack that is relatively smooth with no abrupt changes in the direction until the failure area is reached. Here small, transverse cracks are present. These are believed to have grown, eventually passing through the material to the edge, causing failure. As in sample 2, damage is mostly restricted to the 90 deg plies until the failure area is reached, where the +45, -45 plies are damaged.

Failure
location

Failure
location

a)

b)

Fig. 13.   Edge replicas of specimen #2 after loading close to the
failure load. a) 20X b) 40X magnification.

I-54

Fig. 14. Edge replicas of specimen #3 after loading close to the failure load. a) 20X b) 40X magnification.

Sample 4, Fig. 15, indicates more localized type damage. Very little delamination can be found in this sample. Cracks are found to have passed through the 90 deg ply and started into the +45, -45 plies. The damage is found on both sides of the 0 deg ply, which does not occur in the previous two samples.

When comparing all three samples, it is observed that damage does not occur in the 0 deg ply. Therefore it can be said that the outer plies play a major role in the failure process. Failure of the outer plies causes an increase in the amount of stress applied to the 0 deg plies in a particular area. This increased stress leads to a failure at this area. Another question to be raised deals with the sequence of events during the failure process. In studying the replicas, one must conclude that the damage starts in the 45 deg plies and works its way to the surface by means of delamination and transverse cracking.

X-ray Radiographs

The radiographs shown in Fig. 16 are of sample 2 and confirm the delamination shown by the replicas. The radiographs are for increasing load increments.

The first radiograph (low load) indicates a higher density of 90 deg matrix splits at or near the failure area. Although the entire sample is not shown here, the damage shown is by far the most visible. This initial damage must play a role in the development of damage located on the opposite side of the sample, as shown in the next radiograph (medium load). This radiograph indicates a delamination which starts at the edge plus a large number of 90 deg matrix cracks. These cracks are observed throughout the material and not just at the

Fig. 15. Edge replicas of specimen #4 after loading close to the
          failure load. a) 20X b) 40X magnification.

I-57

a)

b)

c)

Fig. 16.   Penetrant enhanced X-ray radiographs at an a)low b) medium
c) high level of tensile load.

eventual rupture location. The initial damage located on the opposite side of the sample had not changed very much at this point. The last radiograph shows how the area of delamination grew even more with increased load (approximately 1.5 times as big). This radiogjraph was taken very close to actual failure and corresponds to the edge replica for this sample.

VI. Error Analysis

The purpose of this section is to briefly examine the methods of research and to reach a determination of the accuracy and reliability of the resulting data.

Stress wave factor methods took many hours of trial and error sample runs to develop. The procedure which was developed was strictly followed with regard to variables such as transducer positioning, couplant application, instrument setting variations, transducer weights, surface preparation, etc., being carefully controlled. For example, every event in the testing procedure that could be time dependent was carefully timed. A special testing platform was designed to control transducer positioning. To control couplant film variations, practice runs were performed until a smooth consistent film could be applied. To assure adequate preamplifier battery power throughout the testing period for each sample (approximately 2 hrs.), the preamplifier was turned on only 20 seconds for each measurement. Of this 20 seconds, the first 10 provided time for any transient effects to dissipate and the last 10 seconds were used for testing. To control unclean surface problems the transducers and sample surface were cleaned after every measurement. To assure good transducer to sample contact, special weights were used.

Other controls, such as using the same transducers to transmit and receive each time, insured reasonably reproducible results. The error in this process was estimated to be approximately 5% and markings indicating this have been placed on all graphs in this report.

The accuracy of the edge replicas should be high. Errors dealing with the replicas come basically with their examination. One must not mistake dirt, dust, fingerprints, etc., for flaws in the material. Good replicas are a product of practice and patience from which comes accurate prints.

The X-ray radiographs can sometimes be misleading, so caution should be taken when examining them. Zinc iodide was used in the radiographic procedures so that internal flaws would appear on the film. It was applied while the samples were under load so that it could seep into small cracks. The problem here is that the zinc iodide does not penetrate completely into the material. Because of this the center of the sample may appear undamaged; this seems to be the case in this project. No damage appears to have occurred in the center of the samples on the radiographs. Whether or not this is so cannot be determined with the techniques used here. Therefore all conclusions drawn from the radiographs are most appropriate for the outer edges and not for the center of the sample.

The next question that must be raised deals with the reliability of data and resulting conclusions. Since only three samples were considered for analysis, a reliability problem exists. With such a small sample number, the overall reliability cannot be determined. Although the results from the project may possibly be accurate, their reliability cannot be determined without further testing. Three tested

samples do not lay a foundation for a sufficient statistical basis. Because of this fact, the confidence level of these results is low. Therefore the conclusions from this experiment should not be used for the basis of any engineering decisions, but rather be used to motivate further investigation.

VII. Conclusion

It can be concluded from the results produced by this experiment that there are damage characteristics that are directly related to areas of failure in a graphite epoxy composite laminate under uniaxial tension. The edge replication and X-ray radiographic techniques were good detectors of damage after it had been established in the material. The material used in this experiment showed delamination and transverse matrix cracks that started and grew in the failure area. In the samples tested, these distinguishing features seemed to be good characteristics of the failure area since their severity increased in these areas. Edge replication and X-ray radiography were very useful in locating a failure location after gross amounts of structural damage had already been initiated. Visual techniques require an extensive amount of damage just to be detected. What is to be done if the damage is not visual and a failure area is to be established? To answer this question the SWF results must be interpreted.

The results from the stress wave factor analysis point to the fact that damage can be detected. The results showed that predictions of locations of low strength areas in a material can be made with an accuracy of less than ±3/4 inch within the limitations discussed in the results section of this paper. Since structural damage in a material

affects its strength, and low SWF values seem to be related to low strength areas, structural damage should be related to low SWF values. Based upon this reasoning, one can say that low SWF values are a damage characteristic. It should also be pointed out that imperfections such as those encountered during the production process of the material can also cause low SWF values. Because of this, a low SWF values does not necessarily mean that damage is present.

Another interesting conclusion appeared while examining the results. Because of the fact that visual damage was observed in the same general location of low SWF values and this damage was the first significant damage to appear on the replicas and radiographs, it can be said that initial damage is a local event. In other words, the damage does not initiate as a global event, occurring everywhere on the sample and then localizing immediately before failure occurs. This experiment suggests that initial damage is a local event and although damage occurs throughout the sample during further loadings, the failure will occur at this localized area.

References

1. ASM Handbook Committee, Nondestructive Metals Handbook 10, 8th edition (1975).

2. Vary, A. and Bowles, K. J., "Use of an Ultrasonic Acoustic Technique for Nondestructive Evaluation of Fiber Composite Strength," NASA TM-73813, 1978.

3. Vary, A. and Lark, R. F., "Correlations of Fiber Composite Tensile Strength with the Ultrasonic Stress Wave Factor," NASA TM-78846, 1978.

Appendix

Instrument Specifications

A. Stress Wave Factor Set-Up:

    Transducers

        Panametric Inc.
        Width 11/16 in.
        Freq. approx. 5 MHz
        Serial no. 43026
                  43022

    Preamp

        Panametrics Ultrasonic Preamp
        40-60 db.

    Pulser & Gate

        Panametrics Model 5052ua
        Ultrasonic Analyzer

    Counter

        Hewlett Packard 5326 Timer-
           Counter-DVM

B. Instrument Settings for SWF:

    Panametrics Ultrasonic Analyzer

Rep. Rate	200
Damping	200
Energy	2
Attenuation	6 db.

Sample Specifications

Width	8/16 in.
Length	12-16 in.
Thickness	.041 in.

The Use of an Improved Transducer

For the Study of Wave Propagation in

Composite Plates

Thomas S. Lubnow, Jr.

Abstract

The performance of the Proctor Conical Transducer developed at the
National Bureau of Standards as applied to composite materials has been
evaluated and deemed satisfactory with the exception of the method of
electrical grounding employed. Incorporation of the conical transducer
into the Stress Wave Factor scheme yielded evidence of the possible
plate wave mode of propagation in thin composite plates.

I. Introduction

Fiber-reinforced composite materials are gaining widespread use in industrial and military settings. Unfortunately, the development in understanding of mechanical behavior and of failure theories has not kept pace with the rapid increase in applications. This is in part because delaminations, voids, matrix cracks, and broken fibers contribute to a very complex damage state in composites. An increased dependence on nondestructive testing and the development of new NDT techniques is a result of the need to better understand the performance of these materials. One such technique is termed acousto-ultrasonic testing or acousto-ultrasonics (AU).

A relatively recent development in the field of nondestructive evaluation of materials, acousto-ultrasonics combines the advantageous aspects of acoustic emission and ultrasonic testing techniques. With this technique, the acoustic pulse is generated outside the specimen, sent through the material, and received by another transducer a short distance away (Fig. 1). The received signal may be analyzed in both the frequency and time domains. In theory, the extent and nature of damage in the region of material between the sending and receiving trnsducers can be determined. Vary [1] has developed a counting scheme to perform this analysis in the time domain while more recent techniques have attempted to correlate various moments of frequency spectrum of the received signal with stiffness and strength [1,11,15]. Vary and subsequently other investigators have termed this quantitative parameter the Stress Wave Factor (SWF). A major limitation of the current technique is that this parameter changes dramatically with changes in
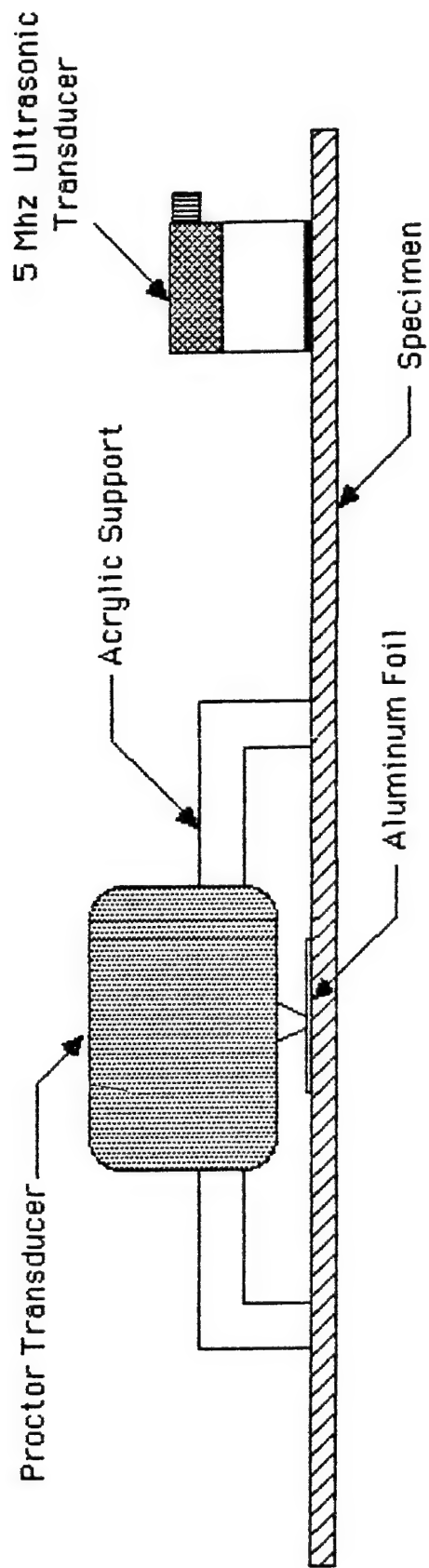
Fig. 1 a. Schematic of the Stress Wave Factor Measurement Procedure
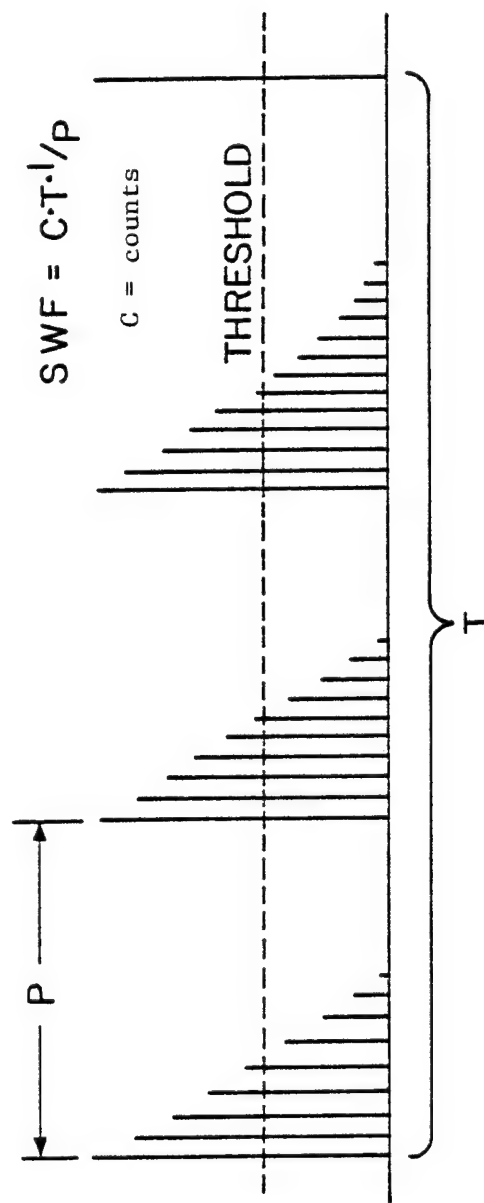
$$SWF = C \cdot T^{-1}/P$$

C = counts

Fig. 1 b. Procedure for calculating the SWF measure.

such experimental variables as the receiving and sending transducer specifications, the couplant used, gating, sample interval and threshold voltage. Thus, the SWF, as it exists now, yields only information on the relative strength, stiffness, and damage between different specimens tested with the same parameters. A current research interest is to improve this scheme so that it will yield a meaningful quantitative value independent of the previously mentioned conditions. Separating the signal modifications caused by the material from those resulting from the interfaces and the electronics is an important step in this process [4,8], Fig. 2. After this material transfer function is isolated, a greater understanding of wave propagation in composites will be made possible and the transfer function may then be related to the precise state of damage in the material.

Of primary importance in understanding the manner in which ultrasonic waves interact with the material is the determination of the type of wave that is propagating. An extensive literature review yielded no information on the nature of wave propagation in composite plates. Literature on wave propagation of anisotropic materials focuses on such factors as grain size and orientation which have little direct relevance to propagation in fiber-reinforced composite material. Fortunately, there is an abundance of literature on wave propagation in isotropic materials, some of which is relevant to composites.

The two predominant wave types involved with ultrasonic analysis are Rayleigh and Lamb waves. These waves vary in the way in which they propagate and in the way they intereact with the material [6,7], Fig. 3.

Rayleigh waves are elastic waves which propagate near the free surface of a solid and decay rapidly with depth. Because Rayleigh waves

Input

↓

INTERFACE TRANSFER FUNCTION

↓

MATERIAL TRANSFER FUNCTION

↓

INTERFACE TRANSFER FUNCTION

↓

RECEIVING TRANSDUCER TRANSFER FUNCTION

↓

SIGNAL CONDITIONING TRANSFER FUNCTION
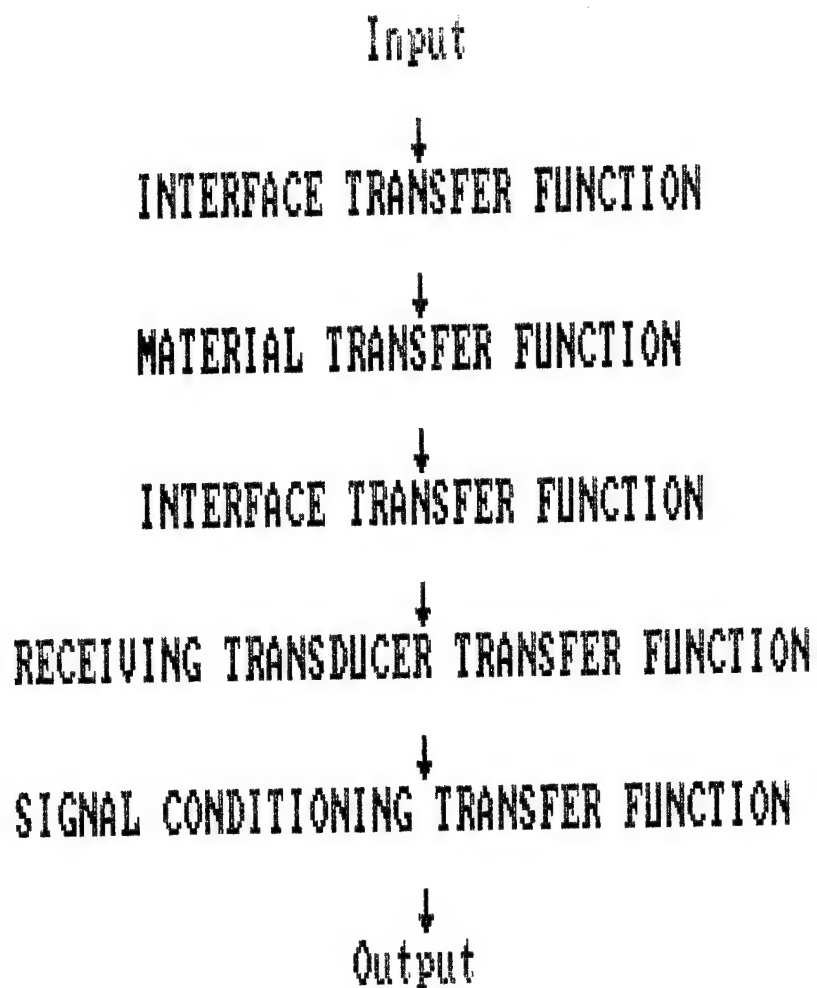
↓

Output

Fig. 2 Progressive altering of input prior to final output.
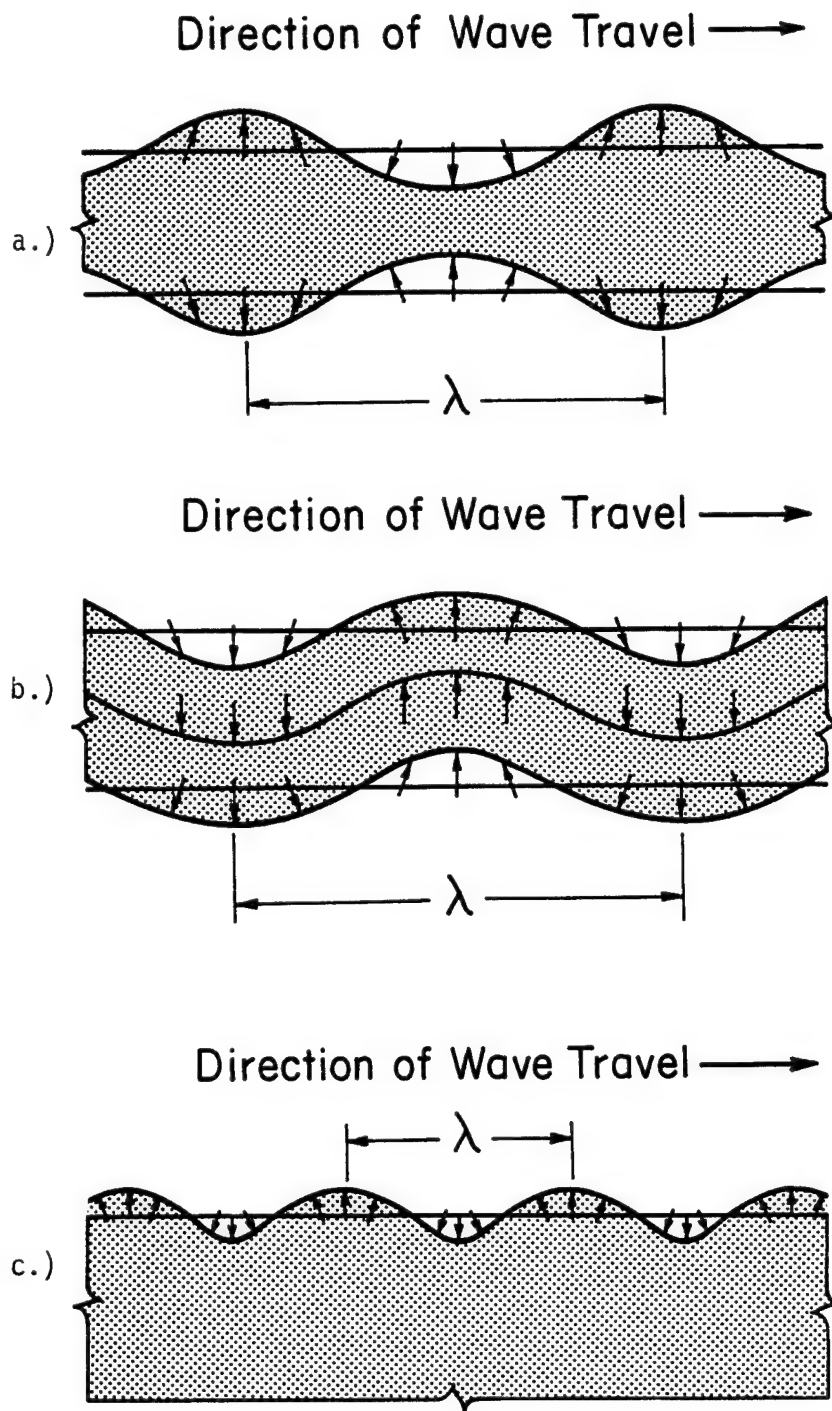
Fig. 3 a.) Symmetric Lamb wave motion, b.) Assymmetric Lamb
wave motion, c.) Surface wave motion

spread in only two dimensions, they fall off more slowly with distance than do other three-dimensional wave types. This geometric decay is much less than that caused by scattering. Rayleigh waves interact very strongly with surface defects which causes significant attenuation. Absorption is analogous to that seen in longitudinal and transverse waves because the Rayleigh wave is a combination of these two wave types. Rayleigh waves do not exhibit phase velocity dispersion.

Lamb (or plate) waves propagate in a plate with free boundaries. Displacements occur both in the direction of wave propagation and perpendicular to the plane of the plate. Lamb waves exhibit dispersion and tend to interact more uniformly through the volume of the material. These waves tend to occur if the wavelength is greater than or equal to the thickness of the plate. They have, in general, both symmetric and antisymmetric components. These two modes propagate independently of one another.

The purpose of this investigation is to use an improved transducer developed at the National Bureau of Standards in the study of wave propagation in composite materials and thus improve the state of the art in acousto-ultrasonic testing. It is also hoped that the use of this transducer will yield some insight as to the wave type being propagated in this technique.

In the past, most AU work has been done using conventional piezoelectric pulse/echo transducers. These transducers have been designed for both reception and transmission of ultrasonic signals. In pulse/echo techniques the signal is travelling parallel to the transducer axis and the transducer is designed with this in mind. However, propagation in AU techniques is generally perpendicular to the

axis, presenting far different demands on the transducer. Most of the pulse/echo transducers have a narrow bandwidth, making them relatively insensitive to part of the wide spectrum of frequencies in AU analysis. In order to further develop AU techniques, these limitations must be overcome through the use of an improved transducer.

For AU applications, a transducer must have a flat frequency response over a wide frequency range. It must produce electrical signals that are accurate depictions of one independent physical quantity, such as normal surface displacement, while showing negligible response to other parameters such as velocity, acceleration, and tangential displacement [8]. Finally, the ideal transducer would have a very small aperture, thus limiting the effect of surface integration and the interference effects associated with signal direction. One such transducer recently developed by Proctor at the National Bureau of Standards is the NBS Conical Transducer.

The NBS Transducer [9] is a piezoelectric transducer consisting of only two pieces, a truncated cone-shaped piece of lead-zirconate-titanate, which is the active element, and a brass cylinder backing. The 1.5 mm diameter of the truncated cone surface is quite small in relation to wavelengths of the signals of interest and in relation to the 13 mm diameter transducers most often used previously. This small contact area size makes the transducer a close approximation to a point receiver. The backing of the transducer serves as the non-grounded electrode for signal detection. Figure 4 illustrates the geometry and structure of the transducer.

Glass capillary break tests have documented the NBS transducer's ability to electronically depict surface displacements accurately. A

Fig 4   Schematic diagram of the NBS conical transducer.
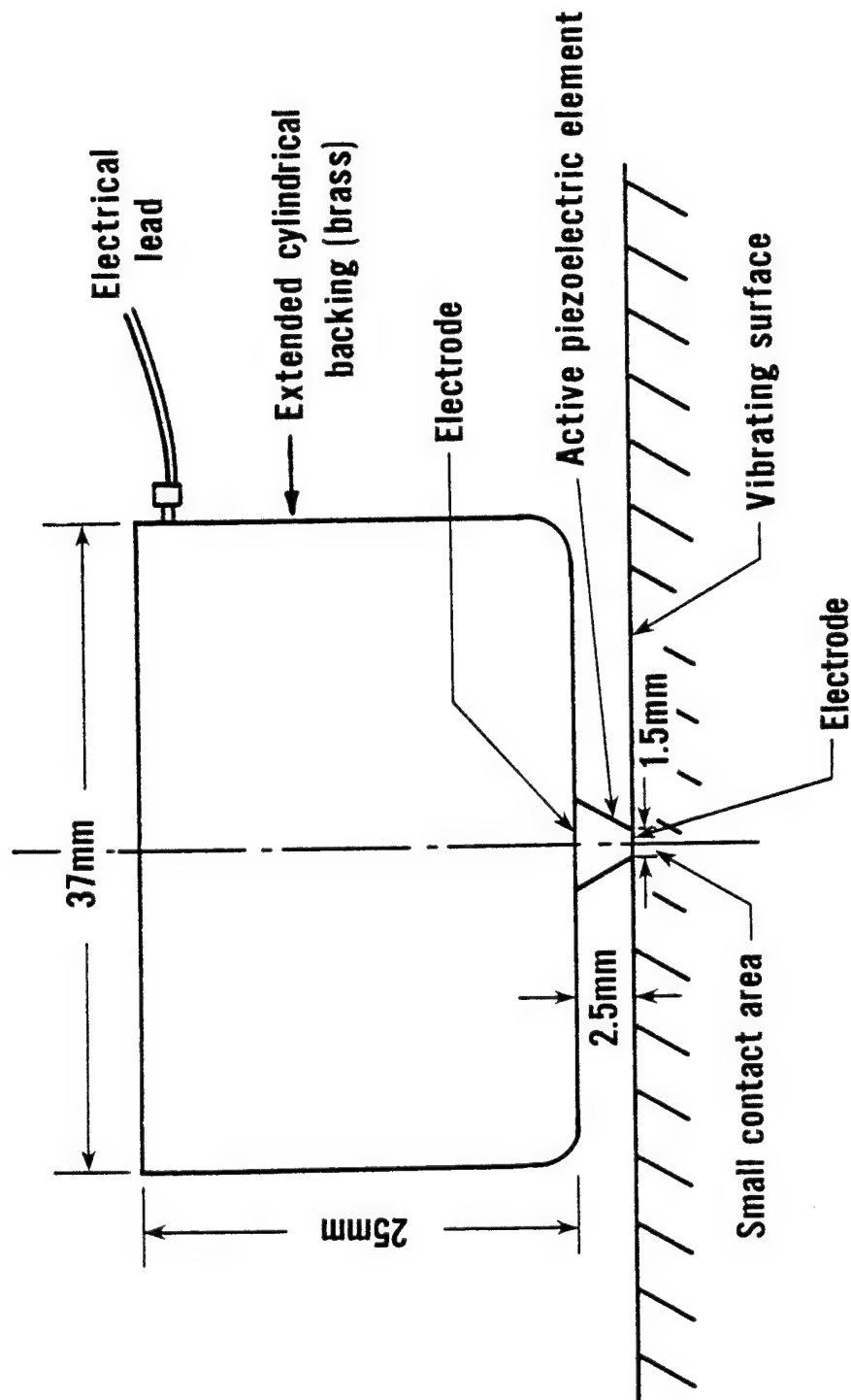(after Proctor)

The labels in the figure read:

Electrical lead

Extended cylindrical backing (brass)

Electrode

Active piezoelectric element

Vibrating surface

Electrode

37mm

25mm

2.5mm

1.5mm

Small contact area

step function input is applied to a large thick steel specimen by breaking a glass capillary on the surface, Fig. 5. In Figs. 6 and 7, the electrical signal received a short distance away by the NBS Transducer is compared to the theoretical surface displacement. As shown, the NBS Transducer signal is almost exactly as predicted by theory [10].

II. Experimental Procedure

The design of the conical transducer is such that the tip of the transducer must be grounded. This creates some problem with use on composite specimens due to the relatively poor conductive epoxy resin on which the transducer is to rest. This was thought to be remedied through the application of a thin coat of conductive epoxy paint (Bipox Traduct). This paint was applied to the region of the 0.5" wide, 6" long graphite epoxy test specimen to be contacted by the transducer and an electrical lead was attached. The voltage drop across the region was checked and found to be minimal. The transducer was then placed on the specimen. The ground wire was attached to the shielding which was in turn wired to an aluminum base plate upon which the specimen rested.

Electrical noise was the dominant feature of the output signal. It was thought that possibly the reason for the poor response of the transducer was lack of out of plane surface displacements in the wave type being propagated in the material. It has been reported by Henneke and Stiffler that acoustic emission signals in composites are primarily in-plane in nature. Thus, if AU signals propagate in the same manner as acoustic emission signals generated inside the specimen, poor response would be expected. Support for this argument was generated when a PVDF

BREAKING GLASS CAPILLARY EVENT

N.B.S. STANDARD
CAPACITANCE TRANSDUCER

STEEL BLOCK

NBS CONICAL TRANSDUCER AT
THE EPICENTER POSITION FOR
THROUGH PULSE CALIBRATION

10cm

90cm

43cm

NBS CONICAL TRANSDUCER AT
SYMMETRICAL POSITION FOR
SURFACE PULSE CALIBRATION

Fig 5 Schematic of the surface-pulse and through-pulse
(epicenter) experimental arrangements. (after Proctor)

I-74

Fig 6   Actual voltage/time response of the NBS capacitance
standard transducer as measured for a step force event produced
by a breaking glass capillary on a large steel block. (after Proctor)

Fig 7 The seismic surface pulse according to Pekeris Abscissa, time in microseconds. Ordinate, normal surface displacement in picometers. Input, point-force-step-function. (after Proctor)

transducer (sensitive primarily to in-plane displacements) was attached to the specimen and a strong signal was generated. However, when the sending transducer was placed on the underside of the specimen and a situation was created in which out of plane displacements were without a doubt present, no signal could be received by the NBS transducer. Other reasons for this problem were then sought out.
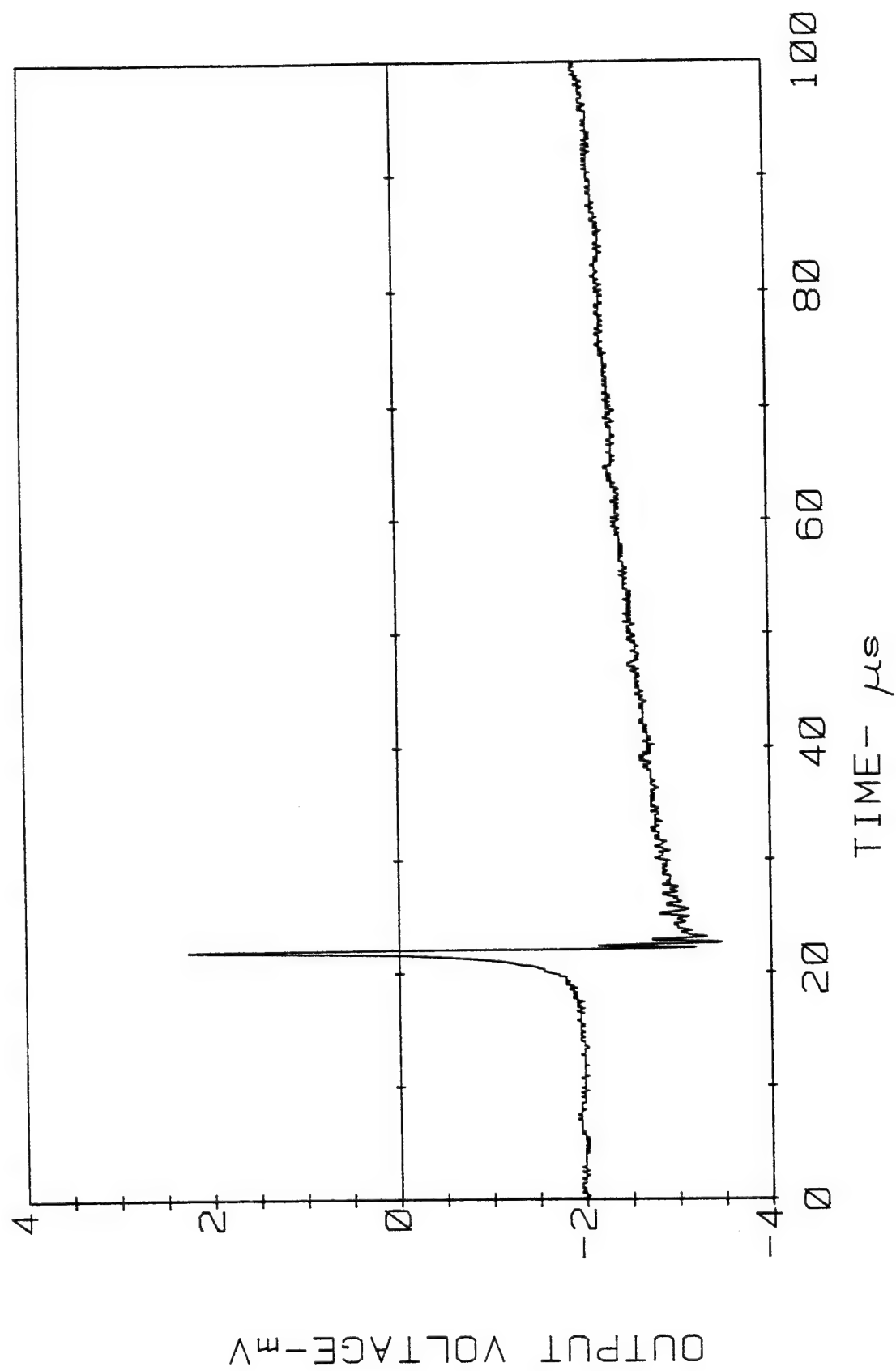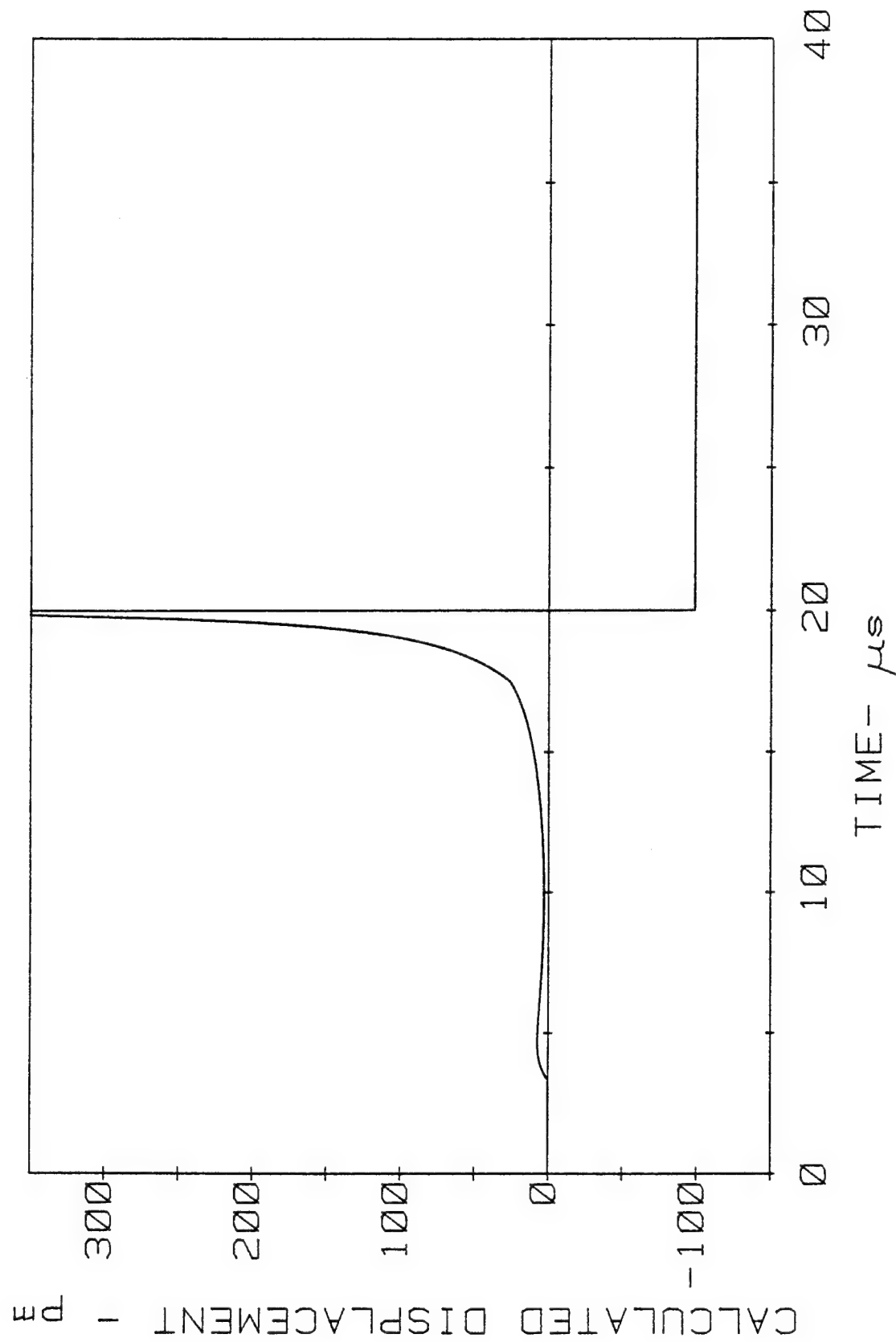
Electrical noise continued to be the only feature of the output when inputs were from lead break tests, from glass capillary break tests, and from transducers ranging from 5 to 15 mHz. Couplants with a wide range of viscosity were also used. Additional amplification was attempted as were alternate triggering schemes. The transducer was then rested on an aluminum plate and a strong clear signal was received with all of the above mentioned inputs. Thus, although at first it appeared to be an adequate method of grounding, the unpredictable electrical properties of the graphite epoxy composite prohibited it from being grounded with the conductive paint.

Because the grounding on the aluminum plate seemed to be adequate, the conductive epoxy was abandoned in favor of a thin piece of aluminum foil. The foil was bonded to the composite specimen with a thin layer of Panametrics couplant. The other end of the aluminum foil was attached to the transducer shield. It was hoped that the foil would be thin enough so as to not affect the signal, yet thick enough to allow adequate grounding. A strong and relatively noise free signal resulted from all of the signal input methods.

It was decided that in order to minimize reflections and edge effects and better isolate the AU signal of interest, a wide graphite epoxy plate should be used for the remainder of the investigation. A unidirectional 25-ply, .125" thick, 12" square plate was used. A grid

I-77

```fortran
      IMPLICIT REAL*8 (A-H,O-Z)
      INTEGER N,IWK(14),IA(16384)
      REAL*8 AI(8193),WK(1),AMP(8193)
      REAL*8 PHASE(8193)
      REAL*8 TIME(8193),FREQ(8193)
  900 FORMAT(A16)
      COMPLEX*16 X(8193),CDABS
      READ(10,900)GARBAGE
      DATA PI,N/3.141592654,2048/
      SMPINT=0.1
      TTOT=SMPINT*16384.
      NCOUNT=0
      READ(10,1000)(IA(I),I=1,N)
      DO 5 MM=2049,16384
    5 IA(MM)=0
      AIMAX=0.
      TMXAMP=0.
      N=16384
      DO 10 K=1,N
      AI(K)=IA(K)
      IF(AI(K).GT.127.)AI(K)=AI(K)-256.
      IF(DABS(AI(K)).GT.AIMAX)AIMAX=DABS(AI(K))
   10 CONTINUE
      CALL FFTRC(AI,N,X,IWK,WK)
      NNH=N/2+1
      DO 20 K=1,NNH
      TIME(K)=K*SMPINT
      AMP(K)=CDABS(X(K))
      FREQ(K)=2.*PI*K/TTOT
      TN=AIMAG(X(K))/REAL(X(K))
      PHASE(K)=DATAN(TN)*180./PI
      IF (PHASE(K).LT.0.)NCOUNT=NCOUNT+1
      PHASE(K)=PHASE(K)+NCOUNT*90.
      IF(AMP(K).GT.TMXAMP)TMXAMP=AMP(K)
   20 CONTINUE
      DO 30 K=1,NNH
      AI(K)=AI(K)/AIMAX
   30 AMP(K)=AMP(K)/TMXAMP
      WRITE(20,1010)(AI(I),TIME(I),I=1,1024)
      WRITE(30,1010)(PHASE(I),FREQ(I),I=1,350)
      WRITE(40,1010)(AMP(I),FREQ(I),I=1,200)
 1000 FORMAT(I3,17I4)
 1010 FORMAT(2E13.5)
      END
```

Fig. 8 Fortran program used to compute the FFT.

of radial lines eminating from the transducer at 10 deg increments was drawn on the plate. Quarter circles of 2" and 4" radii were then drawn so that a matrix of 20 data locations was generated, Fig. 9. Thus the effects of distance from the source and angle relative to the fiber direction could be analyzed.

The AU signal was generated by a Panametrics pulser and sent into the plate via a 5 MHz Panametrics wideband acoustic emission transducer. The transducer was coupled to the specimen with a high viscosity Panametrics couplant. Following reception by the Proctor Transducer, the signal is sent through a preamplifier. The signal is then digitized, stored, and sent to an oscilloscope for viewing. The Biomation signal digitizer was triggered by a signal from the pulser. The settings on the Biomation were as follows:

Input Range .... 1 volt

Delay Following Trigger ...... 2.4 μ sec

Sample Interval .... 0.05 μ sec

Trigger Level .... 0.5 volts

When the distance between transducers was increased to 4", the delay was increased to 2.9 μ sec because of the longer distance that the signal had to travel through the material. The delay also had to be increased (to 3.1 μ sec) after the 50 deg reading corresponding to the slower velocity associated with propagation perpendicular to the fibers. Subsequent tests were run with sample intervals of 0.1 μ sec and 0.2 μ sec and without preamplification. It was determined that the preamplification had no effect on the nature of the signal and that the original instrumentation readings generated the best results. Therefore, all analysis was performed on the original 20 data sets.
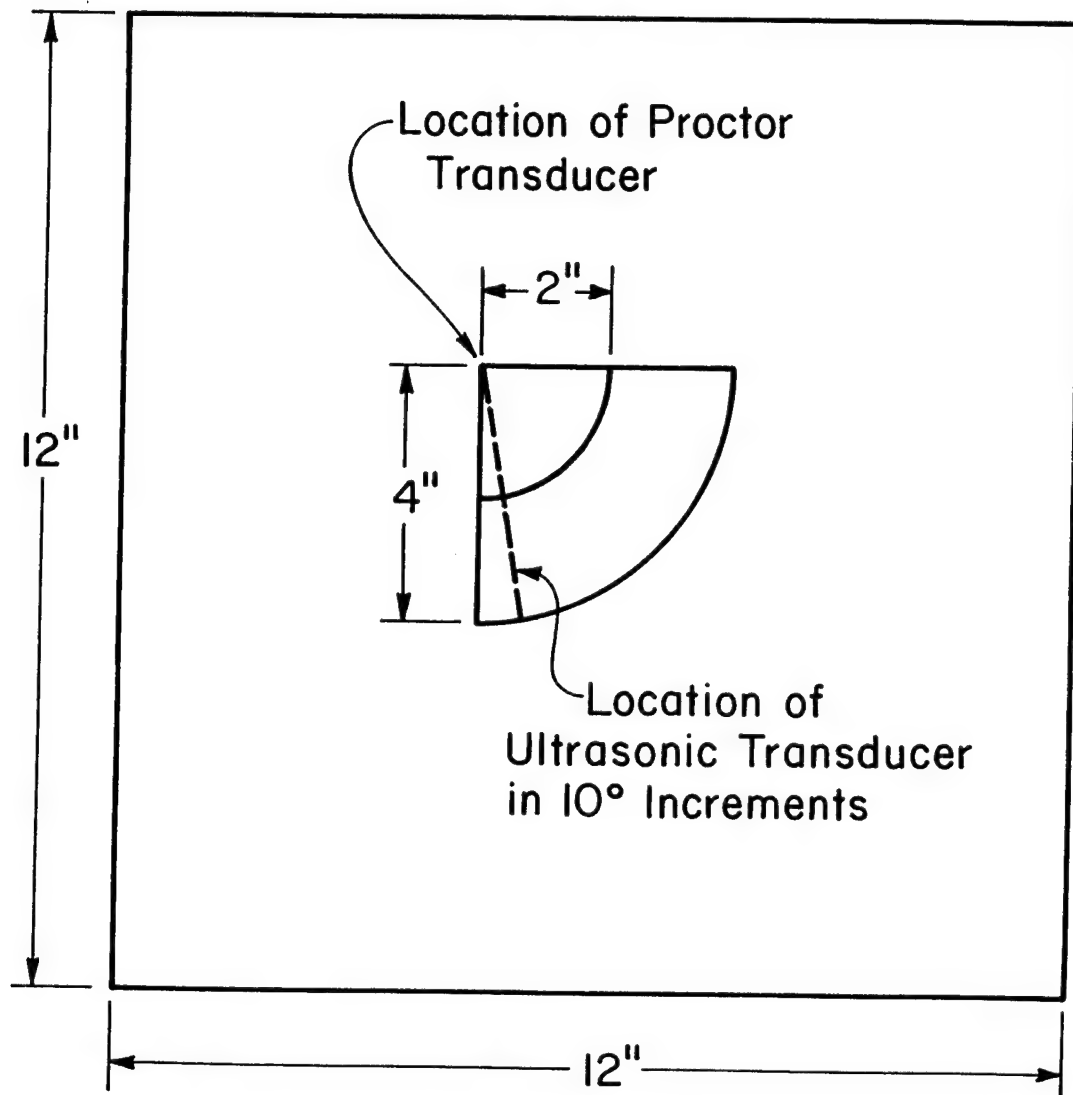
Fig. 9 Schematic diagram of transducer locations

I-80

The digitized signal was processed by the Virginia Tech mainframe computer system. The program, shown here, generates plots of amplitude versus time, and using a Fast Fourier Transform algorithm, generates plots of phase angle versus frequency and amplitude versus frequency. These plots were then analyzed to determine the behavior of the wave in the material.

III. Discussion and Results

Most of the current research in acousto-ultrasonics is concerned with analysis of the frequency spectrum of received signals. It is not then surprising that the most interesting results of this investigation are the plots of signal amplitude versus frequency. However, there are a few significant points to note concerning the phase-frequency and amplitude-time graphs.

The primary importance of the amplitude-time plot is that it consists of the raw data from which all other information is generated. The gating, threshold, and other instrumentation settings, which have a great effect on the subsequent signal analysis, are determined by looking at the amplitude-time curve on the oscilloscope and adjusting the instrumentation to improve the signal quality. For example, in all of the curves we see a spike of maximum amplitude within 10 to 15 microseconds, followed by a decay of the signal. Because the Biomation is triggered by the pulser and we wish to keep most of the decaying signal within our range of data collection (2048 points * 0.05 μ sec/point=102.4eμ sec) the delay time had to be increased corresponding to slower velocity perpendicular to the fibers and longer distance form the 4" points. Because the plots are normalized and the

delay time was changed between the 2" and 4" data sets, the hard-copy plots shown here do not show that the signal amplitude decreased as the distance from the NBS Transducer was increased. Neither do these plots show that the maximum amplitude spike occurred later in the cross-fiber direction, although necessary adjustments in instrumentation indicate this. The plots do indicate broadening of the curves as the angle increases with respect to the fiber direction, Figs. 10,11. Thus, in the direction of least stiffness we have a flat, broad signal in contrast with the sharp burst associated with the fiber direction. This broadening indicates that dispersion is likely to be occurring.

Dispersion occurs when different frequencies propagate at different rates. The incident pulse is a sharp burst and Fourier analysis indicates that sharp bursts contain many frequency components [12]. In a medium that exhibits dispersion, the amplitude versus time curve broadens due to these differences in velocity between the frequency components.

The dispersion of the signal is indicative that Lamb type waves may be propagating. Other time domain evidence of the existence of plate wave modes is the fact that both in-plane and out-of-plane displacements were recorded [18].

The phase angle versus frequency plot (Figs. 12a,12b) shows a very consistent linear relationship between phase angle and frequency. Previous investigators [13] have shown that this linear relationship is characteristic of unflawed materials, correlating sharp changes in elastic modulus with changes in the derivative of this plot. The use of phase angle data is still in its beginning stages. This recent development is a direct result of improved transducers, such as the
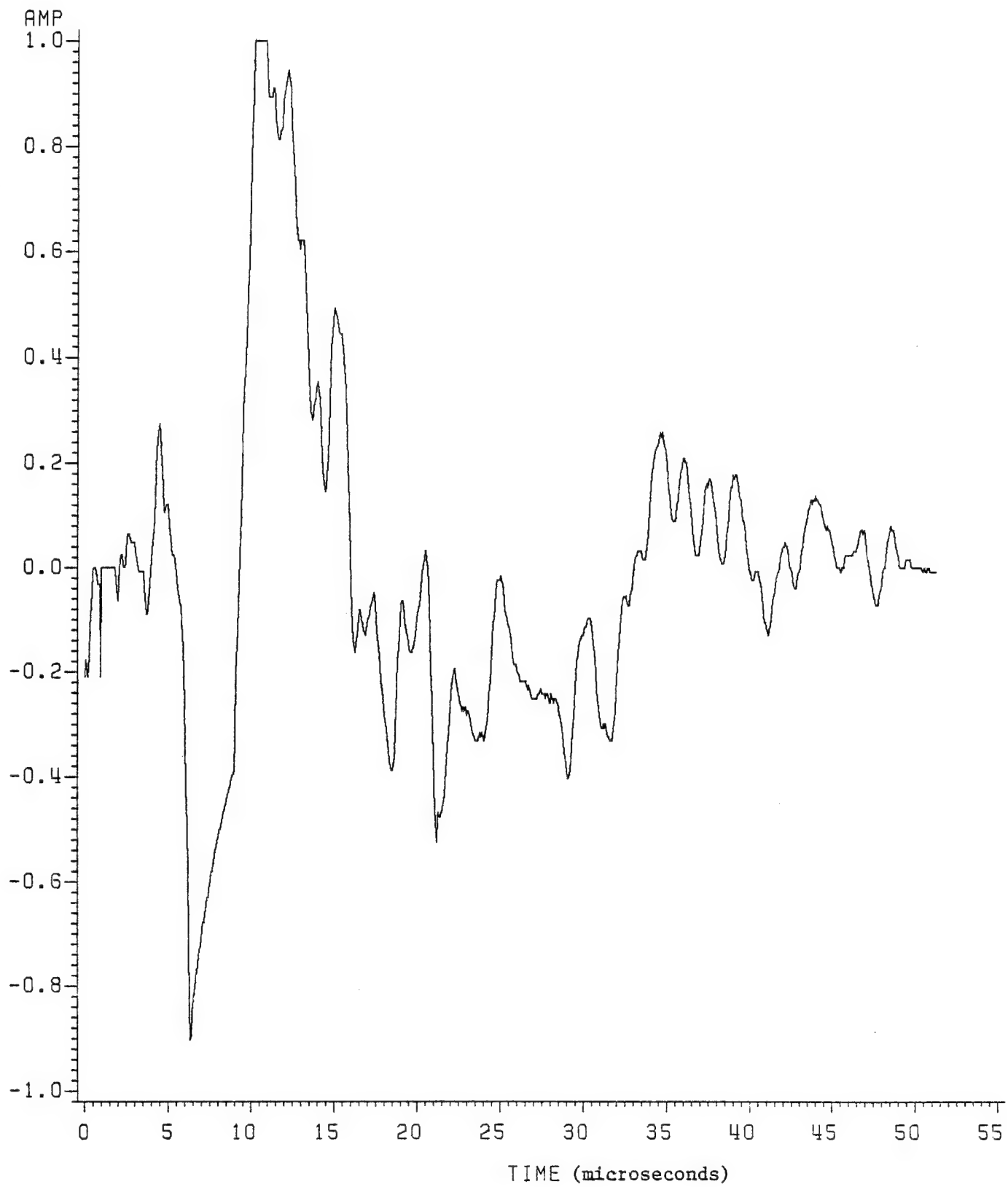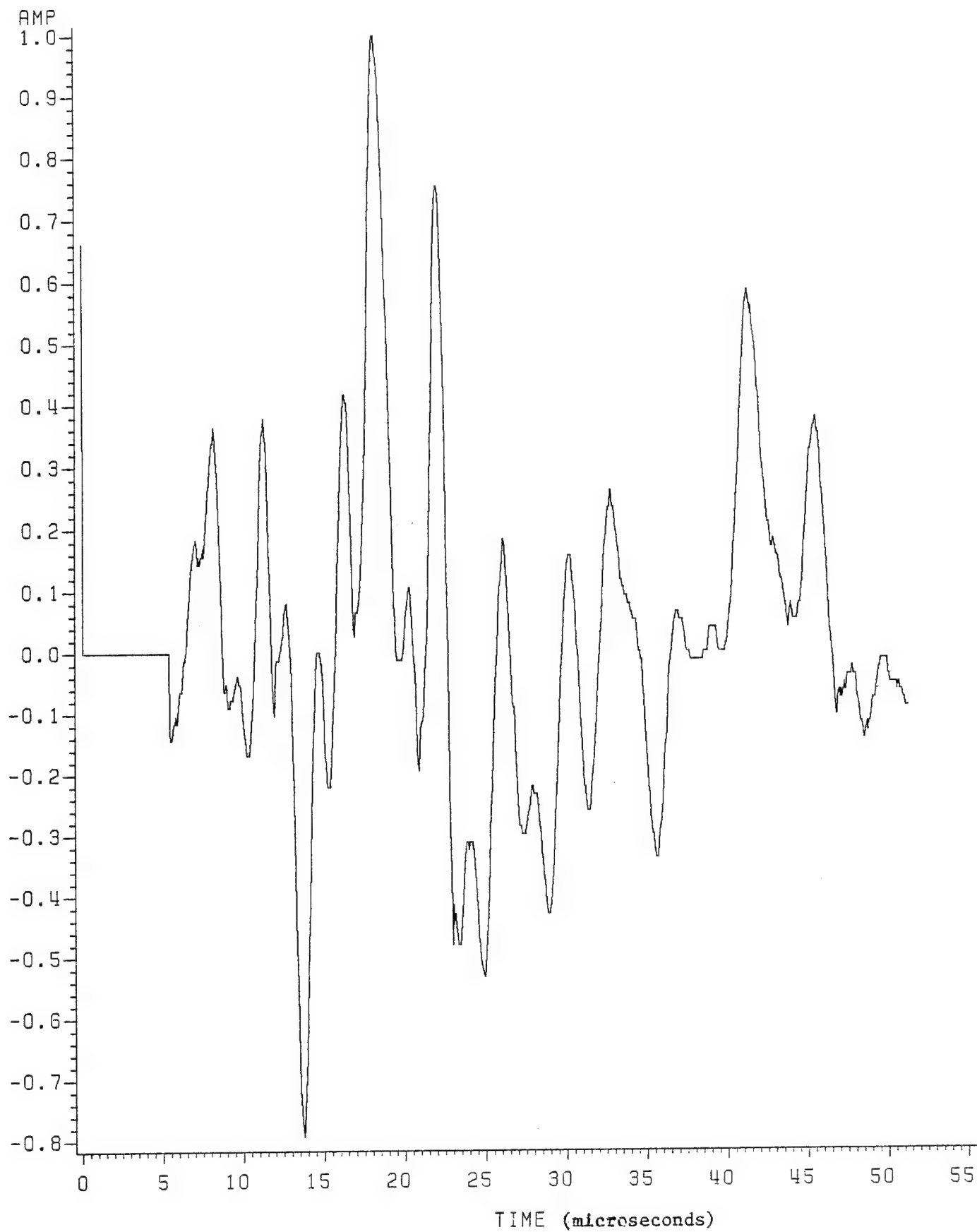
Fig. 10. Amplitude vs. Time 0 Degrees.

I-83

Fig. 11.   Amplitude vs. Time 90 Degrees.
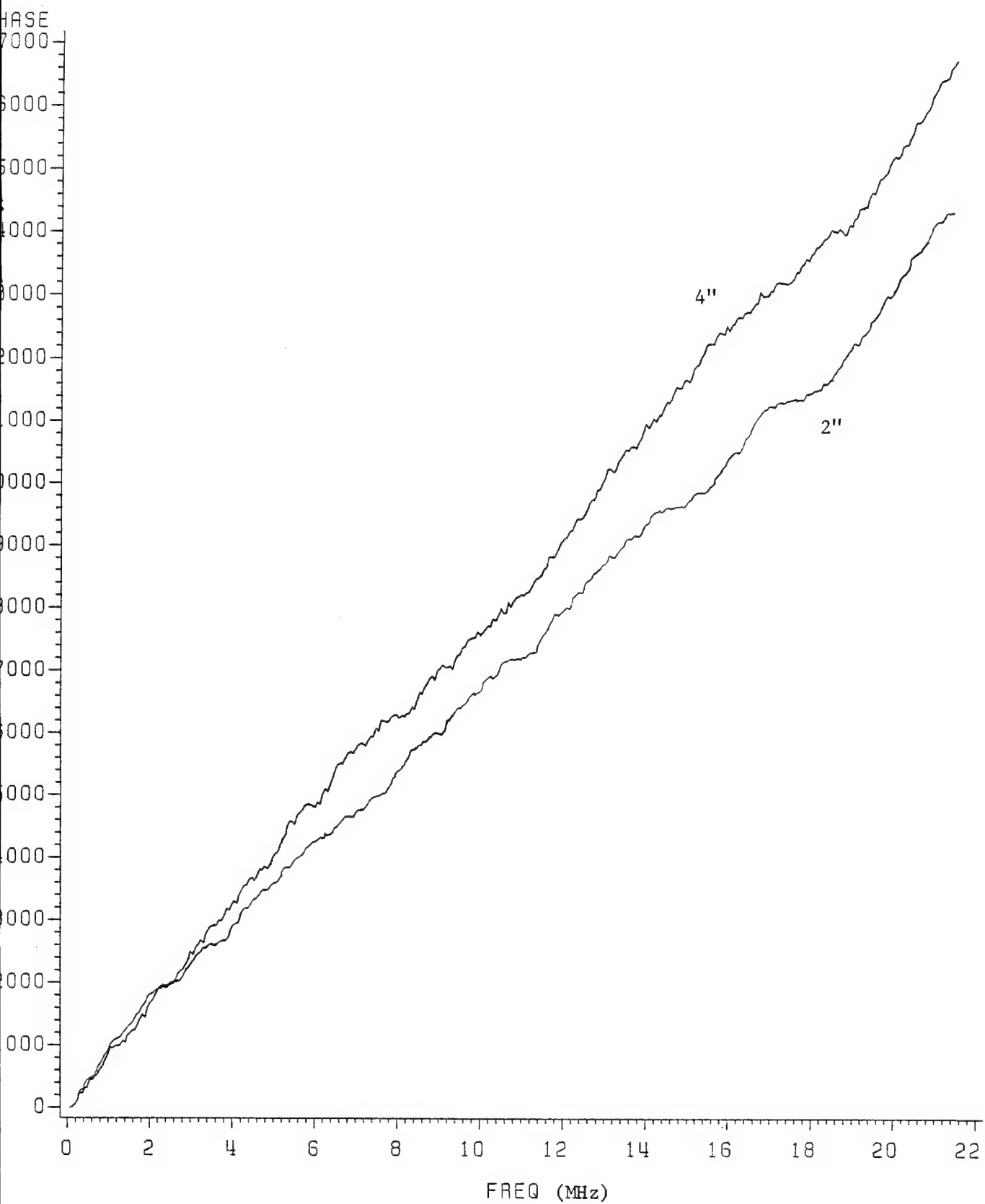
I-84

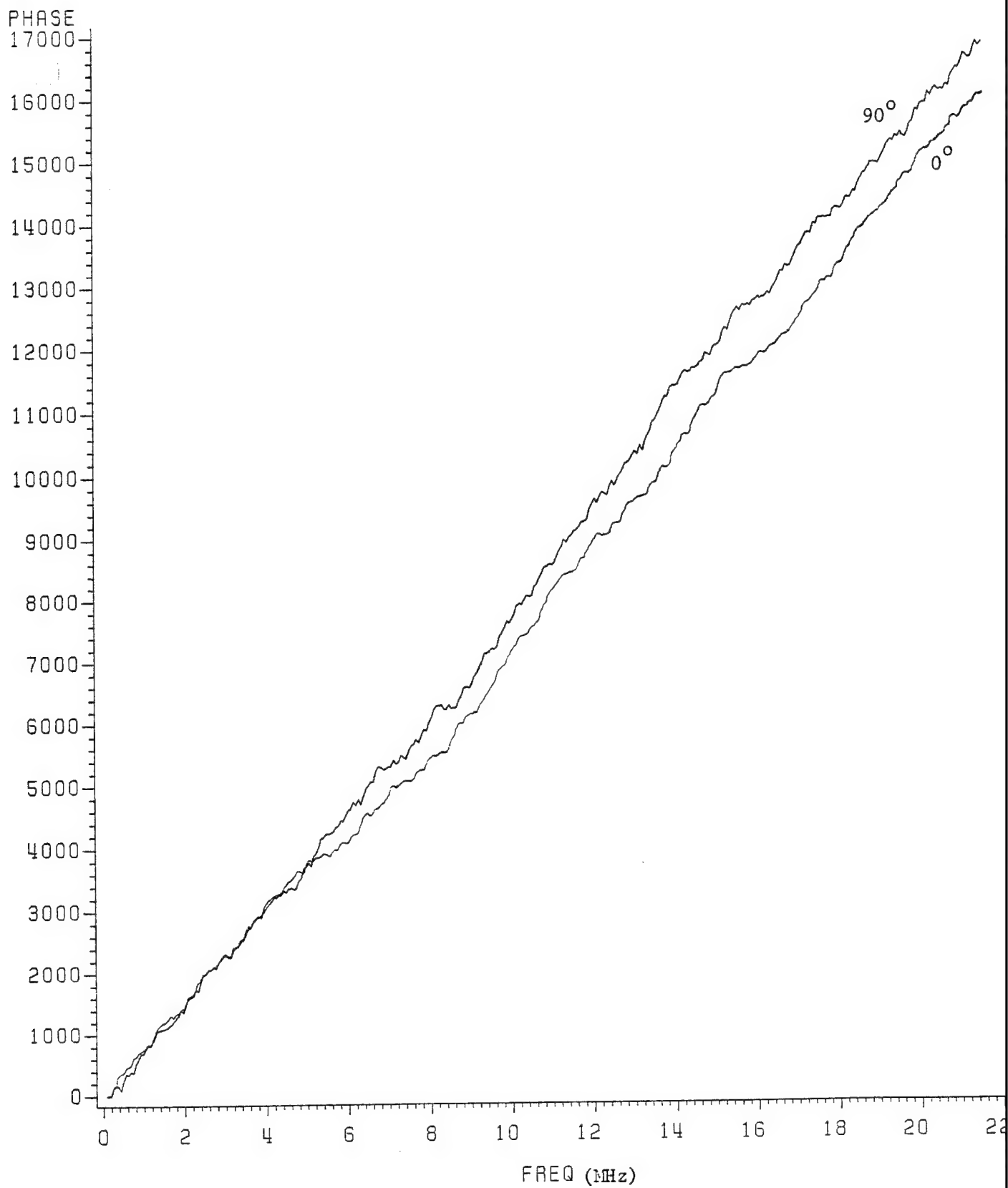Fig. 12a.   Phase Angle vs. Frequency for 30 Degrees at 2 and 4 Inches.

Fig. 12b. Phase Angle vs. Frequency for 0 and 90 Degrees.

conical transducer, because these transducers enable one to separate material prompted slope variations from those created by the integration process over the finite dimensions of the transducer surface.

It also must be noted that in all cases, the slope of the 4" data plot was 5 to 10% higher than that from the shorter distance at the same angle. No trends were noticed in comparing slopes from various angles. Further analysis and development of the technique must be conducted before any conclusive statements regarding the significance of this phase angle information can be made.

There are four major characteristics of the plots of amplitude versus frequency graphs, Figs. 13-22. They are:

-- spreading of the frequency spectrum as the angle approaches 90 degrees, high amplitudes are more likely to exist at higher frequencies in the cross-ply direction.

-- regular spacing between peaks and valleys of all frequency spectra

-- increased number of peaks and valleys within a given frequency band as the angle approaches 90 degrees, more narrow peak and valley width at large angles

-- received frequencies were predominantly in the range of 0.2 to 2.0 MHz

It is easy to trace the development of the SWF technique which is based on moments of the frequency spectrum by noting the spreading of the spectrum due to the increased stiffness. For example, in the 0 deg direction, no amplitudes greater than $0.15*V(max)$ exist at frequencies greater than 1.4 MHz, whereas in the 90 deg direction these amplitudes

Fig. 13.   Amplitude vs. Frequency for 0 Degrees.

Fig. 14.   Amplitude vs. Frequency for 10 Degrees.

I-89

Fig. 15. Amplitude vs. Frequency for 20 Degrees.

Fig. 16. Amplitude vs. Frequency for 30 Degrees.

Fig. 17. Amplitude vs. Frequency for 40 Degrees

Fig. 18.   Amplitude vs. Frequency for 50 Degrees.

I-93

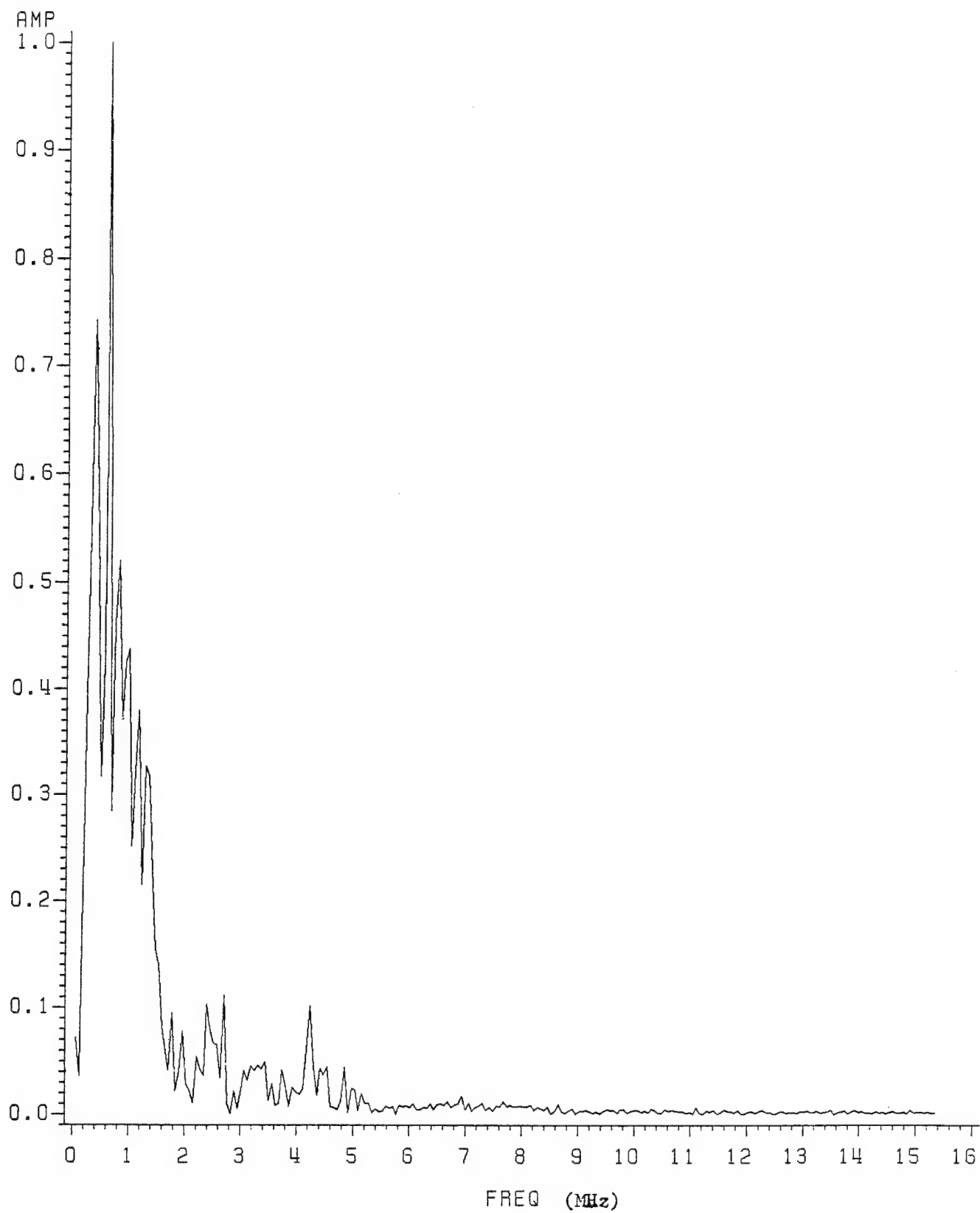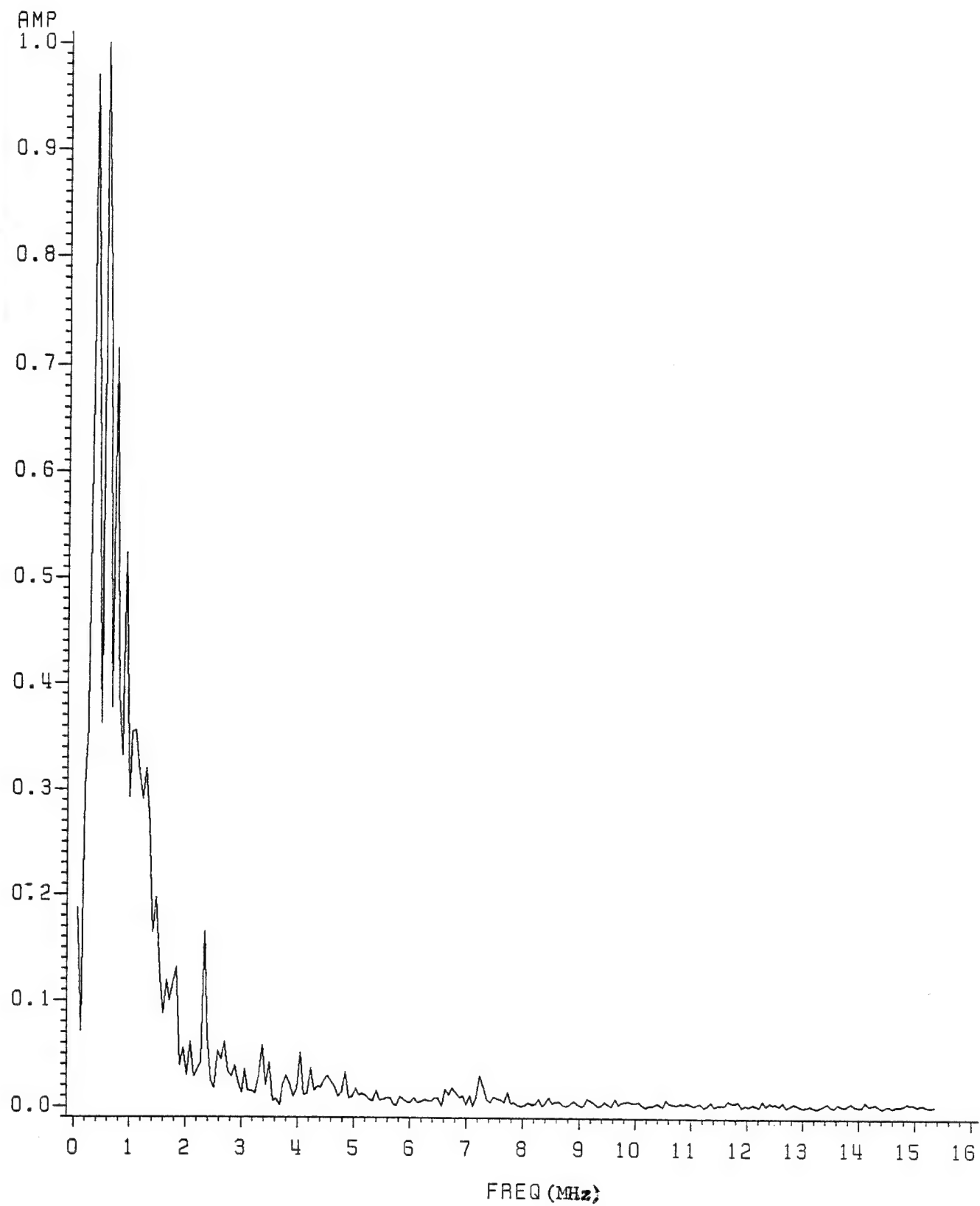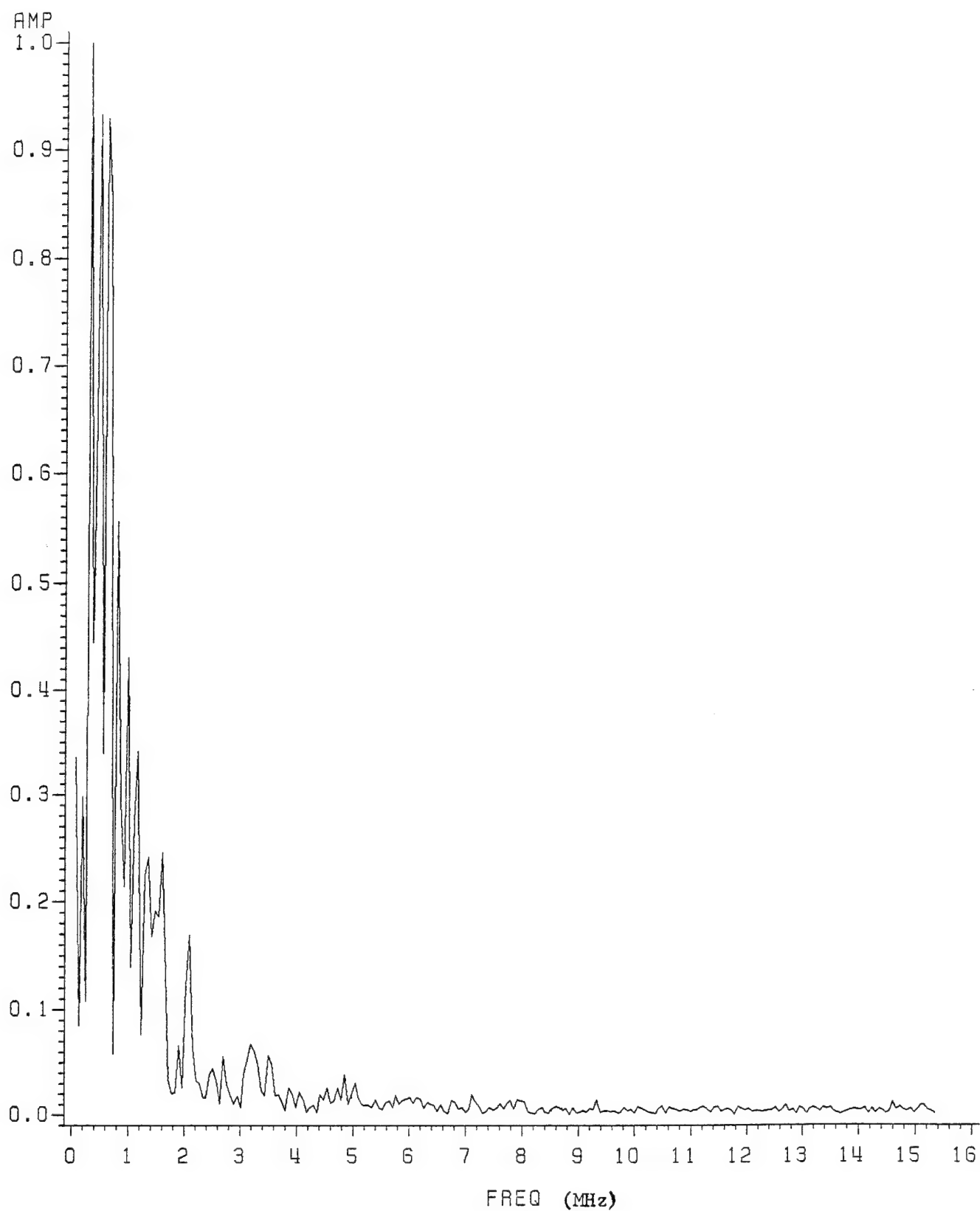Fig. 19.   Amplitude vs. Frequency for 60 Degrees.
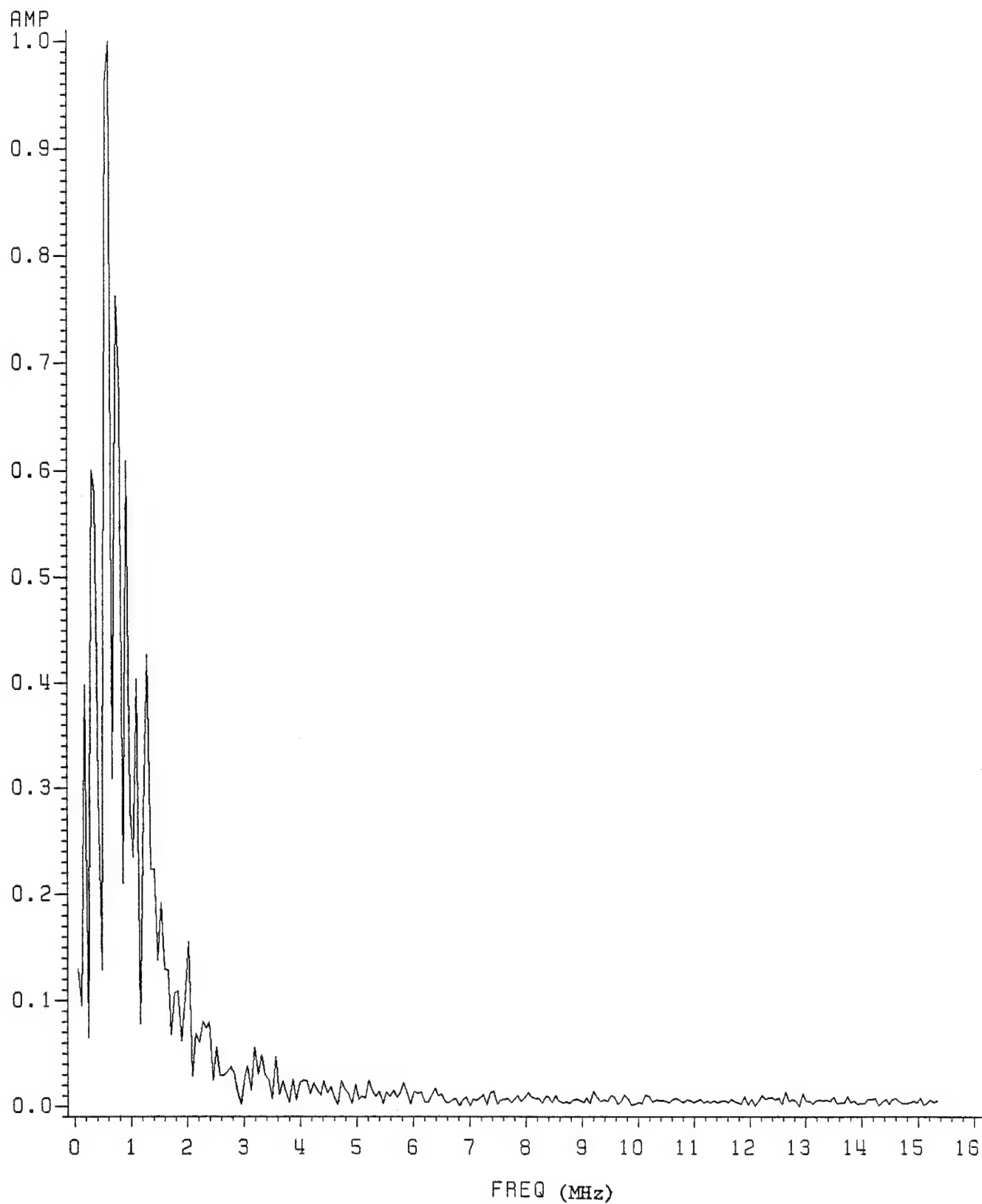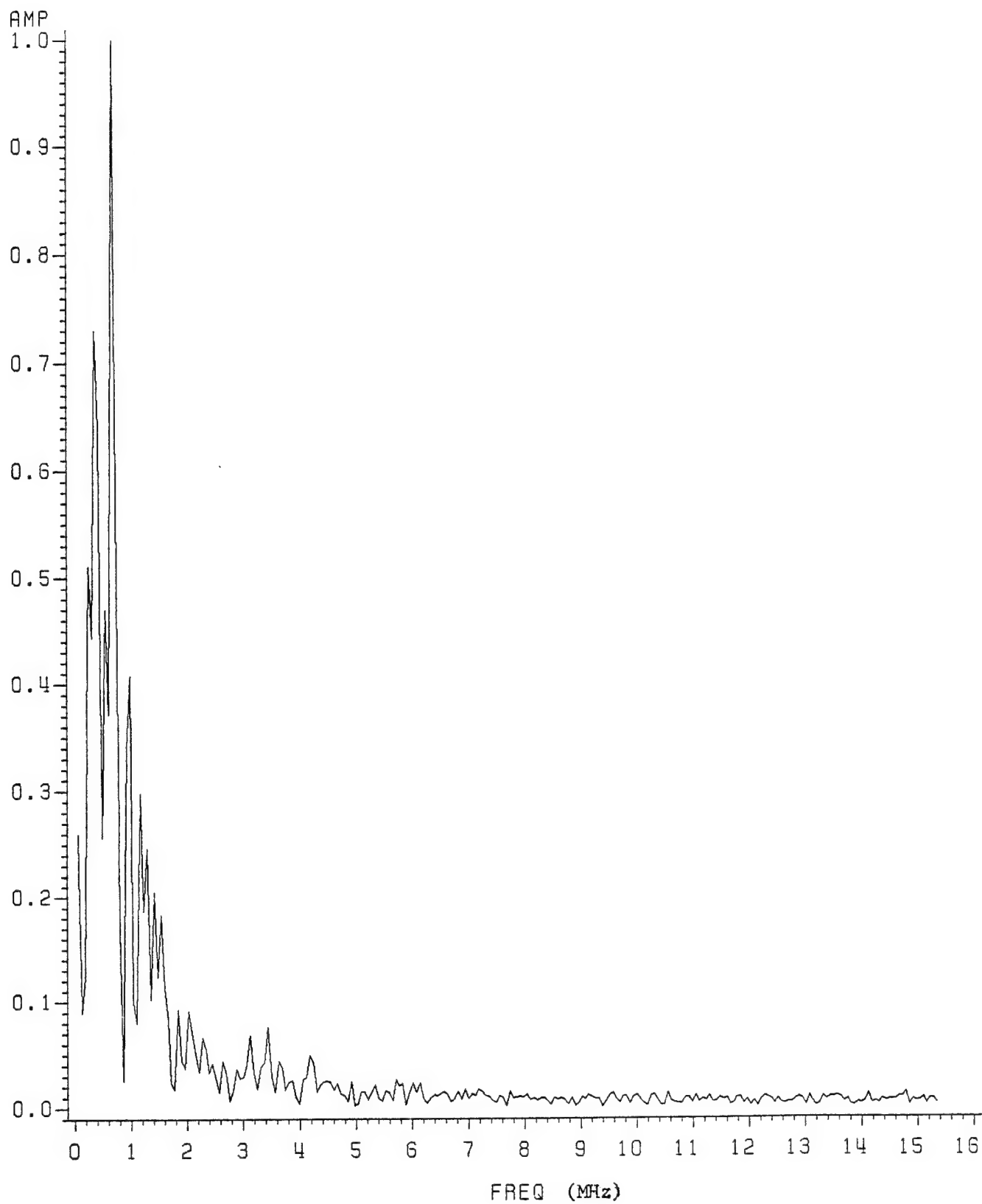
I-94

Fig. 20. Amplitude vs. Frequency for 70 Degrees.

Fig. 21.   Amplitude vs. Frequency for 80 Degrees.

Fig. 22. Amplitude vs. Frequency for 90 Degrees.

Fig. 23. Amplitude vs. Frequency 0 Degrees.

exist out to 2.0 MHz. This trend is continuous through the angles
tested and in both 2" and 4" data sets. This spreading tends to
indicate an inverse correlation between stiffness and first moment of
area of the power spectrum.

The regular spacing between the peaks and valleys of the spectrum
can be explained by bandstop and bandpass phenomena which are
characteristic of plate waves. Selected frequencies interfere
destructively upon reflection from the back of the plate before they can
propagate down the plate to the receiving transducer. These frequencies
are given by [14,15]:

$$w = \frac{n\pi v}{b}$$

where: v = velocity of the wave

b = plate thickness

n - some integer value

For example, taking the thickness to be 0.33 cm and the distance
between frequency valleys to be 0.2 MHz, the calculated velocity is
$2.1*10^4$ cm/s. This calculated velocity is far less than the through-
the-thickness velocities cited in the literature for graphite epoxy
laminates of $2.0*10^{\frac{5}{6}}$ to $18*10^{\frac{5}{6}}$ cm/s. This numerical inconsistancy can
best be explained by differences in velocity and reflections from matrix
rich layers between plies, the thickness of the couplant, and from the
thickness of the foil layer.

In light of previous SWF work done, it was encouraging to note that
the predominant frequencies were below 2 MHz. A previous investigation
[17] yielded similar results and there was some doubt as to the validity

of the tests due to a problem in the FFT algorithm and due to the transducer used. This data seems to substantiate the previous work despite those problems. The reason for the predominance of the low frequencies despite the fact that the incident pulse was centered around 5 MHz may involve the resonant frequency of the plate although a different plate geometry was used in the previous investigation.

It is thought that most of these characteristics can be explained by considering the possible conversion of the incident longitudinal wave to a plate type wave. This process is quite complex and much of the mechanism is still not clearly understood. However, it is thought that the signal which is incident normal to the plate begins to propagate along the plate due to a difference in pressure between the transducer-plate interface the the air-plate interface or through the excitation of resonance frequencies of the plate. The plate, in addition to its incident z component of velocity, begins to develop both x and y components. The magnitude of the x or y component compared to that of the z component, and thus the number of relfections from the front and back surfaces necessary to travel a given distance, is dependent on the orientation of the fibers relative to that direction. The recorded frequency spectrum is a function of both number of reflections and the manner in which the frequency components interact upon reflection. This indicates the complex manner in which the frequency spectrum depends on the fiber orientation [18]. Much more analysis is needed before this understanding is clear.

IV. Conclusions

The NBS Conical Transducer has been found to be a valuable tool in the analysis of wave propagation in composite materials. This illustrates the possible role of this type of transducer in the improvement of the SWF scheme. Future modifications of the transducer should include an alternate scheme of grounding so that the transducer can be conveniently applied to nonconductive materials. Frequency spectrum analysis coupled with information from the time domain has substantiated the idea that plate wave modes are being propagated in the Stress Wave Factor analysis of thin composite plates.

References

1. Vary, Alex, "Concepts and Techniques for Ultrasonic Evaluation of Material Mechanical Properties," _Mechanics of Nondestructive Testing_, W. W. Stinchcomb, Ed. (Plenum Press, New York, 1980).

2. Talreja, Ramesh, Anil Govada and E. G. Henneke, "Quantitative Assessment of Damage Growth in Graphite Epoxy Laminates by Acousto-ultrasonic Measurements," Review of Progress in Quantitative Nondestructive Evaluation, Vol. 3B, D. O. Thompson and D. E. Chimenti, Eds. (Plenum Press, New York, 1984) pp. 1099-1106.

3. Henneke, E. G., Duke, J. C., Stinchcomb, W. W., Govada, A. and Lemascon, A., "A Study of the Stress Wave Factor Technique for the Characterization of Composite Materials," NASA Contractor Report 3670, Grant NSG 3-172 (Feb. 1983).

4. Eitzen, Hsu, Carasso, Proctor, "Deconvolution by Design -- An Approach to the Inverse Problem of Ultrasonic Testing," NBS report.

5. Krautkramer and Krautkramer, _Ultrasonic Testing of Materials_, (Springer-Verlag, New York, 1969) p. 91.

6. Viktorov, _Rayleigh and Lamb Waves_ (Plenum Press, New York, 1967).

7. Kolsky, _Stress Waves in Solids_ (Dover Publications, New York, 1963).

8. Green, Robert E., "Basic Wave Analysis of Nondestructive Testing," _Mechanics of Nondestructive Testing_, W. W. Stinchcomb, Ed. (Plenum Press, New York, 1983) pp. 55-76.

9. Information Packet on NBS Conical Transducer for Acoustic Emission, Dec. 1981.

10. Proctor, "An Improved Piezoelectric Acoustic Emission Transducer," _J. of the Acoustic Society of America_ (May 1982).

11. Stiffler, Richard and Henneke, E. G., "The Application of Polyvinylidene Fluoride as an Acoustic Emission Transducer for Fibrous Composite Materials", _Materials Evaluation_, _41_, no. 8, July 1983, pp. 956-960.

12. Henneke, E. G., Private Communication, April 1985.

13. Mercier and de Belleval, "Use of the Phase of a Signal in Ultrasonic Spectral Analysis to Evaluate Flaws," _Ultrasonic Int'. 81 Conf. Proceedings_ (IPC Business Press Limited, U.K., 1981).

14. Brekhovskikh, L. M., _Waves in Layered Media_, R. T. Beyer, translator (Academic Press, New York, 1980).

15. Stiffler, R. C., Ph.D. Dissertation, Virginia Polytechnic Institute, to be published, 1985.

16. Kriz, R. D. and Stinchcomb, W. W., "Elastic Moduli of Transversely Isotropic Graphite Fibers and Their Composites," <u>Experimental Mechanics</u>, <u>19</u>, no. 1 (1979) pp. 41-49.

17. Govada, A. K., "Nondestructive Assessment of Composite Material's Condition by Means of Acousto-Ultrasonics," Master's Thesis, VPI & SU, 1984.

18. Stiffler, R. C., Private Communication, Apr. 1985.

Part II

LOW FREQUENCY PLATE WAVE MODES

Richard C. Stiffler

and

Edmund G. Henneke, II

ESM Department

Virginia Polytechnic Institute and State University

Blacksburg, Virginia 24061-4899

Abstract

The quality assurance and mechanical serviceability of advanced filament reinforced composites is of great concern because of the increasing use of these materials in many engineering structures. For quality control and maintainability of composites, tests based on strong fundamental and well understood physical principles must be established which can be used to ascertain and predict the design serviceability of finished composite parts. The acousto-ultrasonic, or stress wave factor, method has been found to be especially useful for providing a quantitative parameter which correlates well with certain mechanical properties of composite materials. However, our basic understanding of the type of wave modes established in the material when one applies the SWF technique is insufficient. This work investigates the propagation of Lamb, or plate, waves in anisotropic, homogeneous, materials. By influence of analytic and experimental observations, it is suggested that the stress wave factor technique causes the establishment of the first few fundamental plate wave modes in a composite laminate. It is in large part propagation characteristics of these plate modes which an investigator measures when applying the SWF method.

I. INTRODUCTION

The quality assurance and mechanical serviceability of advanced filament reinforced composites is of great concern because of the increasing use of these materials in many engineering structures. Because of the inherent anisotropy and inhomogeneity of composite materials, damage development and failure is distinctly different from that of homogeneous isotropic materials. Damage can no longer be defined as the formation and growth of a self-similar crack until a critical flaw size is reached, at which time the crack catastrophically propagates under the load condition. Rather, damage development in composite materials is a complex sequence of matrix cracks, delaminations, fiber breakage, fiber-matrix disbonds, and so forth, which form and coalesce until some critical damage state is reached, at which point the structure fails.

Because composites are a relatively new material, there are not many years of experience upon which engineering decisions can be based. There is no simple accept-reject criterion for in-service structures constructed from composite materials. Composite materials have no analog to homogeneous isotropic materials whose critical flaw size can be calculated from fracture mechanics and whose flaw size in a structural element can be used as the accept-reject criterion.

For example, one type of in-service damage that is not readily detected is impact damage. If a piece of sheet metal is impacted with an object having enough energy to cause damage, the damage is usually manifested as a visible dent in the material. However, a composite structure can suffer significant impact damage and can have extensive

internal damage such as delaminations and matrix cracks, yet show no external visible signs of damage.

Another way in which composites differ from other materials is that of fabrication. Because composites are typically manufactured in one-step processes, there are no intermediate stages at which one is able to check the quality of the material used nor for manufacturing defects which include porosity, matrix rich areas, matrix poor areas, improper curing, missing plies, misoriented plies, delaminations, interlaminar inclusions, etc. So, both in quality control and maintainability there must be established tests based on strong fundamental and well understood physical principles which can be used to ascertain and predict the design serviceability of finished composite parts.

A number of nondestructive test methods have been developed for the study of composite materials and have their own particular strengths and weaknesses. Experience with the thermoset matrix composites has indicated that generally a more complete understanding of the damage development and damage state is obtained if several NDT techniques are used. In particular, different NDT methods have been found to be more sensitive to different types of damage. Some methods such as X-ray radiography, thermography, vibrothermography, and ultrasonic C-scan give an indication of the field of damage. Of these, X-ray radiography shows the most microstructural detail, and thermography, the least. On the other hand, thermography gives an indication of the integrated effect of the damage field. Some NDT methods such as ultrasonic attenuation, acousto-ultrasonics, acoustic emission, stiffness reduction measurement, and thermography give real-time information. Some are directly related to the mechanical properties such as monitoring stiffness reduction and

measuring ultrasonic wave speed. Hence, several techniques, each providing complementary information, are usually required to obtain an understanding of the response and damage development in composite materials.

Although there are a number of tests to interrogate a composite material; at this time there is still a need for simple tests which can yield quantitative parameters descriptive of the mechanical state of the material. In particular, one would like to have test methods which yield parameters which can be used to predict the important mechanical properties of strength, stiffness, and life. The measurement of ultrasonic wave speed is directly related to material stiffness and hence is a quantitative parameter which yields information directly about one of the needed mechanical properties. It may also be related indirectly to information concerning strength and life, although knowledge concerning the reasons these materials fail is in too immature a state at present to say anything definitive about this.

Much work has been performed using through-the-thickness ultrasonic attenuation and velocity measurements to monitor damage and evaluate material properties in composites. However, little or no information can be obtained about the in-plane properties. Vary's stress wave factor or acousto-ultrasonics [1-3] is one technique that does give in-plane information. The stress wave number has been correlated with a number of material parameters but there presently is little understanding of why it works.

It is well known that an acoustic or electromagnetic waveguide will allow only propagation of a wave having a particular frequency or any of its harmonics for a given wave vector. For the case of an acoustic wave

guide, the free surfaces cannot support a normal stress; thus acoustic waves propagating through a wave guide that have normal stress amplitudes other than zero at the free surface will be rapidly attenuated due to destructive interference. However, there will be one fundamental wave length or an integral multiple of this wave length that can propagate through the wave guide for a given wave vector and still maintain the stress free boundary conditions.

Wave propagation in plates can be separated into several regimes depending on the wavelength with respect to the thickness. If the wavelength is much larger than the thickness of the plate, then low frequency plate modes are set up. For the low frequency extensional modes, the wave vector is in the plane of the plate and there is no variation in displacement through the thickness. This mode can propagate for all frequencies, is nondispersive, and can be easily applied to angle-ply laminates. Its interpretation is fairly straightforward. This may be the mode that can be most easily applied to the nondestructive testing of plates.

Recently, analytical and experimental research has been conducted, under the sponsorship of General Electric Co. [1], on low frequency wave propagation in anisotropic plates with application to material characterization. It included: (1) a theoretical study conducted to compute low frequency plate phase velocities, and (2) measurement of the phase velocities in the principal directions of the plate. The variation of phase velocity with frequency was used to construct the fundamental, low frequency dispersion curves.

The results of this study provide significant new insight into the nature of the wave propagation that occurs in the stress wave factor

technique. This work has included calculating the low frequency fundamental plate wave modes in composite materials. It should be pointed out that for the analysis described here, the composite plate has been treated as a macroscopically homogeneous, but anisotropic, material having the elastic constants of the composite material in question. This assumption is reasonable as long as the wave lengths are long in comparison with the fiber diameters, fiber spacing, and ply thicknesses, which is a reasonable assumption for frequencies less than those normally used for ultrasonic investigation (i.e., less than 10 MHz).

Preliminary experimental work has shown that the flexural phase velocity in the plate varies as a function of frequency due to the highly dispersive nature of the plate. The dispersion curves, i.e. curves for frequency versus velocity, are characteristic for a plate having a particular thickness and elastic properties. Once established, this analysis allowed good correlation of experimental dispersion relations with plate extensional stiffnesses, A_{11} and A_{22} and plate bending stiffnesses D_{11} and D_{22}. Analytical and experimental results, to date, show good correlation at the longer wave lengths. It appears from these results that fundamental plate wave modes are established by placing a transducer flat upon the surface of a plate. These plate wave modes propagate along the plane of the plate and can be detected by a similarly placed transducer "downstream" of the transmitter.

II.   EXTENSIONAL AND FLEXURAL WAVE PROPAGATION

IN COMPOSITE PLATES

In order to make clear the implications of our previous analytical work [1], a condensed presentation of the analysis is briefly reviewed in this section.   The low frequency approximation described earlier gives several simplifying factors for formulating wave propagation in plates, namely:

1) For extensional and in-plane shear waves, the displacements are uniform across the thickness of the plate and out-of-plane inertial effects are negligible.

2) For flexural waves, rotary inertia and transverse shear are negligible.

With these approximations, classical laminate theory can be used as the basis for developing the low frequency wave equations.

Again, it should be noted that this two-dimensional development is valid only for wavelengths larger than the thickness of the plate. For short wavelengths, the thin plate assumption is no longer valid because the displacements will be a function of the thickness coordinate necessitating an analysis using three-dimensional elasticity.

2.1   In-plane Wave Propagation

For in-plane waves, the stress free surface condition is immediately satisfied by assuming a plane state of stress.   The equations of motion for a plane state of stress are:

$$\frac{\partial \sigma_1}{\partial x_1} + \frac{\partial \sigma_6}{\partial x_2} = \rho \ddot{u}_1 \tag{2.1a}$$

$$\frac{\partial \sigma_6}{\partial x_1} + \frac{\partial \sigma_2}{\partial x_2} = \rho \ddot{u}_2 \qquad (2.1b)$$

For a laminate that is symmetric with respect to its midplane, the stress-strain relationship is given by

$$
\begin{Bmatrix} \sigma_1 \\ \sigma_2 \\ \sigma_6 \end{Bmatrix} = \frac{1}{d}
\begin{bmatrix} A_{16} & A_{12} & A_{16} \\ A_{12} & A_{22} & A_{26} \\ A_{16} & A_{26} & A_{66} \end{bmatrix}
\begin{Bmatrix} \varepsilon_1 \\ \varepsilon_2 \\ \gamma_6 \end{Bmatrix} \qquad (2.2)
$$

where A_{ij}'s are elements of the extensional stiffness matrix. The calculation of the extensional stiffness matrix is discussed in a number of books [4] on composite materials and is not discussed here.

The strains are given by

$$\varepsilon_1 = \frac{\partial u_1}{\partial x_1}$$

$$\varepsilon_2 = \frac{\partial u_2}{\partial x_2} \qquad (2.3)$$

$$\gamma_6 = \frac{\partial u_1}{\partial x_2} + \frac{\partial u_2}{\partial x_1}$$

The displacements for a plane harmonic wave travelling in the plane of the plate are:

$$u_1 = A\alpha_1 \exp \left(i \left(k \left(x_1 \ell_1 + x_2 \ell_2 \right) - \omega t \right) \right)$$

$$(2.4)$$

$$u_2 = A\alpha_2 \exp \left(i \left(k \left(x_1 \ell_1 + x_2 \ell_2 \right) - \omega t \right) \right)$$

where

A = amplitude of displacement

α_i = displacement component in the x_i coordinate direction

i = $\sqrt{-1}$

k = wave number   = $2\pi/\lambda$

ℓ_i = direction cosine of the wave vector in the x_i

coordinate direction

ω = circular frequency

t = time.

When Eqns. (1) to (4) are substituted into one another and common terms cancelled the following set of homogeneous equations is obtained.

$$\begin{pmatrix} \ell_1^2 A_{16}+\ell_1\ell_2 A_{16}+\ell_2^2 A_{66}-\rho\left(\frac{\omega}{k}\right)^2 & \ell_1^2 A_{16}+\ell_1\ell_2(A_{12}+A_{66})+\ell_2^2 A_{26} \\ \ell_1^2 A_{16}+\ell_1\ell_2(A_{12}+A_{66})+\ell_2^2 A_{26} & \ell_1^2 A_{66}+2\ell_1\ell_2 A_{26}+\ell_2^2 A_{22}-\rho\left(\frac{\omega}{k}\right)^2 \end{pmatrix}\begin{pmatrix} \alpha_1 \\ \alpha_2 \end{pmatrix} = 0 \quad (2.5)$$

For a nontrivial solution, the determinant of the 2x2 matrix above must be equal to zero. This gives a characteristic equation whose eigenvalues ω/k are the phase velocities in the plate. The determinant has two roots which correspond to a quasi-extensional and quasi-shear wave. The respective eigenvectors α_1 and α_2 can then be obtained from Eqn. (2.5). The wave velocities can be determined for any direction in the plate.

For the experimental work, the velocities were measured in the x_1 direction and the x_2 direction and only these directions will be considered in the subsequent analysis.

For $\ell_1 = 1$ and $\ell_2 = 0$, the extensional wave velocity is given by

$$V_1 = \frac{\sqrt{2}}{2\rho} \left((A_{11}+A_{26}) + \sqrt{(A_{11}+A_{66})^2 + 4(A_{11}A_{66}-A_{16}^2)} \right)^{\frac{1}{2}} \tag{2.6}$$

and

$$\alpha_1 = 1$$
$$\alpha_2 = 0$$

That is, for this propagation direction the wave is purely longitudinal.

For a unidirectional laminate or a laminate symmetric with respect to the x_1 axis, the extensional velocity is given by

$$V_1 = \left(\frac{A_{11}}{\rho} \right)^{\frac{1}{2}} \tag{2.7}$$

Likewise for propagation along the x_2 axis, $\ell_2 = 1$ and $\ell_1 = 0$ gives

$$V_2 = \left(\frac{\sqrt{2}}{2\rho} \ (A_{22}+A_{66}) + \sqrt{(A_{22}+A_{66})^2 + 4(A_{22}A_{66}-A_{26})} \right)^{\frac{1}{2}} \tag{2.8}$$

and

$$\alpha_1 = 0$$
$$\alpha_2 = 1$$

For a unidirectional laminate or a laminate symmetric with respect to the x_2 axis the in-plane shear wave velocity is

$$V_2 = \left(\frac{A_{22}}{\rho} \right)^{\frac{1}{2}} \tag{2.9}$$

2.2   Flexural Wave Propagation

The derivation for flexural wave propagation is carried out in a

similar fashion as extensional wave propagation. The governing equation
for flexural wave propagation is

$$\frac{\partial^2 M_1}{\partial x_1^2} + \frac{2\partial^2 M_6}{\partial x_1 \partial x_2} + \frac{\partial^2 M_2}{\partial x_2} = -\frac{d}{\rho}\frac{\partial^2 u_3}{\partial t^2} \qquad (2.10)$$

where

M_i = bending moment about x_i coordinate axis

ρ = mass density

d = thickness of plate

The bending moments are related to the curvature by

$$
\begin{array}{ccc}
M_1 & & D_{11} \quad D_{12} \quad D_{16} \quad \kappa_1 \\
M_2 & = & D_{12} \quad D_{22} \quad D_{26} \quad \kappa_2 \qquad (2.11) \\
M_6 & & D_{16} \quad D_{26} \quad D_{66} \quad \kappa_6
\end{array}
$$

where D_{ij} are the bending stiffnesses and κ_i are the curvatures of the
plate. The curvatures are given by

$$\kappa_1 = -\frac{\partial^2 u_3}{\partial x_1^2}$$

$$\kappa_2 = -\frac{\partial^2 u_3}{\partial x_2^2} \qquad (2.12)$$

$$\kappa_6 = -2\frac{\partial^2 u_3}{\partial x_1 \partial x_2}$$

The displacement of a flexural wave, u_3, is given by

$$u_3 = Ae^{i(k(\ell_1 x_1 + \ell_2 x_2) - \omega t)} \qquad (2.13)$$

where the parameters have the same definitions as for Eqn. (2.4).

Substituting Eqns. (2.10) through (2.13) into one another gives

$$k^4(\ell_1^4 D_{11} + 4\ell_1^3 \ell_2 D_{16} + 2\ell_1^2 \ell_2^2 (D_{12} + 2D_{66}) + 4\ell_1 \ell_2^3 D_{26} + \ell_2^4 D_{22}) = \rho d\omega^2 \qquad (2.14)$$

For flexural waves propagating along the x_1 axis, Eqn. (2.14) reduces to

$$k^4 D_{11} = \rho d\omega^2 \qquad (2.15)$$

Since

$$V_p = \frac{\omega}{k} \qquad (2.16)$$

the phase velocity is

$$V_p = \left(\frac{D_{11}\omega^2}{\rho d}\right)^{\frac{1}{4}} = \left(\frac{4\pi^2 D_{11} f^2}{\rho d}\right)^{\frac{1}{4}} \qquad (2.17)$$

It should be noted that the phase velocity is no longer constant but is a function of the frequency. Thus, propagation of low frequency flexural waves is dispersive.

The group velocity is

$$V_g = \frac{\partial \omega}{\partial k} \qquad (2.18)$$

and hence

$$V_g = \frac{4k^3}{\rho d 2\omega} = \frac{2}{\rho d\omega} \left(\frac{\rho d\omega^2}{D_{11}}\right)^{3/4}$$

2.3 Calculated Velocities for Various Materials

In order to verify that the analysis presented in the previous section represents the characteristics of the waves which are generated and detected during application of the acousto-ultrasonic technique, both analyses and experiments were performed on two different materials, aluminum and graphite epoxy. The aluminum plate was 6061-T6 aluminum, 0.065" thick x 12" x 12". The graphite epoxy panels were positive pressure molded from AS-4(GR)/PR288 and consisted of $[0]_8$, $[0]_{22}$, $[0,90]_{2s}$, and $[0,+45,90,-045]_s$ laminates. The mechanical properties of these materials can be found in Table 1. The laminate properties for the plates can be found in Table 2 and the low frequency extensional and flexural wave velocity can be found in Table 3.

Table 1. Material Properties

	E_{11} (MSI)	E_{22} (MSI)	G_{12} (MSI)	ν_{12}	ν_{21}	ρ (lbf-sec^2/in^4)
6061-T6 Aluminum	10.00	10.00	3.75	0.30	0.30	1.55×10^{-4}
AS-4(GR)/PR288 Graphite Epoxy	18.50	1.30	0.67	0.32	0.02	1.50×10^{-4}

Table 2. Laminate Properties

Material Lay-up		Thickness (inches)	Q_{11} (MSI)	Q_{22} (MSI)	A_{11} $\frac{lb}{in} \times 10^6$	A_{22} $\frac{lb}{in} \times 10^6$	$\frac{D_{11}}{in\text{-}lbs \times 10^3}{in}$	$\frac{D_{22}}{in\text{-}lbs \times 10^3}{in}$
6061-T6 Aluminum	--	0.0625	11.00	11.00	0.69	0.69	0.224	0.224
Graphite Epoxy	$[0]_8$	0.092	18.6	1.31	1.71	0.12	1.21	0.085
Graphite Epoxy	$[0]_{22}$	0.262	18.1	1.31	4.87	0.34	27.8	1.96
Graphite Epoxy	$[0,90]_{2s}$	0.095	--	--	0.940	0.940	.942	.480
Graphite Epoxy	$[0,45,90,-45]_s$	0.097	--	--	0.747	0.747	.891	.268

Table 3. Low Frequency Extensional and Flexural Wavelengths

Material	Stacking Sequence	Extensional Waves		Flexural Waves	
		V_1 (in/sec)	V_2 (in/sec)	V_1 (in/sec)	V_2 (in/sec)
6061-T6 Aluminum	--	207,695	207,695	$153\sqrt{f}$	$153\sqrt{f}$
Graphite Epoxy	$[0]_8$	352,136	93,452	$242\sqrt{f}$	$125\sqrt{f}$
Graphite Epoxy	$[0]_{22}$	352,136	93,452	$405\sqrt{f}$	$210\sqrt{f}$
Graphite Epoxy	$[0,90]_{2s}$	256,836	256,836	$226\sqrt{f}$	$191\sqrt{f}$
Graphite Epoxy	$[0,45,90,-45]_s$	226,583	226,583	$223\sqrt{f}$	$164\sqrt{f}$

III. EXPERIMENTS

A number of experiments utilizing low frequency acoustic waves were performed on several different laminates and aluminum to determine the applicability of the plate wave analysis presented in the previous section. A piezoelectric transducer, which acted as the acoustic generator, was excited using a gated sine wave. The gated sine wave provided an excitation signal with a very narrow frequency band while still retaining a definite leading edge.

A second piezoelectric transducer was used as the receiver. The position of the receiver was advanced a known distance and the change in time for a particular phase point noted from a digitizing oscilloscope. Dividing the displacement by the time yielded the phase velocity, from which the laminate stiffnesses were easily obtained.

3.1 Experimental Arrangement

Figure 3.1 is a schematic of the experimental arrangement for determining the phase speed in the plate. The excitation signal was generated by a signal generator which allowed the signal to be gated. The frequency of the signal was adjusted by the signal generator. The gate signal was created by a pulse generator. The amplitude, width, and repetition rate of the pulses were adjustable. The frequency of the signal was obtained from a frequency counter.

The signal from the signal generator, which had a peak-to-peak voltage of 20 volts was input into a piezoelectric transducer which converted the electrical signal into mechanical vibrations. The transducer was a Panametrics V401, 1"x ½ ", wide band transducer having a center frequency of 1 MHz. The transducer was acoustically coupled to the plate by a water soluble couplant.
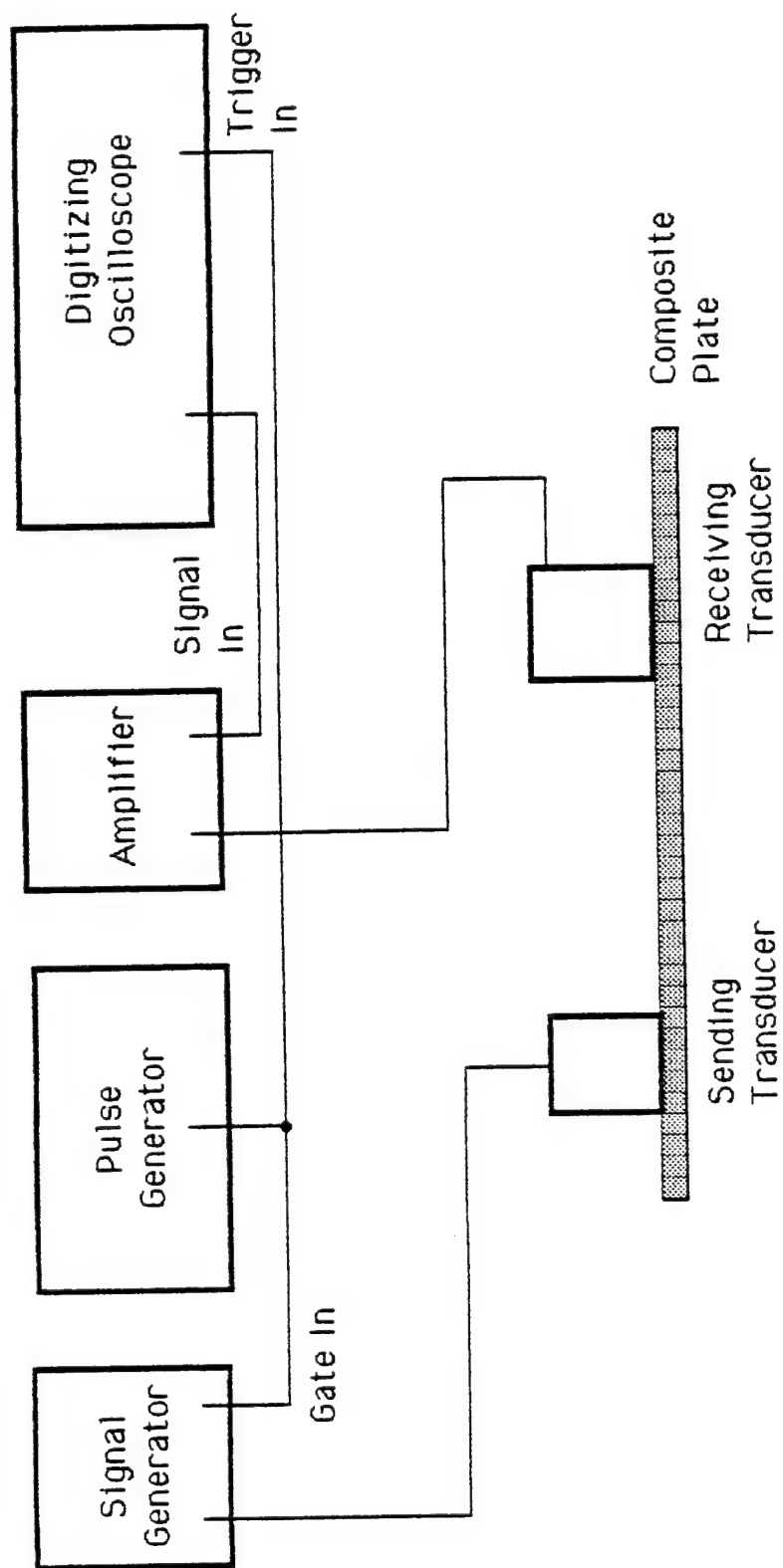
Fig. 3.1. Schematic of experimental arrangement for obtaining phase velocities in plates.

The acoustic signal propagating in the plate was detected by a second transducer which was a Panametrics V109, ½ inch diameter, wideband transducer having a center frequency of 5 MHz. The signal was amplified by a preamplifier and an amplifier and displayed on a digitizing oscilloscope. Both the transmitting and receiving transducers were mounted flat against the specimen surface.

The oscilloscope had movable cursors and a digital readout which corresponded to the position of the cursors in the time domain. This gave an accuracy in the time domain of ±0.5 microseconds. The digital oscilloscope had the capability of storing the waveform on disk and plotting the waveform on an x-y plotter.

3.2 Experimental Procedure

The experimental procedure consisted of first setting the signal generator to the desired frequency, usually between 10 kHz and 1 MHz. The cursor on the digitizing oscilloscope was then positioned on a particular point on the received wave, usually a peak, and the time noted. Next the receiving transducer was translated a fixed amount. The selected phase point on the wave was followed and the time noted again. The phase velocity is given by

$$V_p = \frac{d}{\Delta t}$$

where

    d = distance receiving transducer was translated

    Δt = change in time of point of phase

3.3 Data Reduction

The wave number was obtained from

$$k = \frac{V_p}{2\pi f}$$

for the frequencies at which data were obtained. Next the frequency and wave number were multiplied by the thickness of the plate which gave fd and kd. A plot was then made of fd versus kd. This is a dispersion curve, from which the phase velocities for any fd are obtained by taking the secant to the curve and the group velocities are obtained by taking the tangent of the curve at the value fd.

IV. RESULTS

Numerous tests were conducted on plates made from different materials and having a variety of thicknesses to determine the plausibility of applying the plate wave analysis to the wave modes transmitted in thin plates when one applies the stress wave factor technique. While obtaining data, it was noted that as the frequency of the excitation signal was increased, there existed a frequency at which there was an abrupt change in the phase velocity. Further investigation suggested that this was a change in mode from flexural wave propagation (the lower frequency signal) to extensional wave propagation (the higher frequency signal). Also, from observing the received signal, it was noted that the signals for the lower frequencies were dispersive while the signals at the higher frequencies were not.

Plots of kd versus fd were made with the values obtained from the analysis and from the experiments plotted on the same graph. Figures 4.1 through 4.7 are graphs of the experimental data (points) and theoretical results (curves) for the materials tested. To emphasize how the experimental points were taken, we note the following: Data points were first taken by applying the lower frequencies to the transducers. As the frequency was increased, the data points marched up along the lower curve. At a critical frequency, the generated wave mode changed discontinuously so that suddenly a higher velocity mode was generated. This resulted in a point appearing at the lower end of the higher curve in Figs. 4.1-4.7. With further increase in frequency, the data points marched up along the higher curve.

There is an excellent correlation between the experimental data and theoretical results for the higher (longitudinal) mode , kd=0.5 for all
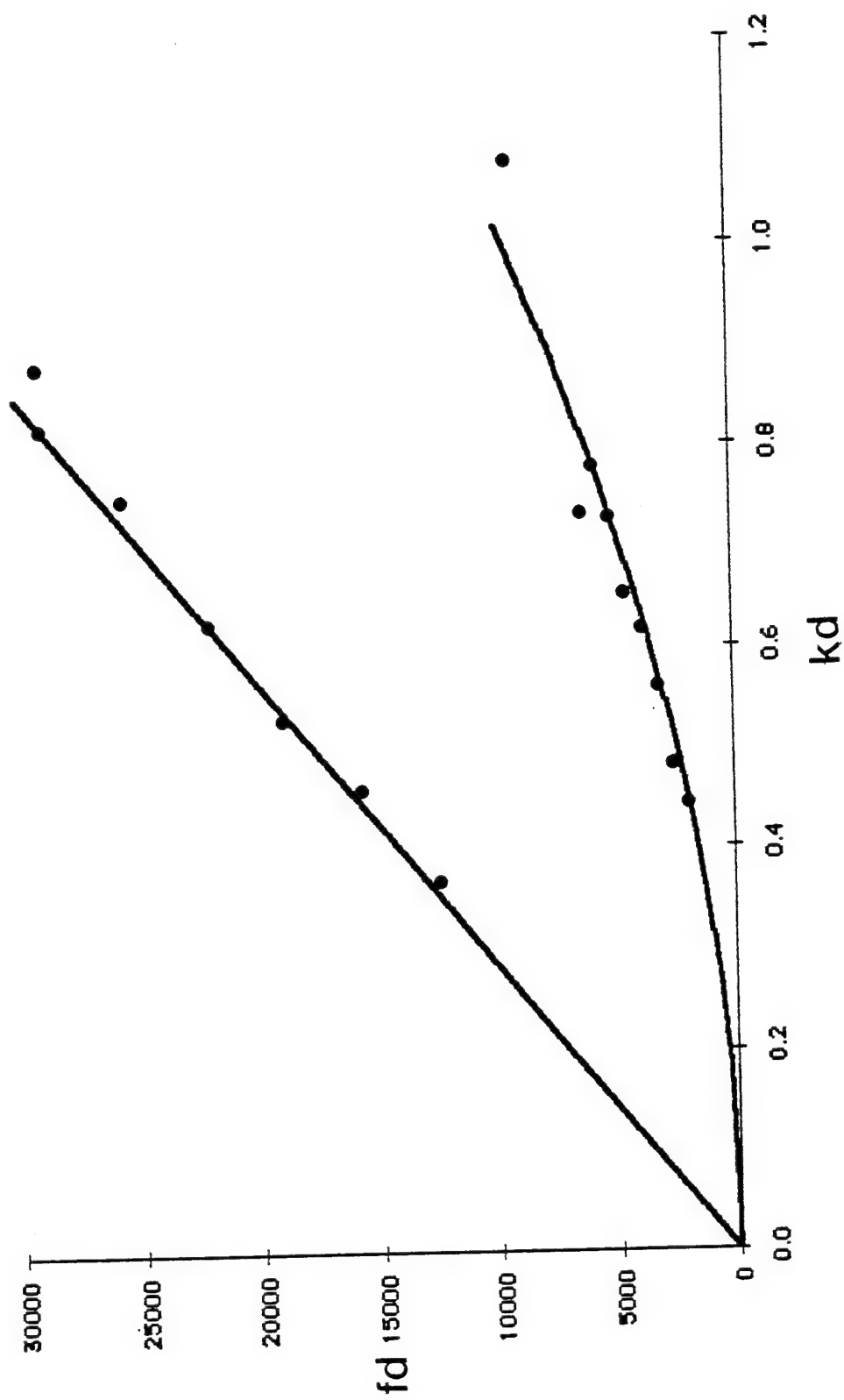
Fig. 4.1. Low frequency dispersion curve for aluminum plate.

Fig. 4.2. Low frequency dispersion curve along the x_1 axis for graphite epoxy plate.

The legend shows:
- ● 0.092" Graphite/Epoxy
- ○ 0.092" Graphite/Epoxy
- ■ 0.262" Graphite/Epoxy
- □ 0.262" Graphite/Epoxy
- —— Calculated Extensional Wave
- —▲— Calculated Flexural Wave

Axes: fd (vertical, 0 to 200000), kd (horizontal, 0.0 to 3.0)

Fig. 4.3. Low frequency dispersion curve along the x_2 axis for graphite epoxy plate.

Legend:
● 0.092" Graphite/Epoxy
○ 0.262" Graphite/Epoxy
— Calculated Extensional Wave
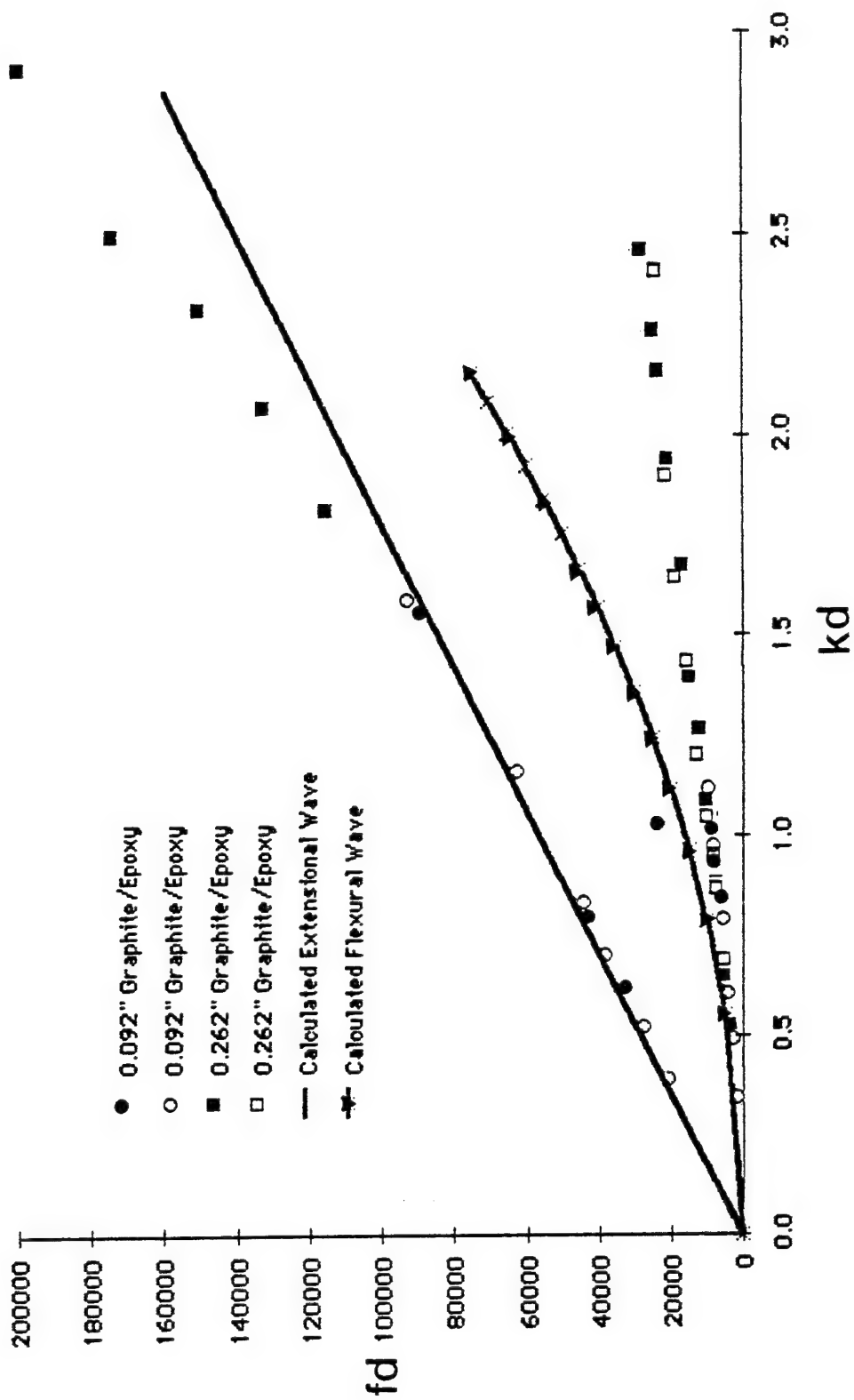+ Calculated Flexural Wave

Fig. 4.4 Low frequency dispersion curve along x_1 axis for $[0,90]_{2s}$ graphite epoxy plate.
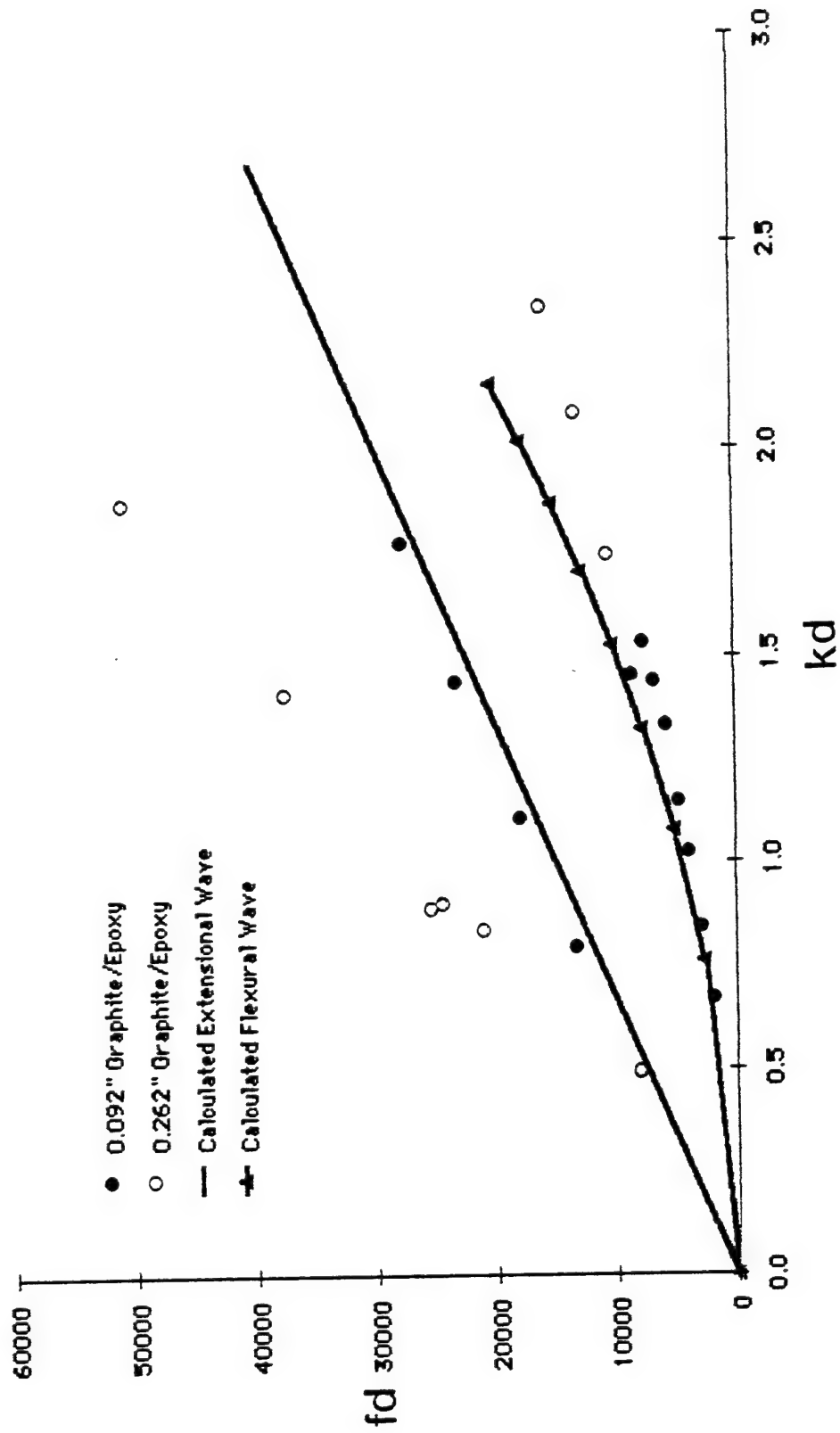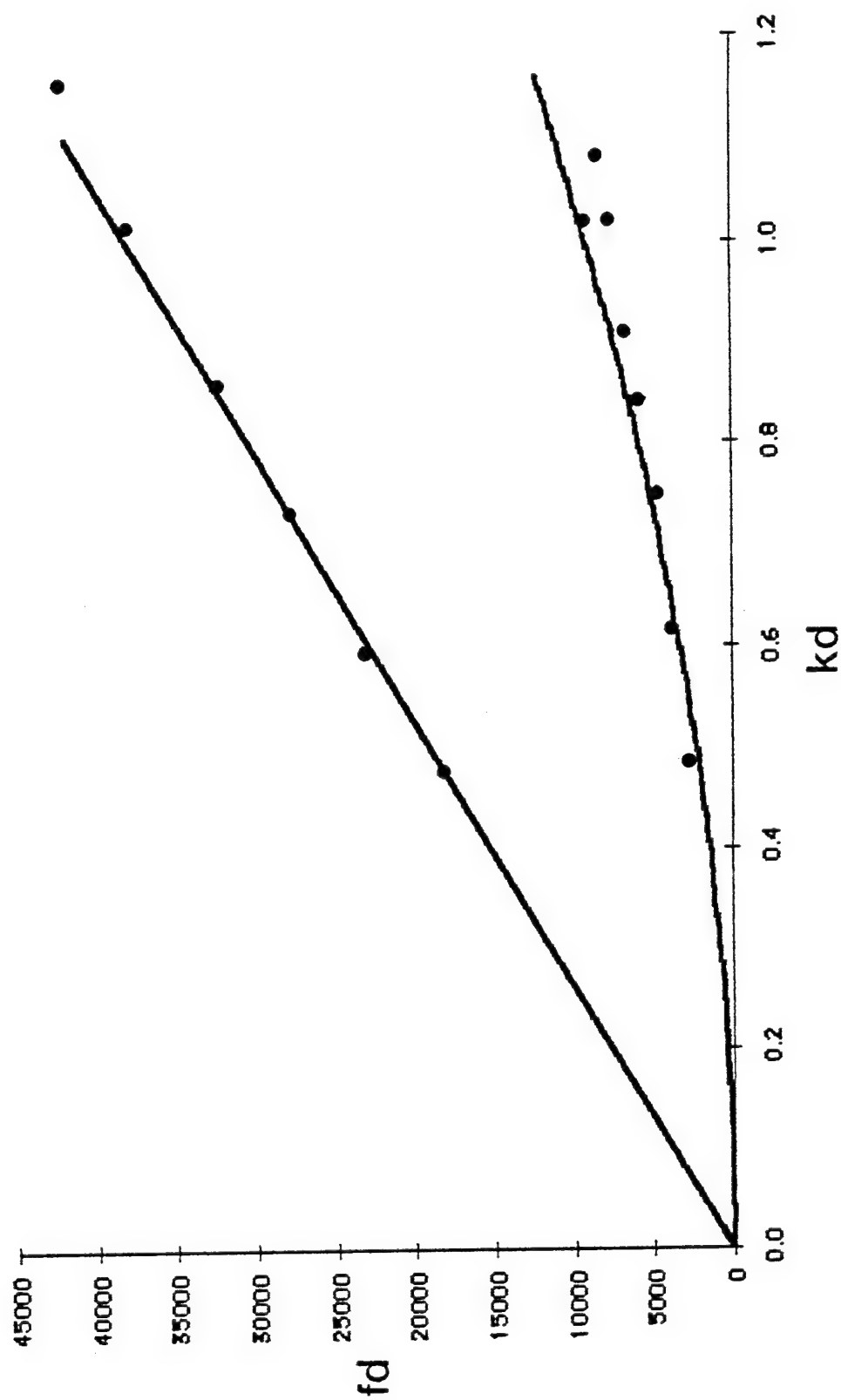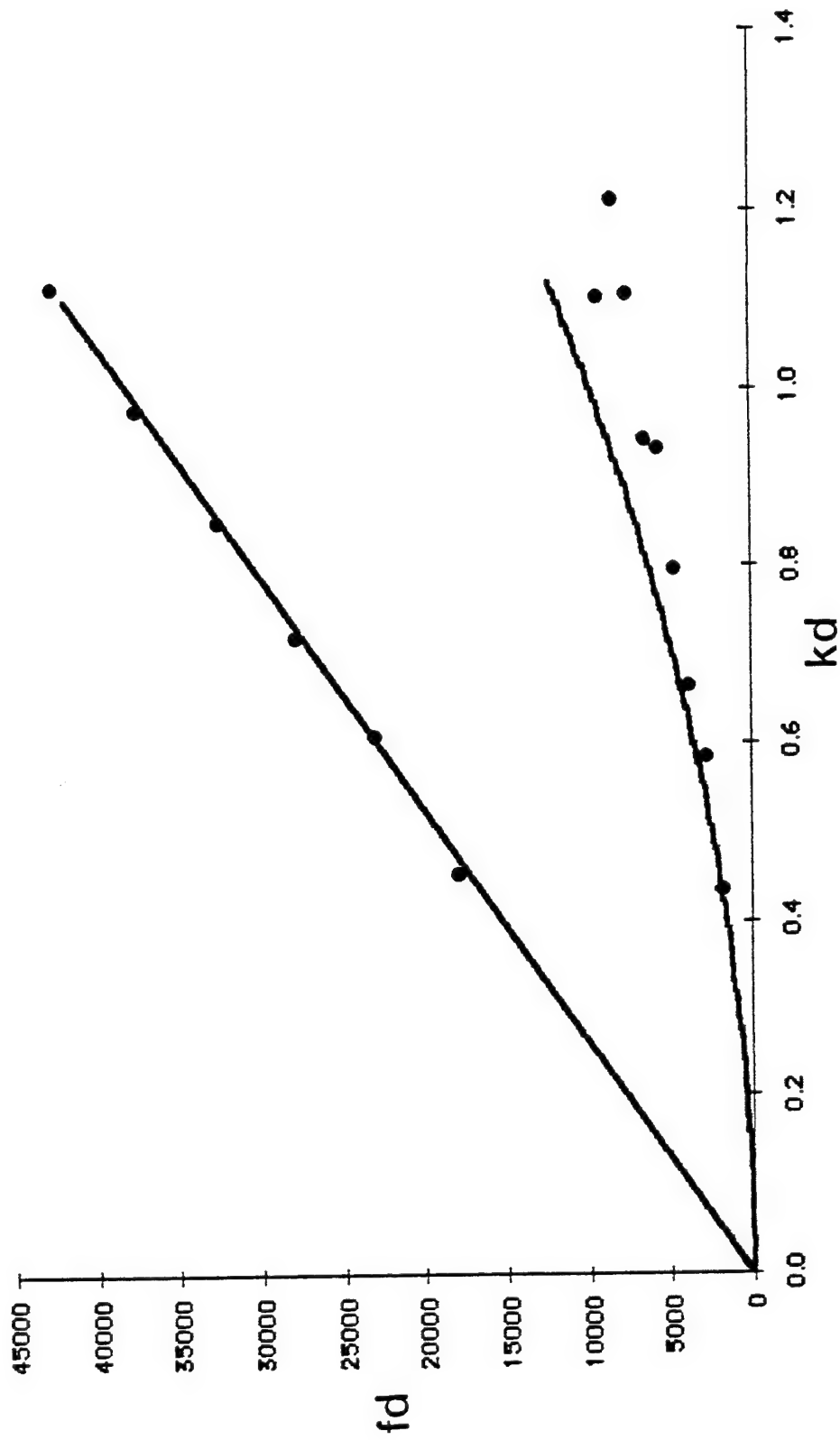
Fig. 4.5   Low frequency dispersion curve along x_2 axis for $[0,90]_{2s}$
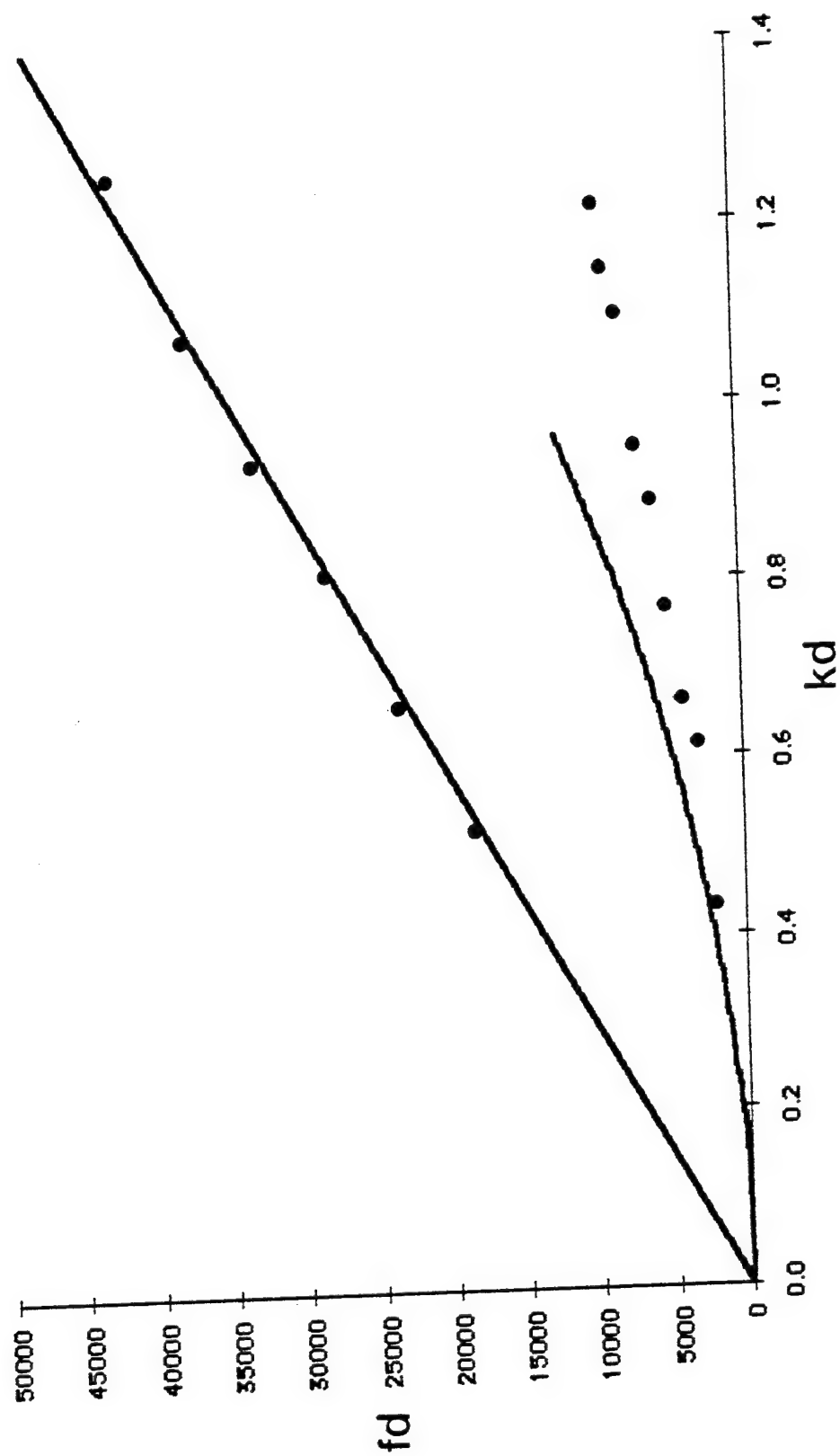graphite epoxy plate.

Fig. 4.6 Low frequency dispersion curve along x_1 axis for [0,45,90,-45]s graphite epoxy plate.
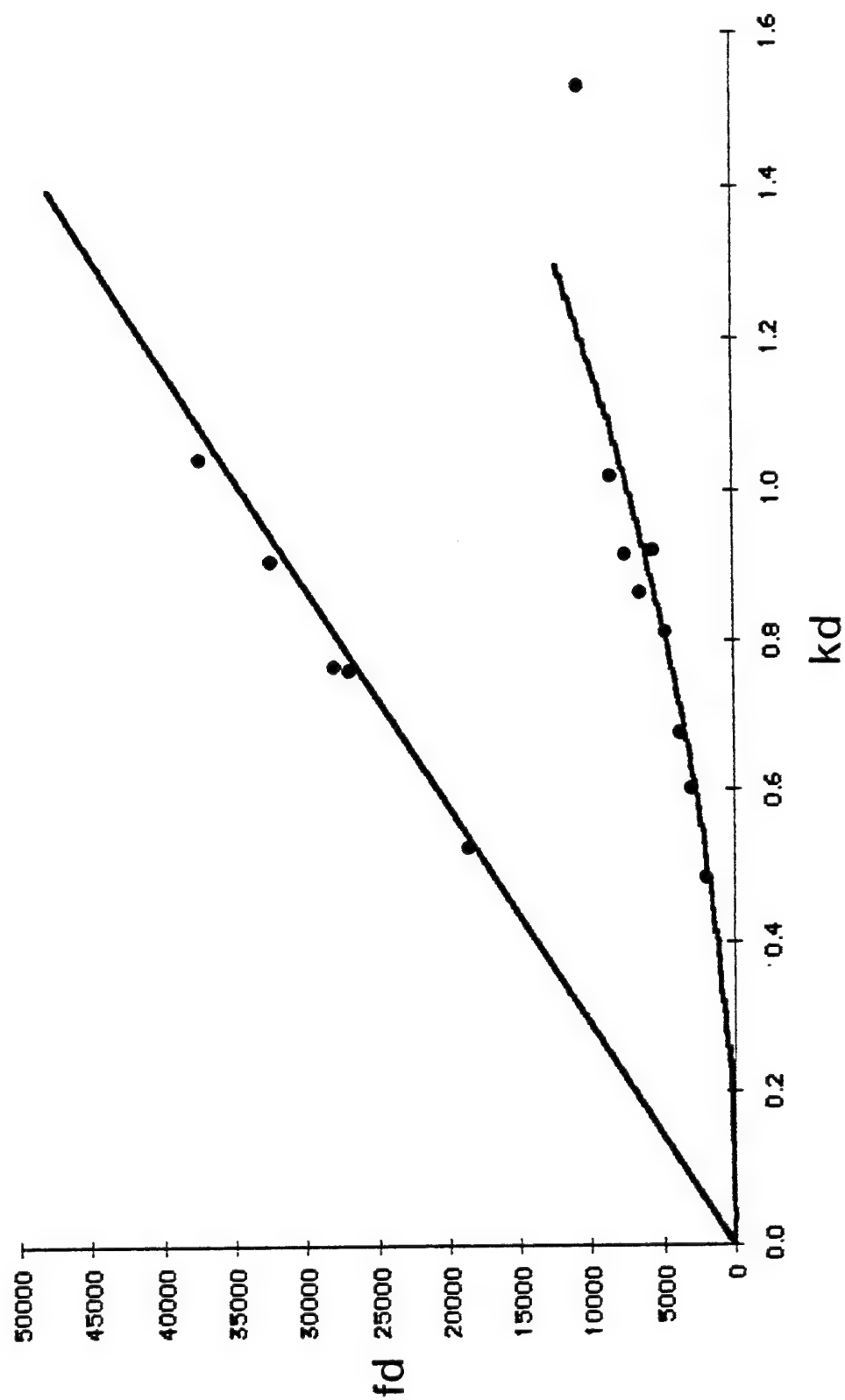
Fig. 4. 7   Low frequency dispersion curve along x_2 axis for [0,45,90,-45]s graphite epoxy plate.

frequencies tested, and for the flexural mode for frequencies up to kd>0.5 the thin plate assumption may no longer be valid for the flexural mode and a better approximation is needed. Also, the flexural mode is noticeably dispersive and it is somewhat more difficult to measure the phase speed. From these plots, the extensional stiffnesses A_{11} and A_{22} can easily be found if the density of the material is known.

The experimental data and analysis clearly indicates that at low frequencies acoustic energy is propagated by the fundamental extensional and flexural plate modes. This could explain the nature of the waves generated when one applies the stress wave factor technique.

For example, Govada [5] used a 5 MHz, wide-band transducer to launch an acoustic wave in a composite specimen. However, a spectral analysis of the received signal showed a frequency content much lower than 5 MHz. For an undamaged $[0,90_2]_s$ graphite epoxy specimen, Govada obtained a tri-modal frequency distribution with frequencies centered around 250 kHz, 750 kHz, and 1 MHz.

With the exception of the fundamental extensional and flexural mode, plate modes exhibit cut-off frequencies for which waves having a frequency content below the cut-off frequency will be attenuated. The lowest cut-off frequency for a plate, which occurs for an antisymmetric mode, is

$$ f = \frac{V_s}{2d} $$

For the $[0,90_2]_s$ coupon, d = 0.030" and V_s = 60,000 in/sec gives the lowest cut-off frequency at 1 MHz. Plate waves having a frequency less than 1 MHz will propagate as one of the fundamental modes. So the type

of plate modes observed in the stress wave technique are in all probability the fundamental extensional and flexural modes.

The reason higher modes do not propagate requires further investigation. It may simply be that higher modes are more rapidly attenuated and hence become lost in the noise level when one is making a measurement.

References

1. Stiffler, R. C. and Henneke, E. G., "The Application of Low Frequency Acoustic Waves for Determining the Extensional and Flexural Stiffnesses in Composite Plates," Interim Report to General Electric Co., Contract No. 14-G-45-480, September 1985.

2. Vary, A. and Bowles, K. J., "Use of an Ultrasonic-Acoustic Technique for Nondestructive Evaluation ofFiber Composite Strength," NASA TM-73813, 1978.

3. Vary, A. and Bowles, K. J., "Ultrasonic Evaluation of the Strength of Unidirectional Graphite-Polyimide Composites," NASA TM-X-73646, 1977.

4. Vary, A. and Clark, R. F., "Correlation of Fiber Composite Tensile Strength with the Ultrasonic Stress Wave Factor," NASA TM-78846, 1977.

5. Jones, Robert M., Mechanics of Composite Materials, (McGraw Hill Book Co., New York, 1975).

6. Govada, A. K., Duke, J. C., Henneke, E. G. and Stinchcomb, W. W., "A Study of the Stress Wave Factor Technique of the Characterization of Composite Materials," NASA CR-174870, February 1985.

Part III

NONCONTACTING DETECTION IN ULTRASONIC NDE OF MATERIALS:
SIMPLE OPTICAL SENSOR AND
FIBER OPTICS INTERFEROMETRIC APPLICATION

A. Sarrafzadeh-Khoee and J. C. Duke, Jr.

Abstract

An optical displacement sensor based on the two-beam interferometry of coherent light using two principal diffracted orders of a fine reflection blazed grating is constructed. The inherent capability of the interferometer for absolute calibration, its maximum sensitivity adjustment, and the simplicity of the configuration of its components are explained.

Utilization of a single-mode optical fiber in the test arm of the interferometer to enhance the geometric flexibility of the optical system is demonstrated.

The sensor's application in the noncontacting detection of stimulated ultrasonic stress waves for nondestructive evaluation of advanced composite materials is emphasized. The detected signal is digitized and recorded using an IBM PC with a plug-in data acquisition board. The combination of high sampling rate capability of the device, Fast Fourier Transformation of data, and optical detection has facilitated the spectral analysis of ultrasonic signals in order to achieve interpretation and quantification of the physical parameters of interest.

Introduction

The acousto-optical techniques for the detection and analysis of ultrasonic stress waves have been of major interest to many investigators due to increased ultrasonic applications in nondestructive testing and materials evaluation [1,2]. Most physical effects are transformed into displacement. Different optical set-ups can be constructed and optimized for looking at a particular particle disturbance (out-of-plane/in-plane displacement) of the material under study. Ordinarily these optical transducers act as displacement sensors; therefore, any other related physical quantities can be derived from the displacement magnitudes.

The main advantages for using optical sensors are that they are noncontacting so that no alteration of actual surface displacement occurs. They can be used in hostile environments, in particular for high temperature materials characterization. They are sensitive -- e.g., displacements of subangstrom magnitudes can be measured. Because of the ability to focus the laser beam on a spot-sized region, point-by-point interrogation of the surface and complete characterization of the displacement field is readily accomplished. Following the suggestion made in Ref. [3], a unique optical arrangement is designed in a Michelson-type interferometer using a blazed diffraction grating as a beamsplitter and recombiner.

System of Two-Beam Interference

A plane reflection blazed grating is shown in Fig. 1. The grating is constructed by a number of densely packed right angle prisms grooved
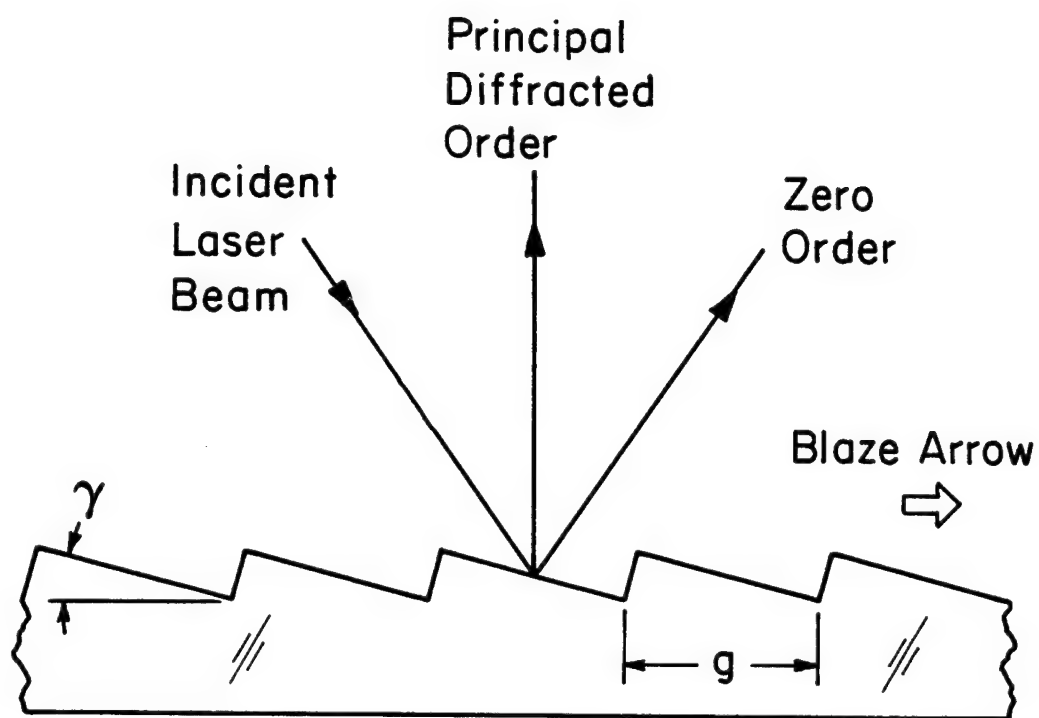
Fig. 1. Single-order blazed reflection grating, (γ = blaze angle, g = grating pitch).

on the surface of a plane glass block on which a thin layer of aluminum has been deposited for increased relfectivity. In contrast to ordinary (amplitude or phase) diffraction gratings where the undiffracted (zero) order has the stronger intensity, in a blazed diffraction grating the stronger intensity is shifted to some higher order. Consequently, the blazed grating has· a higher diffraction efficiency compared to its counterparts. For a given optical wavelength, the intensity of the diffracted beams, in general, is the function of the shape, angle, and depth of the grooved surfaces and of the grating surface reflectivity. The angle of the principal diffraction order is solely determined by the proper choice of the wavelength used and by grating spacing (pitch). As shown in Fig. 1, the angle of incidence can also be chosen so that the dominant diffracted order from the fine blaze grating bisects the angle between the dominant zero order and the incidence. Such an arrangement will provide a single-order blazed diffraction grating with two dominant orders of near equal intensity.

As was mentioned previously, when the correct light wavelength is used, when the spacing of linearly groved surfaces is proper, and when the selection of the blaze angle is correct, the grating behaves such that an incident coherent beam of the laser emerges in two dominant diffracted orders, e.g., the zero and the first order. Referring to Fig. 2, consider the conditions where a) the incident angle is in a direction normal to the grating plane. In this case the undiffracted beam also emerges in the direction normal to the grating and the principal diffracted beam emerges at twice the blaze angle with respect to normal incident direction. The latter is the natural direction of reflection from grooved surfaces. b) The incident angle is twice the
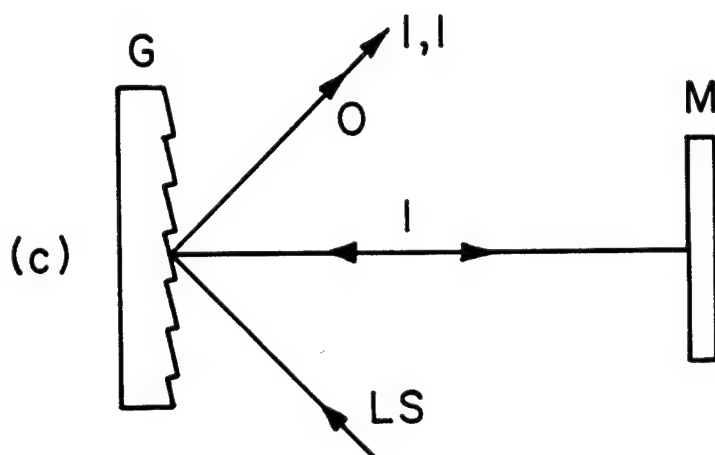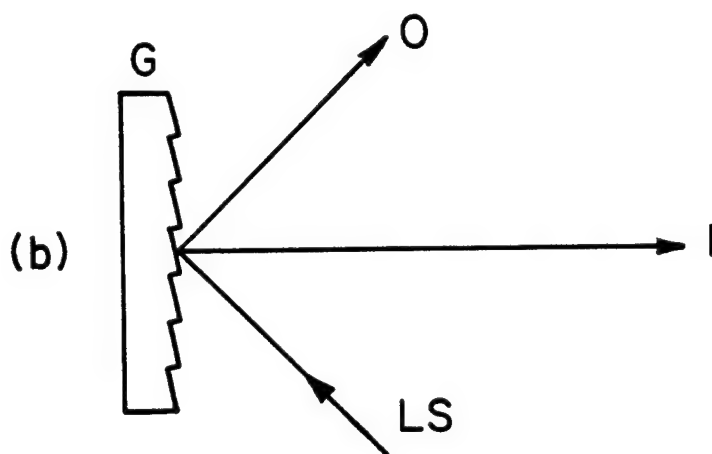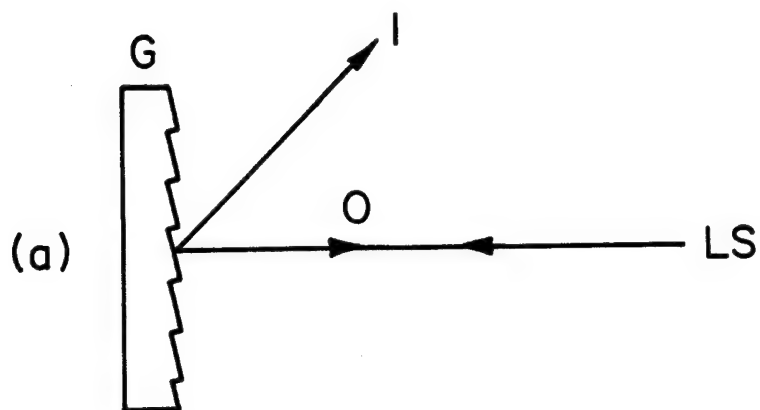
Fig. 2. Diffraction action of a fine reflection blazed grating.
         (a) normal incidence; (b) twice the blaze angle incidence;
         (c) two-beam interference from simultaneous action of (a) and (b).

blaze angle with respect to the grating normal and oriented toward the blaze arrow. In this case the first order beam bisects the angle between the zero order and the incident direction. Interestingly enough, this diffracted beam is along the direction normal to the grating plane. c) In arrangement (b), if a mirror is placed perpendicular to the first order direction and if the action of arrangement (a) is added, a two-beam interferometric system is developed. The reference arm of the interferometer is the zero order -- the natural reflection of the incident beam from grating plane -- and the sensing arm is the first order diffraction. The sensing arm after reflection from the test surface is diffracted again by the action of the grating. Consequently, the resulting first order diffraction of the original first order is superimposed upon the original zero order diffraction and produces an interference pattern. The system of the unequal-path interference of these two beams is the basic optical component of the entire sensor. This two-beam unequal-path interferometer, as well as any of the Michelson-type interferometers, is only sensitive to the out-of-plane displacement of the motion of the surface under interrogation.

Phase Displacement vs. Optical Intensity

The test arm and the reference arm are the two interfering coherent beams of the optical system. The phase change in the test arm with respect to the reference arm is introduced due to the distance between the grating and the surface under study. This distance will change due to surface displacement fluctuation caused by the presence of ultrasonic stress waves. In that case, the phase displacement is written as

$$\phi = 2K1 + 2K\delta$$

where

  1 = optical distance between grating and the test surface

  $K = 2\pi/\lambda$, optical wave number

  $\delta = \Delta\cos \omega t$, amplitude of surface displacement

  $\omega = \pi f$, angular frequency of the oscillation.

The factor of two in the expression for the phase displacement denotes the fact that light travels twice through the optical path between the grating and test surface. If both superposing beams of the interferometer have the same optical intensity (this is a reasonable assumption since both zero order and first order diffractions of the blazed grating have relatively close intensities), upon superposition, the interferometric intensity deviates from a minimum of zero to a maximum of four times the intensity of each beam (I), depending on the phase difference between the two beams. In general, the cosine squared expression for the intensity of the two-beam interference [4] is written as

  $I' = 4I(\cos \phi/2)^2$

   $= 2I[1+\cos(2K1+2K\Delta\cos \omega t)]$.

If the spacing between the grating and the test surface is such that it introduces a phase of $\pi/2$ radians, then

  $I' = 2I[1+\cos[\phi/2+2K\Delta\cos \omega t)]$

   $= 2I - I''$.

The interferometric term is

  $I'' = 2I \sin(2K\Delta\cos \omega t)$.

If the amplitude of the surface displacement is much smaller than the optical wavelength, $\delta \ll \lambda$, the sine can be approximated to be equal to its argument. Thus,

$I'' = rIk\Delta\cos \omega t$. This linear relationship between the instantaneous surface displacement, δ, and the optical intensity (time-averaged of the optical field) is the prime factor in the use of such a two-beam interferometer for detection.

The variation in the light intensity due to surface disturbance of the test sample can be photoelectrically observed. The photodetector converts the optical power into an electrical current. For a photodetector with a quantum efficiency of α, the RF signal current produced by the incident optical intensity is

$$i_s = \alpha I''.$$

The sensitivity of the detected signal is limited to the presence of the noise inherent in the detecting system. This would include: laser noise (optical) caused by fluctuation of laser power output, Johnson noise (thermal) caused by the load resistor of the photodetector, the electronic noise in the electronic signal processing components, and shot noice (photon) of the square-law detector, which is considered to be the most limiting factor in sensitivity. Other sources of noise, which will be taken into consideration in a later section, are low-frequency environmental noises (mechanical and thermal).

The dc optical power, 2I incident on the photodetector, gives rise to the rms shot noise current. That is,

$$i_n = \left(2eI_{dc}B\right)^{\frac{1}{2}}$$

where

I_{dc} = averaged optical intensity on photo-diode

B = detection bandwidth

e = electron charge.

The minimum detectable displacement amplitude is obtained when noise current and signal current are equal (S/N=1), i.e., $i_n = i_s$. Thus, in terms of output laser power, P, the maximum detectable displacement is written as

$$\delta_{min} = (2eB/\alpha\eta P)^{\frac{1}{2}}\lambda/4\pi$$

where η = optical system efficiency. The theoretical minimum detectable displacement for a He-Ne laser, P = 10 mW, α = 0.4 W/A, B = 5MHz, and $\eta \simeq$ 80% is calculated to be about 0.01 Å.

Calibration and Large Phase Shift

The optical interferometer described earlier has the same sensitivity as any of the Michelson-type interferometers. The output of the interferometer can be calibrated so that the absolute magnitude of the surface displacement can be determined. If the surface under study is subjected to large displacement excitations ($\delta > \lambda/4$) and the peak-to-peak signal output is noted, then the magnitude of the smaller displacements ($\delta < \lambda/4$) can be obtained from its peak-to-peak signal output.

As was mentioned earlier, the interference of two equal-intensity beams has a magnitude which varies between two extreme opposite values depending on the relative phase difference (ϕ) between the test and reference beams. For the interferometer to operate at the point of maximum sensitivity (i.e., smallest phase shift giving rise to largest change in intensity), the relative phase must be kept constant halfway between the two limiting phases throughout the operation [5]. Unfortunately, the presence of low-frequency mechanical and thermal fluctuations existing in the testing environment alters the proper

tuning. To solve this problem, a slight modification to the optical system of Fig. 2 may suffice -- the blazed diffraction grating can be driven by a low-frequency piezoelectric crystal at a large displacement amplitude so that the face of the grating translates at least an amount $\lambda/4$. this causes the passage of phase difference through the optimum point of sensitivity at the time of high-frequency transient surface fluctuations. The frequency of the phase shifter should be low enough to allow the entire signal to be detected at the maximum operating condition. Through the use of this large phase shifter, the interferometer can also be calibrated.

Fiber Optics Interferometric Application

The use of optical fibers as a light guiding medium can be a great advantage in optical probing flexibility [6]. In this regard, an attempt has been made to utilize single-mode-step-index fiber optic interferometry. There are special kinds of single-mode optical fibers that preserve the state of linearly polarized light, which is necessary to maintain in the interferometric application. These types of bi-refringent fibers have geometric flexibility and allow the test arm of the interferometer to be isolated from the bulky optical table. There are two classes of fiber optic sensors. In one application the fiber itself is used as a sensing device. In another application it is used to simply guide the optical wave through its medium. The latter has been incorporated into our two-beam unequal-path interferometric system. The optical system shown in Fig. 3 is the optical fiber link extension of the probing arm of the previously discussed interferometer. The test arm of the interferometer in the air medium
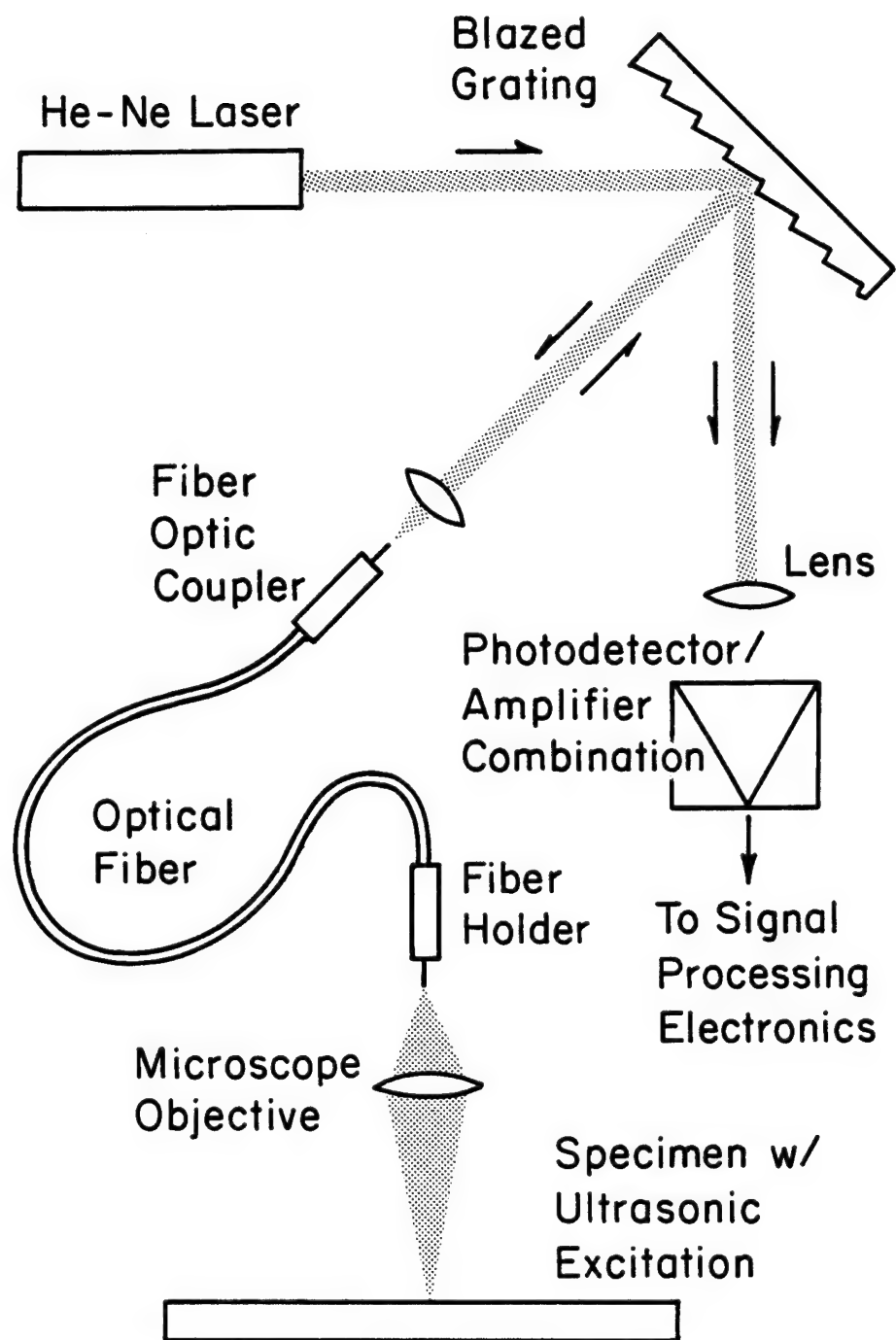
Fig. 3. Schematic diagram of a flexible single-mode fiber optics
interferometric system.

has been coupled into the fiber medium using a microscope objective to focus the beam on the front flat surface of the stripped fiber. The second microscope objective provides the beam illumination and reception from the reflective surface under study. The use of an interferometric fiber optic sensor in this fashion allows the ultrasonic scanning of the reflective surface of a stationary object which is located away from the bulky optical bench.

Spurious fringes may occur as a result of the interference of some reflected light from the front face of the optical fiber (i.e., at the focused laser beam-to-fiber interface). Since these unwanted fringes may superimpose upon the actual interference pattern, care should be taken to minimize this contrast limiting effect. For the maximum fringe visibility, the total optical path length traveled by the test arm of the interferometer must be an integral multiple of twice the laser cavity, as long as it does not exceed the coherence length of the laser source. Thus, by proper positioning of the fiber coupler with respect to the grating, and of the probing fiber coupler with respect to the surface under study, and by correct choice of fiber length, one can establish the condition under which the maximum contrast will emerge in the interference pattern but not in the unwanted fringes.

Preliminary Results

The schematic diagram in Fig. 4 shows a data processing procedure used in optical detection of ultrasonic stress waves. As a demonstrative exercise, a repetitive electronic short pulse was transmitted to drive a 1 MHz PZT transducer of the thickness-dilatation type which was coupled acoustically to one side of a unidirectional
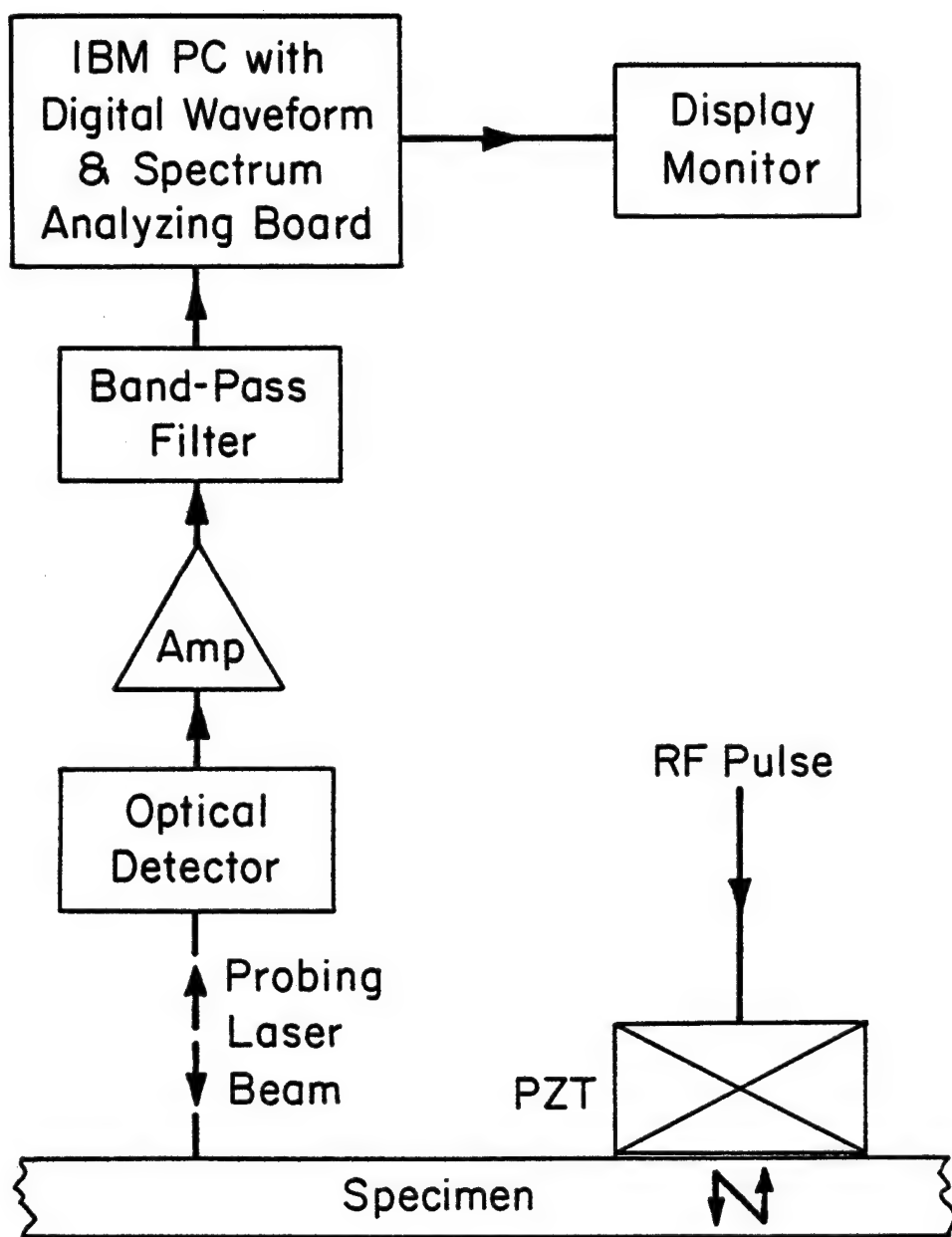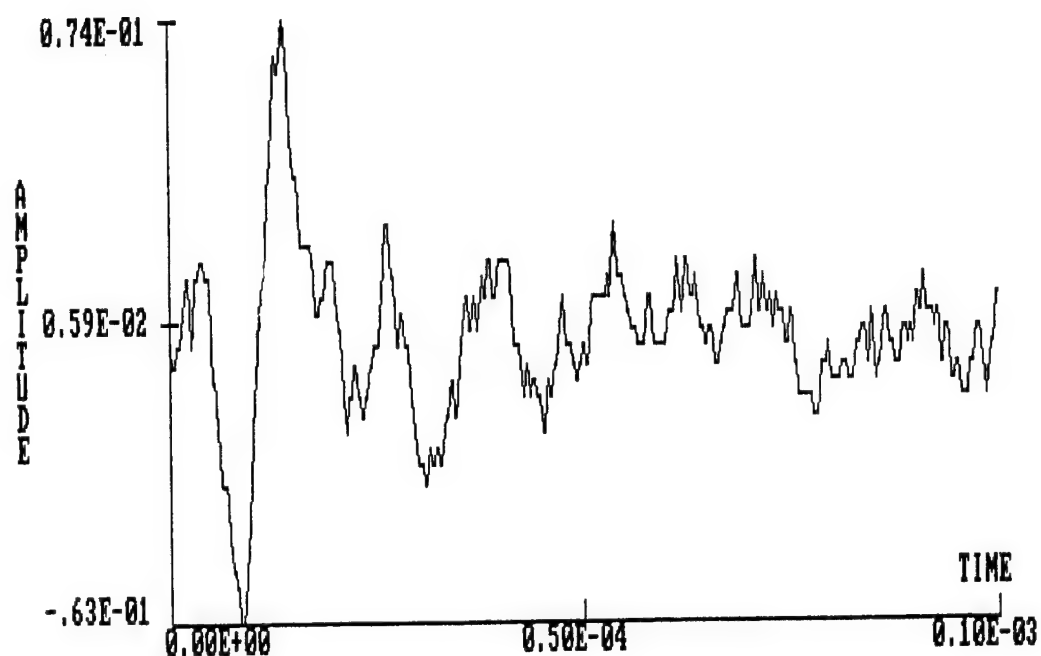
Fig. 4.   Schematic diagram of an NDT using ultrasound, optical detection
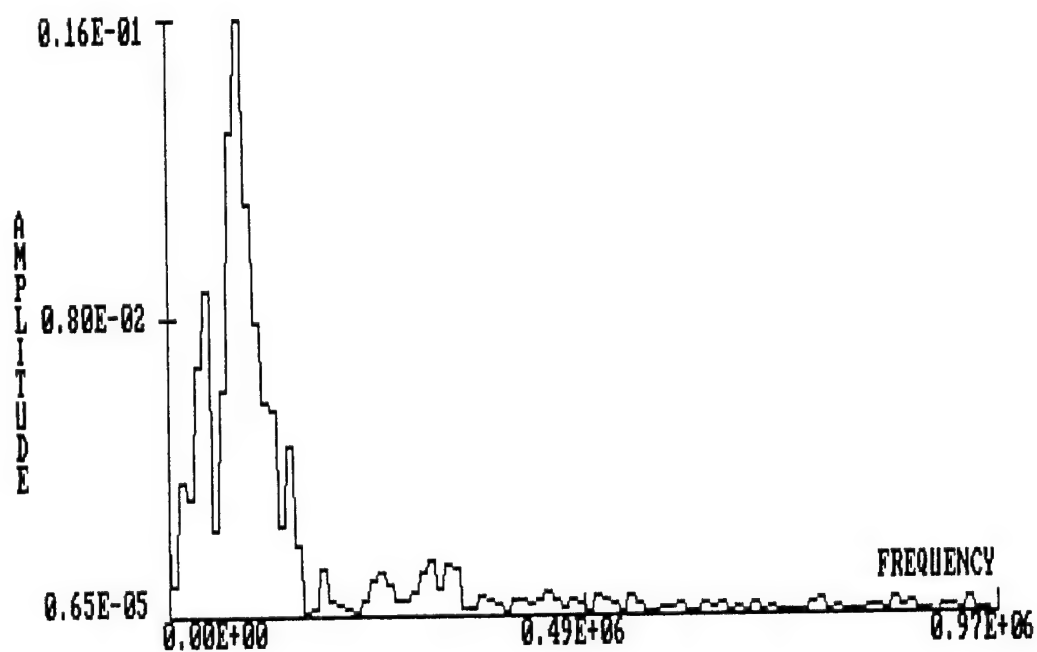and spectral analysis.

fiber-reinforced composite laminate. The interrogation point on the same side of the specimen was mirrorized for light reflectivity. Then three different transducer positions about 1 inch from the point were chosen such that the transducer could propagate plane waves parallel to, off-axis to, and perpendicular to the fiber axis. The resultant surface displacement excitations were detected by the linear optical sensor (arrangement in Fig. 3). After signal amplification and suitable filtering, the information pertaining to the amplitude and frequency of acoustic disturbances was obtained. Both the time-domain and frequency-domain amplitudes of the detected stress waves for the aforementioned transducer positions are shown in Fig. 5(A)-(D), respectively. The spectrum of the signal is not shown for the curves (C) and (D) because no change in spectrum has been noticed for all three of these cases. Note that the magnitude of surface displacement is larger in curve (C) than in curve (A) and is drastically reduced in curve (D). This is contrary to the results found in homogeneous isotropic materials in which the magnitude of signals for all three transducer locations would have been equal.

NDT Applications

Low-power ultrasound is one of the NDT methods which has long been used for materials' mechanical characterization through the determination of acoustic wave parameters of interest (e.g., velocity, frequency, amplitude, attenuation, etc.). The sources for such an ultrasonic regime are generated either by the materials themselves -- acoustic emission -- or by external means -- acoustic stimulation. To
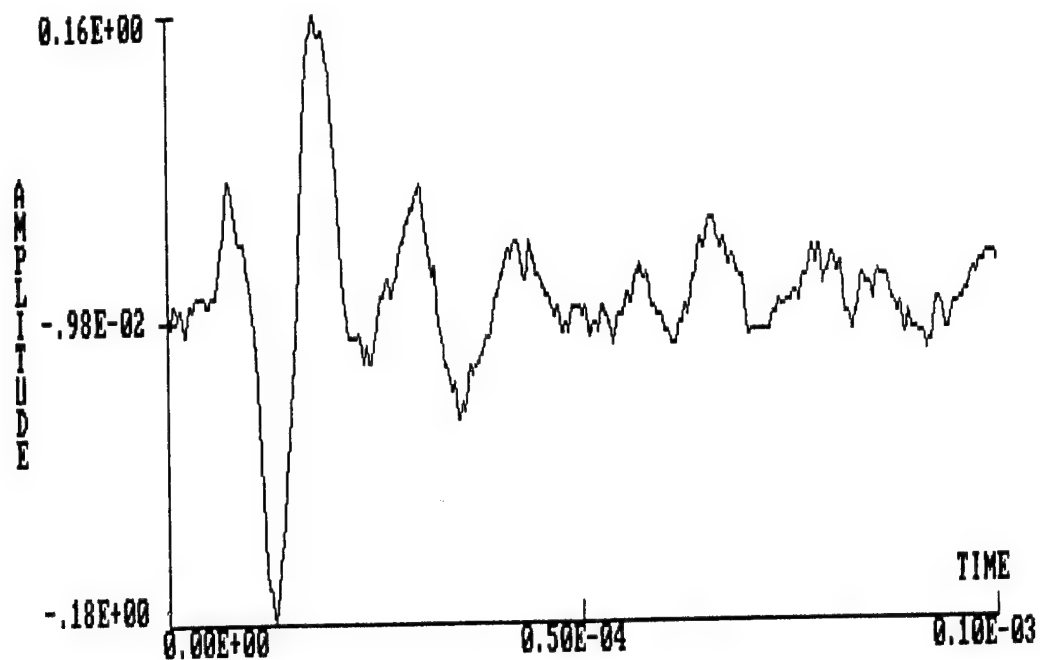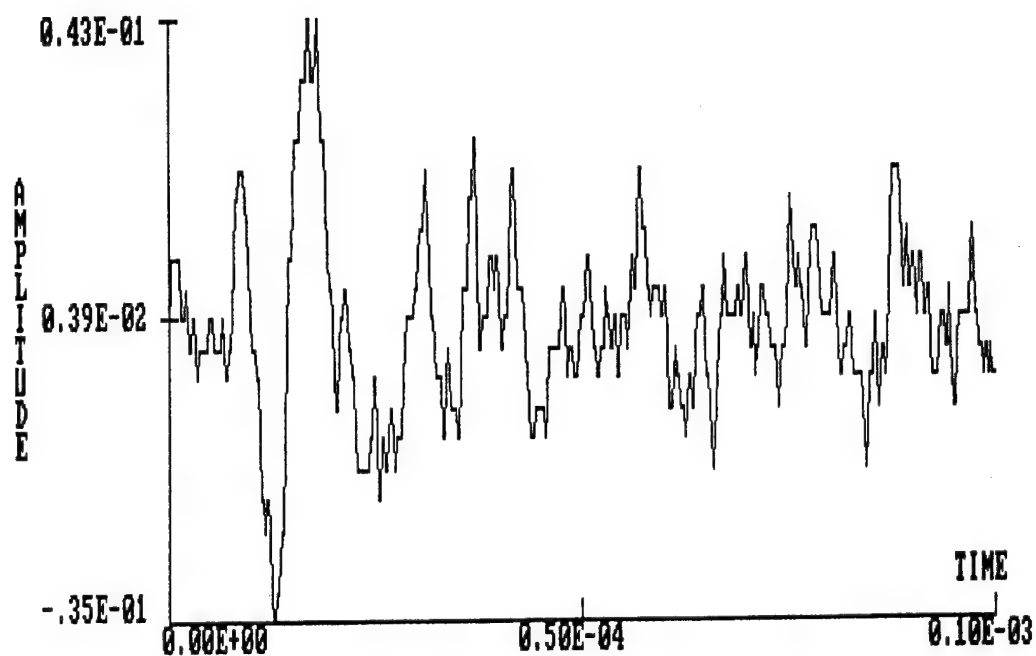
Fig. 5. Plots of optically detected ultrasonic signals. a) Direction of propagation parallel to fiber direction. b) Frequency spectrum of the signal shown in a).

III-15

(c)

(D)

Fig. 5.   (cont.) c) Direction of propagation off-axis to the fiber
          direction.   d) Direction of propagation perpendicular to the
          fiber direction.

III-16

quantitatively characterize materials using ultrasonic methods, a well characterized quantitative detection method in conjunction with a well characterized source of ultrasonic excitation must be used. The applications of noncontacting optical sensors, along with optical generation of ultrasound , are conducive to a more refined analysis in NDE.

Conclusion

The analysis of this optical system shows that the stress wave causes a change in interferometric light intensity due to surface disturbance. The deviation in light intensity is detected photoelectrically. The output signal is found to be proportional to the instantaneous surface displacements. Through suitable calibration of the system, the absolute measurement of surface displacements, is obtained. The ultimate sensitivity of these interferometric optical transducers is limited in part, due to the photodetector shot-noise current, and in part due to optical path length differences. The small optical wavelength gives rise to much smaller optical path length differences which may be less than the atomic dimension.

The basic optical arrangement described in this paper is a simple one in which the reflection blazed diffraction grating is the primary component of the interferometer. Through a simple rearrangement of the previously discussed optical configuration, e.g., by reversing the blaze arrow orientation and selecting the zero order as the sensing arm, a similar two-beam interferometer is formed. In this case, the mechanical movement of the grating does not introduce any optical path difference between the first and the zero order beams of the interferometer.

Therefore, unlike the Michelson interferometer, this arrangement is not sensitive to the low-frequency noise associated with the mechanical vibration of the reference mirror.

In the ordinary Michelson interferometer, only half of the laser power is utilized and the other half is fed back into the laser. The optical intensity returning to the laser might alter the laser power output which in turn might cause an increase in the signal noise level and reduce the sensitivity. The feedback problem is usually solved by using optical or acousto-optical isolators [7] which effectively prevent any light from entering the laser. In another treatment of the problem, a dual-quadrature Michelson interferometer [5,8] is constructed basically to use advantageously the complementary optical intensity pattern which was fed back to the laser. For our interferometer, which utilizes a single-order blazed diffraction grating, most of the energy of the incident laser beam is distributed into the zero and the first order so that very little light corresponding to the second order diffraction is returned to the laser.

The addition of an optical fiber to the test arm of the interferometer as a light-guiding medium has been shown to be a great advantage in optical probing flexibility. For this reason, an attempt to utilize single-mode fiber optic interferometry for remote sensing is justified.

References

1. Palmer, C. H. and Green, R. E. Jr., "Materials Evaluation by Optical Detection of Acoustic Emission Signals," Materials Evaluation, Oct. 1977, pp. 107-112.

2. Palmer, C. H. and Green, R. E., Jr., "Optical Probing of Acoustic Emission Waves," Nondestructive Evaluation of Materials, John J. Burke and Volker Weiss, Eds. (Plenum Press, 1979) pp. 347-378.

3. Munnerlyn, C. R., "A Simple Laser Interferometer," App. Opt. 8(4), 1969, pp. 827-829.

4. Hecht, Eugene, "Optics, Schaum's Outline Series (McGraw-Hill, Inc., 1975) p. 126.

5. Mezrich, R., Etzold, K. F. and Vilkonerson, D., "System for Visualizing and Measuring Ultrasonic Wavefronts," RCA Rev. 35, 1974, p. 483.

6. Dakin, J. P., "Optical Fibre Sensors-Principles and Applications," Proc. No. 53 (Int'l. Conf. on) Fibre Optics, London 1982, pp. 39-47.

7. Kroll, M. and Djordjevic, B. Boro, "A Laser Stress-Wave Probe with Sub-angstrom Sensitivity and Large Bandwidth," 1982 Ultrasonic Symposium, pp. 864-866.

8. Mezrich, R., Vilkomerson, D. and Etzold, K., "Ultrasonic Waves: Their Interferometric Measurement and Display," Appl. Opt. 15, 1976, pp. 1499-1505.

Closure

Ultrasonic methods are unequaled in directly and nondestructively evaluating the mechanical behavior of materials containing damage. The work supported by this grant has expanded the basic understanding of the acousto-ultrasonic method for that purpose.

A summary of the more significant conclusions is listed here.

Part I

1. Acousto-ultrasonic examination of fatigue damage development reveals a sensitivity to damage mechanisms that are undetectable by penetrant-enhanced stereo X-ray radiography or stiffness monitoring procedures.

2. "Weak" regions detected by the acousto-ultrasonic method coincide with the location of initial damage development and final failure for uniaxial loaded specimens.

3. Incorporation of the NBS (Proctor) conical transducer into the acousto-ultrasonic procedures has revealed that a significant portion of the ultrasonic energy is transferred throughout the laminate by plate wave propagation.

Part II

4. Careful analytical consideration of in-plane wave propagation has shown that the dominant frequencies observed in the acousto-ultrasonic method correspond to the fundamental extensional and flexural plate modes.

5. Measurement of plate wave velocities allows for determination of extensional and flexural stiffnesses from place to place in the laminated plates.

Part III

6. Practical, quantitative, noncontact detection of ultrasonic waves used for effecting the acousto-ultrasonic method is possible if optical fibers are integrated into a blazed grating Michelson-type interferometric system.

1. Report No. NASA CR-3976	2. Government Accession No.	3. Recipient's Catalog No.
4. Title and Subtitle Ultrasonic Stress Wave Characterization of Composite Materials		5. Report Date May 1986
		6. Performing Organization Code
7. Author(s) John C. Duke, Jr., Edmund G. Henneke II, and Wayne W. Stinchcomb		8. Performing Organization Report No. None
		10. Work Unit No.
9. Performing Organization Name and Address Virginia Polytechnic Institute and State University Engineering Science and Mechanics Department Blacksburg, Virginia 24061-4899		11. Contract or Grant No. NAG3-323
		13. Type of Report and Period Covered Contractor Report
12. Sponsoring Agency Name and Address National Aeronautics and Space Administration Washington, D.C. 20546		14. Sponsoring Agency Code 506-53-1A (E-2948)

15. Supplementary Notes

Final report. Project Manager, Alex Vary, Structures Division, NASA Lewis Research Center, Cleveland, Ohio 44135.

16. Abstract

The work reported covers three simultaneous projects. The first project was concerned with (1) establishing the sensitivity of the acousto-ultrasonic method for evaluating subtle forms of damage development in cyclically loaded composite materials, (2) establishing the ability of the acousto-ultrasonic method for detecting initial material imperfections that lead to localized damage growth and final specimen failure, and (3) characteristics of the NBS/Proctor sensor/receiver for acousto-ultrasonic evaluation of laminated composite materials. The second project was concerned with examining the nature of the wave propagation that occurs during acousto-ultrasonic evaluation of composite laminates and demonstrating the role of Lamb or plate wave modes and their utilization for characterizing composite laminates. The third project was concerned with the replacement of contact-type receiving piezotransducers with noncontacting laser-optical sensors for acousto-ultrasonic signal acquisition.

17. Key Words (Suggested by Author(s)) Nondestructive testing/evaluation; Stress waves; Acousto-ultrasonics; Fiber-reinforced composites; Damage; Strength; Stiffness; Signal analysis; Laser/piezotransducers	18. Distribution Statement Unclassified – unlimited STAR Category 38

19. Security Classif. (of this report) Unclassified	20. Security Classif. (of this page) Unclassified	21. No. of pages 158	22. Price* A08